

JINANNOUNCED

①

AD-A955 991

VIRTUAL MODE SURFACE DUCT
MODEL FOR FACT

SAI-81-259-WA

by

F. J. Ryan

September 28, 1980

DTIC
ELECTED
JAN 24 1991
S B D

Prepared for:

Code 500

Ocean Programs Office
Naval Ocean Research and Development Activity
Bay St. Louis, Mississippi 39529

Developed Under Contract No. N00014-78-C-0566



SCIENCE APPLICATIONS, LA JOLLA, CALIFORNIA
ALBUQUERQUE • ANN ARBOR • ARLINGTON • ATLANTA • BOSTON • CHICAGO • HUNTSVILLE
LOS ANGELES • MCLEAN • PALO ALTO • SANTA BARBARA • SUNNYVALE • TUCSON

P.O. Box 2361, 1200 Prospect Street, La Jolla, California 92037

DISTRIBUTION STATEMENT A

Approved for public release
Distribution Unlimited

01 7 05 2

TABLE OF CONTENTS

<u>Section</u>		<u>Page</u>
1	INTRODUCTION	1-1
1.1	Background	1-1
1.2	Model Requirements	1-2
1.3	Technical Summary	1-2
1.4	Acknowledgements	1-4
2	TECHNICAL APPROACH	2-1
2.1	Furry Model	2-1
2.2	Virtual Mode Solution	2-1
2.3	Trapped Modes	2-6
2.4	Leaky Modes	2-10
2.5	Eigenfunctions	2-12
2.5a	Trapped Modes	2-13
2.5b	Leaky Modes	2-15
2.5c	Turning Points	2-16
2.5d	Near Surface	2-18
2.6	Rough Surface Effects	2-18
3	MODEL EVALUATION	3-1
3.1	PE Comparisons	3-2
3.2	Normal Mode Comparisons	3-40
3.3	Evaluation Summary	3-42
4	SURFACE DUCT PROGRAM	4-1
5	CONCLUSIONS	5-1
APPENDIX A: EVALUATION OF $T_+ T_-$		A-1
APPENDIX B: SURFACE-DUCT PROGRAM LISTING		B-1
APPENDIX C: SAMPLE EXECUTION		C-1
REFERENCES		R-1

per letter

Distribution/	
Availability Codes	
Dist	Avail and/or
	Special
A-1	

SECTION 1 INTRODUCTION

Since its introduction in April 1973, the FACT Model⁽¹⁾ has proven to be a useful tool for predicting and analyzing long-range low-frequency propagation in range-independent environments. The original development emphasized the incorporation of diffraction and surface-image effects in a fully automated, highly efficient model. For short-range high-frequency surface-ducted propagation, Clay augmented the ray model by an approximate surface-duct model already in use in FACT's predecessor, RP70⁽²⁾. While the Clay Model was recognized to have certain deficiencies, an efficient alternative was not available. This report documents such an alternative which is proposed for incorporation in FACT.

1.1 BACKGROUND

The Clay Model underwent a series of reviews (e.g., Labianca⁽³⁾), and was considered in a comparison by Morris of several models with data from the Surface Duct Sonar (SUDS) experiments⁽⁴⁾. Labianca's analysis showed that the model had an oversimplified depth dependence and the wrong dependence of leakage on environmental parameters. The leakage error resulted from assigning leakage losses to partial reflection from the gradient discontinuity at the bottom of the duct rather than to the correct quantum-mechanical "tunneling" phenomenon. The depth dependence was characterized by a single 10-dB drop in level from that in the duct if one of either the source or receiver were moved below the duct ("cross-layer"). In a number of cases the lack of environmental sensitivity proved critical.

Morris' comparisons showed that the Clay Model, AMOS⁽⁵⁾ and the Bucker surface-duct model⁽⁶⁾ were in fair agreement in a number of cases with none particularly better than the others. Since both the Clay Model and AMOS were largely based on experimental data this result was not altogether surprising. The data set was not a severe test of environmental sensitivity and was apparently contaminated by a range dependence in the sound-speed profile that none of the models were developed to include. Bucker's model clearly had the strongest theoretical basis, however it was

much longer running than the others and based on the comparisons a change was not justified.

In the period following these initial evaluations, considerable progress was made in understanding the basic mechanisms of surface ducted propagation, largely as a result of Labianca's⁽⁷⁾ work on virtual modes. Subsequently, Spofford⁽⁸⁾ identified Labianca's asymptotic expressions for deeply trapped virtual modes with mode bundle ray-equivalents ("smodes") and was able to incorporate rough surface scattering effects. A prototype surface duct propagation code was developed by Spofford, using the smode techniques. While showing improvement over the Clay Model, Spofford's model displayed poor performance for some propagative scenarios.

1.2 MODEL REQUIREMENTS

As FACT saw more and more use, dissatisfaction with the Clay Model increased, and LRAPP authorized the development of a better model subject to the following constraints:

1. increased accuracy for a wide range of environmental parameters;
2. continuity of transmission-loss in depth (including acoustic reciprocity);
3. range-smoothed transmission-loss of the approximate form $A + B \log R + aR$; and
4. sufficient speed to have a minimal impact on overall FACT running time (presently about 4 CPU seconds per 100 nmi).

SAI has developed such a model as reported herein.

1.3 TECHNICAL SUMMARY

The approach used in the new model is a further refinement and extension of Labianca's virtual mode results to include modes near cutoff as well as leaky modes. This permits intensity calculations in ducts below cutoff and/or at short ranges where the leaky modes make important contributions. The WKB work of Spofford was extended to the rough surface losses. A brief description of the model theory is provided here, with detailed discussions postponed till Section 2.

The surface duct model is designed to compute the relative incoherent intensity level from a point source in a canonical bilinear duct. Labianca's formulation of the complex pressure field as a Hankel transform over the continuum eigenspectrum is the theoretical starting point. An approximate, yet highly accurate, evaluation of the transform results in the relative incoherent intensity \tilde{I} being given as a finite sum of virtual modes

$$\tilde{I} \approx \frac{2\pi}{r} \sum_m e^{-\alpha_m r} I_m(z_s) I_m(z_r)$$

where r is the range and $z_s(z_r)$ is the source (receiver) depth. The I_m are modal intensity amplitudes and the α_m are modal attenuation coefficients. Individual terms in the sum arise from resonances in the kernel of the Hankel transform due to the proximity of Regge poles in the complex energy plane. The resonances in the transform occur at locations along the real energy axis corresponding to the real part of the Regge pole E_m .

The intensity amplitudes I_m are related to normalized depth functions and are expressible in terms of Airy functions. Efficient expansions for the Airy functions provide a rapid means for evaluation of the virtual mode sum, while preserving numerical accuracy. For the deeply trapped modes, Labianca's results are obtained as limiting cases.

The modal attenuation coefficient α_m incorporates volume, surface and diffractive losses. Volume losses are obtained from standard absorption loss formulas presently included in FACT. The diffractive portion of α_m is obtained from the imaginary component of the Regge pole and physically arises from leakage of acoustic energy into the region below the duct. The surface loss portion of α_m is computed by using conservation of energy applied to the virtual modes' ray-equivalent reflecting from the rough ocean surface. Each interaction of the ray-equivalent with the surface yields an effective reflection loss which is then accumulated continuously over the ray's cycle distance. The rough surface reflection losses are computed in a separate module as a function of the ray's surface grazing angle, sea state and frequency.

The virtual mode model was compared to a series of benchmarks generated using both the parabolic-equation (PE) code⁽¹⁶⁾ and the NOSC n-layer normal mode (NM) code⁽¹²⁾ for a representative surface duct. The model shows excellent agreement with both PE and NM calculations. Details of the comparisons are described in Section 3.

1.4 ACKNOWLEDGEMENTS

This work was supported by the Ocean Programs office of NORDA (Code 500), under the program management of Mr. Bob Wheatley. The support of technical staff at the Naval Ocean Systems Center (NOSC), particularly Mr. M. A. Pedersen and Dr. D. F. Gordon, in making the normal mode computer runs, is gratefully acknowledged. At SAI, prior work by Dr. H. L. Wilson on modeling surface scattering using the transport equation and by Mr. C. W. Spofford and Ms. R. E. Keenan on rough surface loss was incorporated into the surface duct model. Ms. E. Holmes assisted in making the parabolic equation runs used in the model evaluation. The author is grateful to Mr. C. W. Spofford for initially suggesting this problem and for discussions related to the virtual mode model.

SECTION 2

TECHNICAL APPROACH

This section describes the theoretical basis for a new surface duct model proposed for use in FACT. The model is an extension of previous work by Labianca on virtual mode representations and by Spofford on ray-mode equivalents. The model is designed to compute the incoherent acoustic intensity from a point source in a range independent ocean surface duct as a function of source/receiver geometry. The ocean surface duct is approximated by a canonical bilinear model first analyzed by Furry⁽⁹⁾ in connection with the transmission of electromagnetic waves in the atmosphere.

2.1 FURRY MODEL

Furry's model approximates the square of the refractive index n^2 with the bilinear form [Fig. (2.1)]

$$n^2(z) = \left[c_0 / c(z) \right]^2 = 1 - g_- z , \quad 0 \leq z < d$$

$$= 1 - g_- d + g_+ (z-d) , \quad z \geq d$$

unit: ?
 g_+, g_-
 are gradient
 $\frac{d}{dz}$
 so have m^{-1}

where d is the depth of the surface duct, $g_-(g_+)$ is the gradient within (below) the duct, c_0 is the surface sound speed, and $c(z)$ is the depth dependent sound speed. The Furry model has been employed by a number of authors in the context of ocean acoustics, with the conventional Fourier-Bessel or longitudinal wavenumber (λ) representation being used by Marsh,⁽¹⁰⁾ Hall⁽¹¹⁾ and Pedersen and Gordon,⁽¹²⁾ while the transverse wavenumber (κ) representation was employed by Labianca.⁽⁷⁾ The latter is used in this report.

2.2 VIRTUAL MODE SOLUTION

In polar cylindrical coordinates, the complex pressure field \underline{P} from a unit strength monopole source satisfies the Helmholtz equation

$$\left[\frac{1}{r} \frac{d}{dr} r \frac{d}{dr} + \frac{d^2}{dz^2} + k_0^2 n^2(z) \right] \underline{P}(r, z_r, z_s) = \frac{-1}{2\pi r} \delta(r) \delta(z_r - z_s) .$$

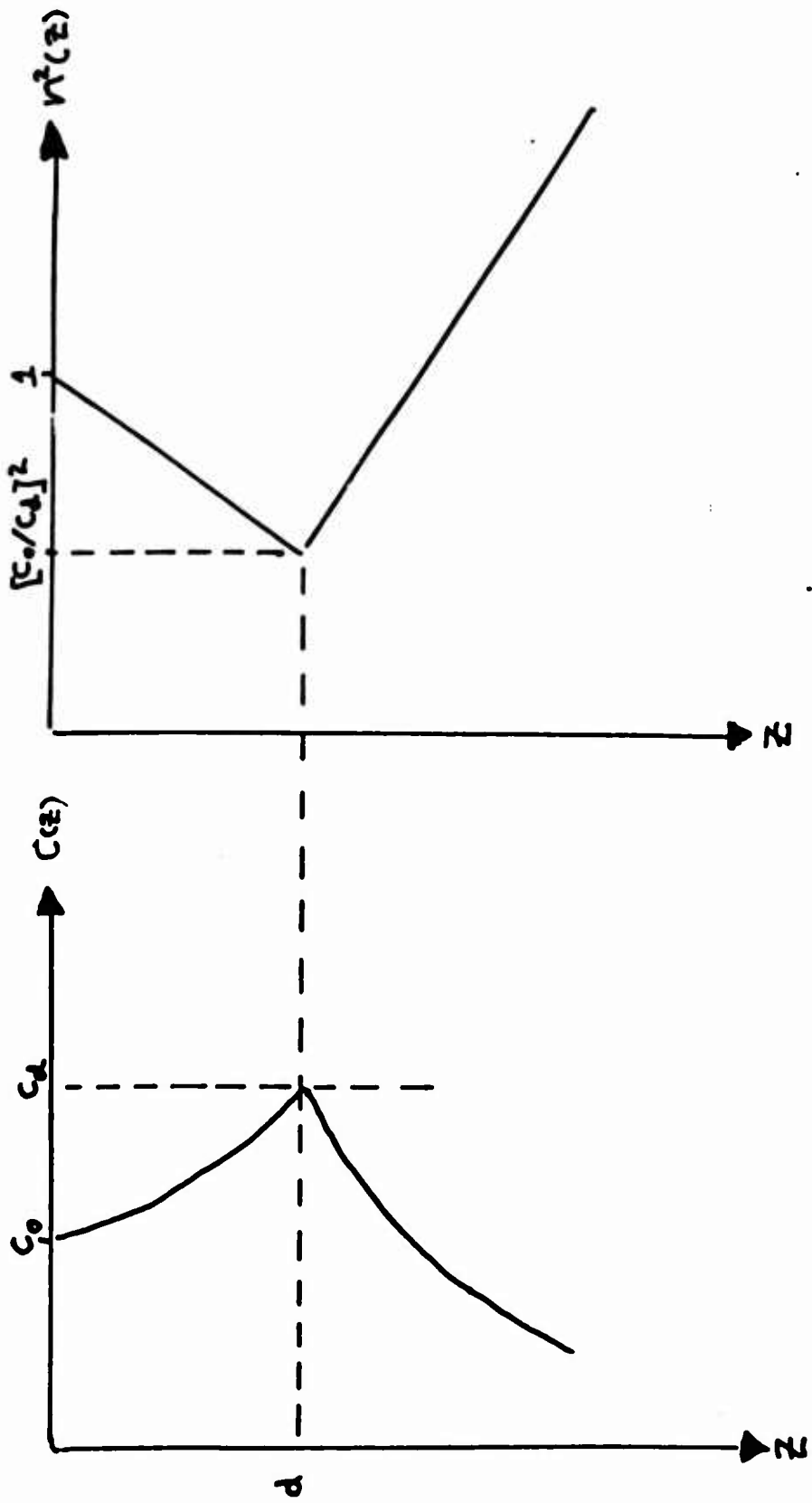


Figure 2-1. Furry Model Profile.

A harmonic time dependence, $\exp(-i\omega t)$, is suppressed with ω the angular frequency and $k_0 = \omega/c_0$. The source is located at $\vec{r} = (0, z_s)$, the receiver at $\vec{r} = (r, z_r)$ and P is to satisfy a pressure release boundary condition ($P=0$) at the surface and a radiation condition at deep depths.

Employing standard separation of variables techniques, the pressure is represented by the convolution

$$P(r, z_r, z_s) = \frac{-1}{8\pi} \int_{\Gamma} H_0^{(1)} \left[r(k_0^2 - \kappa^2)^{\frac{1}{2}} \right] g(\kappa^2, z_r, z_s) d\kappa^2 \quad (2.1)$$

where the depth Green's function g satisfies

$$\left[\frac{d^2}{dz^2} + k_0^2 (n^2 - 1) + \kappa^2 \right] g = -\delta(z_r - z_s)$$

with κ the transverse wavenumber ($k_0^2 = \lambda^2 + \kappa^2$).

The depth Green's function is expanded in a complete set of orthonormal eigenfunctions $\hat{\phi}$ of the homogeneous equation

$$\left[\frac{d^2}{dz^2} + k_0^2 (n^2 - 1) + \kappa^2 \right] \hat{\phi} = 0 \quad , \quad (2.2)$$

subject to the pressure release boundary condition. For the Furry model the eigenfunctions $\hat{\phi}$ form a continuous spectrum and the integral in Eq. (2.1) becomes

$$P(r, z_r, z_s) = \frac{i}{4\pi} \int_{-\infty}^{\infty} H_0^{(1)} \left[r(k_0^2 - \kappa^2)^{\frac{1}{2}} \right] \hat{\phi}(z_r, \kappa^2) \hat{\phi}(z_s, \kappa^2) d\kappa^2 \quad .$$

Analytic solutions for the eigenfunctions are readily obtained by introducing a natural unit of length, $H = (g_+ k_0^2)^{-\frac{1}{2}}$, whereby Eq. (2.2) becomes

$$\left[\frac{d^2}{dx^2} + E - Q(x) \right] \psi(x, E) = 0 \quad . \quad (2.3)$$

The new independent variable is $x = (z - d)/H$, and the "energy" E and "potential" Q are

$$E = H^2 \kappa^2 - s^3 D ,$$

and

$$\begin{aligned} Q(x) &= s^3 x , \quad x \leq 0 \\ &= -x , \quad x > 0 \end{aligned}$$

with $s^3 = g_- / g_+$ and $D = d/H$. Solutions of Eq. (2.3) may be expressed in terms of the Airy functions. Within the duct,

$$\psi(x, E) = \frac{\pi}{s} \left[Ai(-q) Bi(-q_0) - Ai(-q_0) Bi(-q) \right] , \quad x \leq 0 \quad (2.4a)$$

with $q_0 = w + sD$, $q = w - sx$ and $w = E/s^2$, and below the duct

$$\psi(x, E) = \frac{\pi^{1/2}}{2} \left[T_+(E) h_1(p) + T_-(E) h_2(p) \right] , \quad x > 0 \quad (2.4b)$$

with $p = E + x$. The h functions are

$$h_1(p) = Ai(-p) - i Bi(-p)$$

and

$$h_2(p) = Ai(-p) + i Bi(-p) .$$

Continuity of ψ and $d\psi/dx$ at the duct bottom fixes the T coefficients, leading to

$$T_+(E) = -i\pi^{1/2} \left[\psi'(0, E) h_2(E) - \psi(0, E) h_2'(E) \right] , \quad (2.5a)$$

and

$$T_-(E) = i\pi^{1/2} \left[\psi'(0, E) h_1(E) - \psi(0, E) h_1'(E) \right] . \quad (2.5b)$$

The pressure field integral, Eq. (2.1), is then given in terms of the new variables x, ψ as⁽¹³⁾

$$P(r, x_r, x_s) = \frac{i}{4\pi H} \int_{-\infty}^{\infty} H_0^{(1)} \left[r(k_0^2 - \kappa^2)^{\frac{1}{2}} \right] \frac{\psi(x_r, E)\psi(x_s, E)}{T_+(E)T_-(E)} dE , \quad (2.6)$$

with $\kappa^2 = (E + s^3 D)/H^2$.

The kernel of the Hankel transform in Eq. (2.6) has resonances along the real E axis from Regge poles in the lower half E plane. The Regge poles are the complex roots of $T_-(E_m) = 0$, with the real part of E_m corresponding to the resonance position and the imaginary part of E_m proportional to the resonance width. An approximate, yet highly accurate, evaluation of the integral in Eq. (2.6) is obtained by evaluating the integrand in the region of the resonances. The incoherent intensity, $\tilde{I} = |P|^2$, is then given in the far field $\left[r(k_0^2 - \kappa^2)^{\frac{1}{2}} \gg 1 \right]$ as⁽¹⁴⁾

$$\tilde{I} \simeq \frac{2\pi}{r} \sum_m e^{-ra_m^L} \frac{I_m(x_s)I_m(x_r)}{|k_0^2 - \kappa_m^2|^{\frac{1}{2}}} \quad (2.7)$$

with $\kappa_m^2 = (E_m + s^3 D)/H^2$,

$$\alpha_m^L = 2 \operatorname{Im} \left[(k_0^2 - \kappa_m^2)^{\frac{1}{2}} \right] ,$$

$$I_m(x) = |\psi_m^2(x, E_m)/N_m|$$

and

$$N_m = H \int_{-D}^{\infty} \psi_m^2(x) dx . \quad (2.8)$$

The ψ_m have been termed virtual modes by Labianca.

When the imaginary part of E_m is small (low attenuation) the depth function $\psi_m(x)$ is contained or "trapped" within the duct. The trapped modes

are capable of propagating acoustic energy to long ranges. Conversely, modes with large imaginary part are not localized in the duct and are termed "leaky".

Trapped modes have $E_r = \text{Re}(E_m)$ negative, and there are two zeroes (turning points) of $E_r - Q(x)$ denoted by x_1 and x_2 (Figure 2.2). When $x < x_1$, or $x > x_2$ ψ_m is oscillatory; when $x_1 < x < x_2$ ψ_m is exponential. The region between the turning points acts as a barrier, confining the depth function to the duct. ψ_m has an imaginary component that is essentially zero until below the barrier ($x > x_2$) and then spirals about the origin of the complex plane in a counter-clockwise sense with increasing magnitude as x increases.

Leaky modes have positive E_r and complex turning points. ψ_m is oscillatory and complex everywhere with no enhancement in the duct. While of lesser importance at long ranges, the leaky modes may make significant contributions at short ranges and need to be included in the residue series.

A ray-equivalent may be associated with ψ_m by defining a surface grazing angle θ_m through

$$\sin\theta_m = \left[g_+ H(E_r + s^3 D) \right]^{1/2} = \left[g_+ + s^2 - g_- d \right]^{1/2}$$

now the leaky modes
grazing angle

The trapped modes are thus seen to have ray-equivalents which turn within the duct, while the leaky modes correspond to ray-equivalents with large grazing angle.

The major effort in using the virtual mode series is in finding the Regge poles E_m . The roots of $T_-(E_m) = 0$ are generally obtained using complicated numerical methods as was done by Pedersen and Gordon.⁽¹²⁾ A different approach will now be discussed which provides accurate approximate expressions for the E_m , yet is very efficient.

2.3 TRAPPED MODES

The Regge pole E_m satisfies $T_-(E_m) = 0$, which upon using Eq. (2.5b) becomes the transcendental equation

$$\psi'(0, E_m) h_1(E_m) = \psi(0, E_m) h'_1(E_m) .$$

Pedersen use
numerical solution
Newton-Raphson
technique

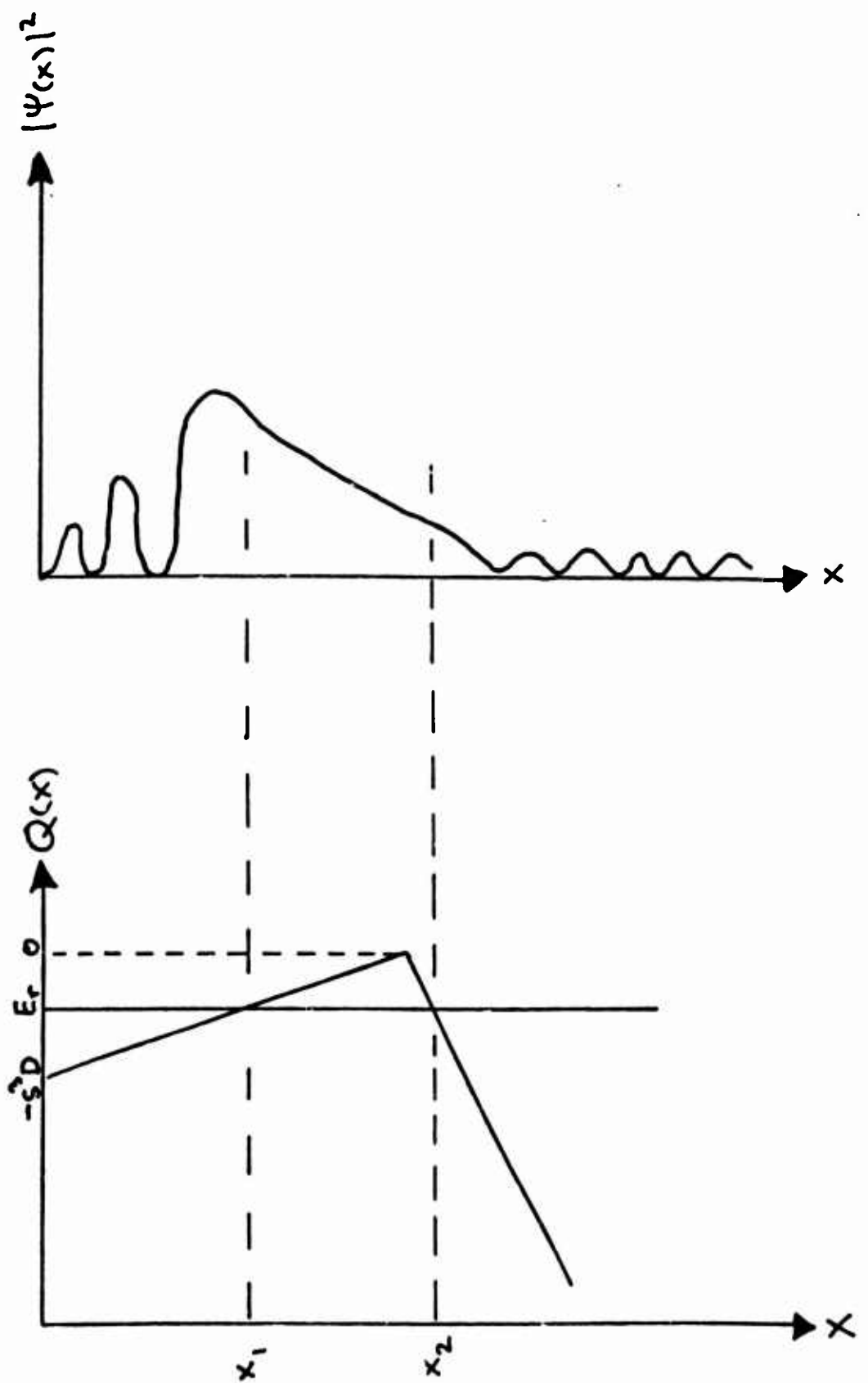


Figure 2-2. Potential $Q(x)$ and Schematic of Trapped Eigenfunction.

Using ψ from Eq. (2.4a), the above eigenvalue equation can be recast as (the mode subscript will be suppressed on E)

$$\frac{Ai(-q_0)}{Bi(-q_0)} = \frac{Ai'(-w) - Z(E)Ai(-w)s}{Bi'(-w) - Z(E)Bi(-w)s} . \quad (2.9)$$

with the effective "impedance" Z of the duct bottom expressed as

$$Z(E) = h_1'(E)/h_1(E) \quad (2.10)$$

and where $w = E/s^2$ and $q_0 = w + sD$.

If phase integral (WKB) methods were used to solve for the trapped eigenvalues, the m-th mode quantization condition would be

$$\int_{-D}^{x_1} (E - s^3 x)^{\frac{1}{2}} dx = \frac{2}{3} q_0^{\frac{3}{2}} = (m - \frac{1}{4})\pi \quad (2.11)$$

where x_1 (complex) is the upper turning point. Since the imaginary part of E is small for the trapped modes, a good approximation for x_1 is to assume it to be real. This corresponds to q_0 in Eq. (2.11) being an approximate root of $Ai(-q_0) = 0$, and suggests a zeroth order approximation to E as $E \sim E_0 = (q_0^* - sD)s^2$ where q_0^* is a real zero of Ai. Zeroes of Ai lie along the negative real axis and are tabulated in Abramowitz and Stegun.⁽¹⁵⁾

Next, expand the left side of Eq.(2.9) around q_0^* with $q_0 = q_0^* + \Delta q$ and use the Wronskian relation of the Ai and Bi to give

$$\left. \frac{Ai}{Bi} \right|_{-q_0} \simeq \Delta q \pi Ai'(-q_0^*)^2 + O(\Delta q^2) \quad \begin{array}{l} \text{automatically} \\ \text{get imaginary} \\ \text{term} \\ E_0 + iEi \end{array} \quad (2.12)$$

$$= \Delta q q_0 , q_0 = \pi Ai'(-q_0^*)^2 .$$

Finally, expanding the right side of Eq. (2.9) around E_0 yields the linearized form

$$a_0 \Delta q = \left| \begin{array}{c} Ai' - Z_0 Ai \\ Bi' - Z_0 Bi \end{array} \right| , \quad Z_0 = Z(E_0) \quad (2.13)$$

$-E_0/s^2$

from which the perturbed eigenvalue is $E = E_0 + \Delta q s^2$. This perturbation solution for E , using Δq from Eq. (2.13), is fast and direct unlike the complicated iterative solution of the original equation (2.9). Furthermore, since E_0 is real, the Airy functions have real arguments greatly simplifying numerical calculations.

For well trapped modes ($E_0 \ll 0$), asymptotic expansion of the Airy functions gives

$$a_0 \Delta q = - \left[\frac{(1+s^3)e^{-\zeta}}{16(-E_0)^{3/2}} + \frac{i}{4} e^{-\zeta(1+s^3)} \right] \quad (2.14)$$

$$\text{with } \zeta = 4(-E_0)^{3/2}/3s^3.$$

The expression for Δq in Eq. (2.14) is based on large argument asymptotic expansions of Ai and Bi . Careful analysis of these expansions indicate that this form is not valid if $w, E \gtrsim -3.5$. Instead, when E_0 is not large and negative (or s^3 not small), Z_0 is evaluated from Eq. (2.10) and Δq computed by direct methods from Eq. (2.13). Compared with the numerical calculations of Pedersen and Gordon, this procedure yields excellent agreement for the trapped modes [$\text{Re}(E) < 0$].

The perturbation expression for Δq [Eq. (2.13)] is only valid if q_0 is near a zero of Ai . Thus a "cutoff" condition is $sD > 2.338$, the first zero of Ai . Ducts with smaller values of sD cannot support trapped modes. Using the asymptotic formulas for zeroes of Ai , an approximate expression for the number of trapped modes N_{vm} is

$$N_{vm} \simeq .25 + (sD)^{3/2}/1.5\pi .$$

2.4 LEAKY MODES

The leaky wave [$\text{Re}(E_m) > 0$] Regge poles are difficult to calculate by solving for roots of $T_-(E)$ as was done for the trapped modes. The imaginary part of the pole is comparable to the real part and recourse is usually made to iterative numerical solutions of Eq. (2.9). Instead a different approach will be used for the leaky modes, which gives an approximate, yet accurate, solution.

As discussed previously, the integrand in Eq. (2.6) resonates for real values of E corresponding to the real part of E_m . Expanding the product $T_+(E)T_-(E)$ using modulus and phase representations for the Airy functions (Appendix A) yields

$$T_+(E)T_-(E) = C(E)G^2(E)$$

where

$$G^2(E) = \beta^2 \sin^2 x_+ + \sin^2 x_- + 2\beta \sin x_+ \sin x_- \cos \Delta . \quad (2.15)$$

The envelope $C(E)$ is a slowly varying function of the energy while G^2 has resonances. The various terms in Eq. (2.15) are

$$\beta = M(w)N(E)/sN(w)M(E) ,$$

$$\Delta = \phi(E) - \theta(E) , \quad \delta = \phi(w) - \theta(w) ,$$

$$x_{\pm} = (x \pm \delta)/2 ,$$

and

$$x = 2\theta(q_0) - \phi(w) - \theta(w) .$$

The M , N , θ , and ϕ functions are the moduli and phases of the various Airy functions and their derivatives.

All the terms in Eq. (2.15) are slowly varying functions of E with the exception of the angle x . Analysis shows that minima in G^2 occur at those energy values E_r where x is a negative multiple of 2π

$$x(E_r) = -2m\pi , \quad m = 1, 2, \dots \quad (2.16)$$

When $E_r \gg 0$, the asymptotic expansions for the phase functions θ and ϕ yield

$$\chi(E_r) \sim \pi/2 - \frac{4}{3} q_0^{3/2} - \pi + \frac{4}{3} w^{3/2} = -\frac{\pi}{2} - \frac{4}{3} (q_0^{3/2} - w^{3/2}) \quad (2.17)$$

and thus the eigenvalue condition is

$$\left. \frac{4}{3} (q_0^{3/2} - w^{3/2}) \right|_{E_r} = \frac{4}{3s} 3 \left[(E_r + s^3 D)^{3/2} - E_r^{3/2} \right] = 2\pi(m - 1/4) \quad . \quad (2.18)$$

But, the phase integral between the surface and duct bottom is just

$$J(E_r) = \int_{-D}^0 (E_r - s^3 x)^{1/2} dx = \frac{2}{3} (q_0^{3/2} - w^{3/2}) \quad , \quad \begin{matrix} \text{phase} \\ \text{integral} \\ \text{action integral} \end{matrix} \quad (2.19)$$

so the eigenvalue condition for highly leaky modes is just $J(E_r) = \pi(m - 1/4)$, or the usual WKB quantization condition. Equation (2.17) in practice proves to be a good approximation even for small values of E_r , and is used to solve Eq. (2.16) numerically.

Once the real part E_r of the Regge pole is obtained from the extremum in G^2 , the imaginary portion E_I is found from conservation of energy. From the form Eq. (2.7), E_I gives rise to an attenuation coefficient a^L :

$$a^L = 2 I_m \left\{ \left[k_0^2 - (E_r - iE_I + s^3 D)/H^2 \right]^{1/2} \right\} \quad .$$

Using the ray-equivalent to the leaky mode, a^L is

$$a^L = - \ln [R(\theta_m)] / D(\theta_m) \quad (2.20)$$

where θ_m is the surface grazing angle of the ray-equivalent defined by

$$\sin^2 \theta_m = g_+ H(E_r + s^3 D) \quad ,$$

$R(\theta_m)$ is the reflection coefficient of the ray equivalent by the gradient discontinuity in refractive index at the duct bottom, and where $D(\theta_m)$ is the ray's cycle distance. The cycle distance $D(\theta_m)$ is given by

$$D(\theta_m) = -2k_0 H^2 \frac{\partial}{\partial E} X(E_r) \sim 4k_0 H (q_0^{1/2} - w^{1/2})$$

where X from Eq. (2.17) has been used.

The reflection coefficient $R(\theta_m)$ is found to be

$$R(\theta_m) = R(E_r) = \frac{\beta^2 + 1 + 2\beta \cos(\delta + \Delta)}{\beta^2 + 1 + 2\beta \cos(\delta - \Delta)},$$

with limiting values

$$R = (1 + s^3)/(1 + s)^3, \quad E_r \rightarrow 0$$

$$R = \frac{(1 + s^3)^2}{64 E_r^3}, \quad E_r \rightarrow \infty$$

The results [Eqs. (2.18) and (2.20)] obtained for the leaky modes are suggestive of WKB formulas. As pointed out by Furry, however, (Ref. 9) phase integral solutions for the bilinear profile are not strictly valid due to the non-analytic nature of the refractive index profile. In particular the phase integral methods do not give the proper above barrier ($E_r > 0$) reflection coefficient Eq. (2.22) arising from gradient discontinuities in n at the duct bottom.

2.5 EIGENFUNCTIONS

Once the eigenvalues E_m are known, the virtual mode depth functions $\psi_m = \psi(x, E_m)$ are obtained from Eq. (2.4a) or Eq. (2.4b). The latter can be simplified, by making use of continuity across the duct bottom, to

$$\psi_m(x) = \psi_m(0) h_1(p)/h_1(E_m) \quad , \quad x > 0 \quad (2.23)$$

with $p = E_m + x$. The normalization N_m is easily obtained from properties of the Airy functions and Eqs. (2.4a) and (2.23) as

$$N_m = H \int_{-D}^{\infty} \psi_m^2(x) dx = \frac{H}{s^3} \left[1 + (1 + s^3) \psi_m^2(0) \frac{d}{dE_m} \left(h_1'/h_1 \right) \right] . \quad (2.24)$$

The calculation of ψ_m and N_m involves computing Airy functions of complex arguments (due to the complex nature of the Regge pole E_m), which tends to be time consuming. Instead various approximations are used to significantly reduce the numerical calculations.

2.5a TRAPPED MODES

Trapped modes have imaginary components E_I of the Regge pole that are small. Since the virtual mode depth functions are analytic with respect to the energy, this suggests a Taylor series expansion about $E_r = \text{Re } E_m$:

$$\psi(x, E) \simeq \psi(x, E_r) + i E_I \frac{\partial \psi(x, E_r)}{\partial E} .$$

For positions within the duct, this yields

$$\psi(x) \sim \frac{\pi}{s} B_1(-q_0^*) \left[(A_1 - \alpha_0 \Delta q_r B_1) + i \Delta q_i (A_1' - \alpha_0 \Delta q_r B_1') \right] \Big|_{-q_r}$$

where $\alpha_0 = \pi A_1'(-q_0^*)^2$, $\Delta q = \Delta q_r + i \Delta q_i$, and $q_r = E_r/s^2 - sx$. The squared amplitude is thus

$$|\psi(x)|^2 \sim \frac{\pi}{\alpha_0 s^2} \left[(A_1 - \alpha_0 \Delta q_r B_1)^2 + \Delta q_i^2 (A_1' - \alpha_0 \Delta q_r B_1')^2 \right] . \quad (2.25)$$

Strongly trapped modes have $|\Delta q| \ll 1$ and therefore

$$|\psi(x)|^2 \sim \frac{\pi}{\alpha_0 s^2} A_i^2 (1 - \alpha_0 \Delta q_r B_i/A_i)^2 , \quad (2.26)$$

where the A_i, B_i are evaluated at $q_r = E_0/s^2 - sx$.

Similar considerations for the below duct region ($x > 0$) lead to

$$h_1(p) \sim h_1(p_r) + i E_i h_1'(p_r) , \quad p_r = x + E_r , \quad E_i = \text{Im}(E)$$

and thus

$$\psi(x) \sim \psi(0) \frac{h_1(p_r) + i E_i h_1'(p_r)}{h_1(E_r) + i E_i h_1'(E_r)} .$$

The squared amplitude of u then is

$$|\psi(x)|^2 \sim |\psi(0)|^2 \cdot \frac{M^2(p_r) + N^2(p_r)E_i^2 - 2E_i/\pi}{M^2(E_r) + N^2(E_r)E_i^2 - 2E_i/\pi}$$

where $M^2(x) = A_i^2(-x) + B_i^2(-x)$, and $N^2(x) = A_i'(-x)^2 + B_i'(-x)^2$. For those modes with $|\Delta q| \ll 1$, this becomes

$$|\psi(x)|^2 \sim |\psi(0)|^2 \frac{M^2(E_0 + x)}{M^2(E_0)} . \quad (2.27)$$

The normalization N_m is

$$N_m = \frac{H}{s^3} \left[1 + (1+s^3) \psi^2(0) \left. \frac{d}{dE} \left(\frac{h_1'}{h_1} \right) \right|_{E_0} \right] ,$$

and for well trapped modes becomes

$$N_m \sim \frac{H}{s^3} \left[1 + \frac{(1+s^3)e^{-\zeta}}{4w_0 a_0 s^2} \right] \rightarrow \frac{H}{s^3} \quad (2.28)$$

where $w_0 = |E_0|/s^2$ and $\zeta = 4/3 w_0^{3/2}$.

2.5b LEAKY MODES

Leaky virtual modes have positive E_r with E_i not small. Asymptotic expansion of the Airy functions with arguments in the sector $|\arg z| < 2/3 \pi$ yield for the in duct form (Eq. 2.4a) of ψ

$$\psi(x, E) \sim s^{-1} (q q_0)^{-1/2} [\sin(\zeta - \zeta_0) - \cos(\zeta - \zeta_0) 5/72 \zeta]$$

where $\zeta = 2/3 q^{3/2}$, $\zeta_0 = 2/3 q_0^{3/2}$ ($|\arg(q, q_0)| < 2/3 \pi$). The squared amplitude of ψ is then

$$\begin{aligned} |\psi(x, E)|^2 &= s^{-2} |q q_0|^{-1/2} |\sin(\zeta - \zeta_0) - \cos(\zeta - \zeta_0) 5/72 \zeta|^2 \\ &= s^{-2} |q q_0|^{-1/2} |\sin(\zeta - \zeta_0)|^2 , \quad |\zeta| \gg 1 \end{aligned}$$

or

$$|\psi(x)|^2 = \frac{1}{2} s^{-2} |q q_0|^{-1/2} (\cosh 2\Delta\zeta_r - \cos 2\Delta\zeta_i) , \quad x < 0 \quad (2.29)$$

with $\Delta\zeta = \Delta\zeta_r + i \Delta\zeta_i = \zeta - \zeta_0$.

Below the duct, similar expansions are made for $h_1(p)$ in Eq. (2.23) to give

$$\begin{aligned} h_1(p) &= A_1(-p) - i B_1(-p) \\ &\simeq \sqrt{\pi} p^{-1/2} e^{i(t-\pi/4)} (1 - i 5/72 t) , \quad |p| \gg 1 \end{aligned}$$

with $p = E + x$, and $t = t_r + i t_i = 2/3 p^{3/2}$.

The squared modulus of h_1 is

$$|h_1(p)|^2 \simeq \pi p^{-\frac{1}{2}} e^{-2t_f} |1 - 15/72t|^2 , \\ \rightarrow \pi p^{-\frac{1}{2}} e^{-2t_f} , \quad (2.30)$$

which leads to ψ having the form

$$|\psi(x)|^2 \sim \frac{|\psi(0)|^2}{|h_1(E_m)|^2} \pi p^{-\frac{1}{2}} e^{-2t_f} \quad (2.31)$$

below the duct. Note that since $E_f < 0$, Eq. (2.31) predicts an exponential increase in the virtual mode amplitude with increasing depth below the duct. This behavior is in precise agreement with the numerical results of Pedersen and Gordon.

2.5c TURNING POINTS

The expressions for the virtual mode depth function ψ_m developed thus far are based on large argument expansions of the Airy functions which fail near turning points (i.e., regions where q or p are zero). However, ψ_m is an analytic function of its arguments and thus can be expanded in a Taylor series about the turning point.

Concentrating on the in-duct form [Eq. (2.4a)] of ψ , a series expansion about the turning point is ($q = E_m/s^2 - sx$)

$$\psi_m(x) = \psi(q) = \psi_0 + q \psi'_0 + \frac{q^2}{2} \psi''_0 + \frac{q^3}{6} \psi'''_0 + \dots \quad (2.32)$$

where $\psi_0 = \psi(q=0)$, $\psi'_0 = \partial\psi(q=0)/\partial q$, etc. The series can be greatly simplified by using the differential equation satisfied by ψ

$$\partial^2 \psi / \partial q^2 = -q\psi$$

to yield

$$\begin{aligned}\psi(q) &= \psi_0 \left(1 - q^3/3! + 4q^4/6! - \dots \right) \\ &\quad + q\psi'_0 \left(1 - 2q^3/4! + 10q^6/7! - \dots \right) .\end{aligned}\quad (2.33)$$

The depth function and its derivative at the turning point are .

$$\psi = c_1 \frac{\pi}{s} \left[Bi(-q_0) - \sqrt{3} Ai(-q_0) \right] , \quad (2.34)$$

$$\psi'_0 = c_2 \frac{\pi}{s} \left[Bi(-q_0) + \sqrt{3} Ai(-q_0) \right] , \quad (2.35)$$

where $c_1 = Ai(0)$ and $c_2 = -Ai'(0)$. Separate asymptotic expressions for ψ_0 , ψ'_0 are obtained depending on whether the mode is trapped or leaky (i.e., depending on q_0).

Trapped modes have q_0 near a zero of Ai , and the perturbation expansion of Eq. (2.12) leads to

$$|\psi_0|^2 \sim \frac{\pi c_1^2}{a_0 s^2} \left[(1 - a_0 \sqrt{3} \Delta q_r)^2 + 3a_0^2 \Delta q_i^2 \right] \quad (2.36)$$

and

$$\psi'_0/\psi_0 \sim \frac{c_2 (1 + a_0 \sqrt{3} \Delta q)}{c_1 (1 - a_0 \sqrt{3} \Delta q)} , \quad \Delta q = \Delta q_r + i\Delta q_i . \quad (2.37)$$

Similar results for leaky modes are obtained by using the complex asymptotic forms of $Ai(-q_0)$ and $Bi(-q_0)$:

$$\psi'_0/\psi_0 \sim -\frac{c_2 \cos(\zeta_0 - \pi/12)}{c_1 \sin(\zeta_0 + \pi/12)} , \quad \zeta_0 = \frac{2}{3} q_0^{\frac{3}{2}} \quad (2.38)$$

and

$$|\psi_0|^2 \sim \frac{4\pi c_1^2}{s^2} |q_0|^{-\frac{1}{2}} |\sin(\zeta_0 + \pi/12)|^2 . \quad (2.39)$$

For both trapped and leaky modes, the amplitude of $|\psi|^2$ is obtained from Eq. (2.33) as

$$|\psi(q)|^2 \sim |\psi_0|^2 \left| \left(1 - \frac{q^3}{3!} + \frac{4q^4}{6!} \right) + q \frac{\psi'_0}{\psi_0} \left(1 - \frac{2q^3}{4!} + \frac{10q^6}{7!} \right) \right|^2 . \quad (2.40)$$

2.5d NEAR SURFACE

Near the surface ($x \sim -D$) the virtual mode depth function can be expanded in a Taylor series as was done for the turning point region

$$\psi(q) = \psi(q_0) + \Delta q \psi'(q_0) + \frac{\Delta q^2}{2} \psi''(q_0) + \dots \quad (2.41)$$

with $\Delta q = q - q_0$ and $q_0 = E/s^2 + sD$ the surface value for q . At the surface $\psi(q_0) = 0$ and $\psi'(q_0) = 1/s$ so Eq. (2.41) becomes

$$\psi(q) = \frac{\Delta q}{s} \left(1 - q_0 \frac{\Delta q^2}{s^3 3!} - 2 \frac{\Delta q^3}{s^4 4!} + \dots \right) \quad (2.42)$$

where $\Delta q = q - q_0 = -s(x+D)$. The amplitude of ψ is then

$$|\psi|^2 \sim (x+D)^2 \left| 1 - q_0 s(x+D)^2 / 6 - s^3 (x+D)^3 / 12 + \dots \right|^2 \quad (2.43)$$

which displays the proper quadratic depth dependence and pressure-release condition at $x = -D$.

2.6 ROUGH SURFACE EFFECTS

The presence of a non-planar ocean surface will modify the Regge poles E_m leading to a larger imaginary component. The virtual mode intensity decays with range at an increased rate due to an additional attenuation term arising from rough surface scattering. The resultant attenuation is the sum

of the previously computed leakage term α^L and the surface scattering term α^S

$$\alpha = \alpha^L + \alpha^S .$$

The surface scattering term is found by applying energy conservation to the modal ray-equivalent interacting with the ocean surface.

A ray-equivalent may be identified with each virtual mode through a surface grazing angle θ_m defined by

$$\sin^2 \theta_m = (E_r + s^3 D) / (k_0 H)^2$$

correction
 previously $\sin^2 \theta_m = g_r / t (E_r + s^3 D)$
the correct \nearrow

and a corresponding cycle distance $D(\theta_m)$

$$D(\theta_m) = 2H \cos \theta_m \int_{-D}^{x_1} [E_r - Q(x)]^{-\frac{1}{2}} dx .$$

x_1 is the upper turning point (real) of the mode and for leaky modes is taken as the duct bottom ($x = 0$). Each interaction of the ray-equivalent with the rough surface is treated as a specular reflection with corresponding reflection coefficient $R^S(\theta_m)$. The intensity decay with range is then modeled as a "loss per bounce" applied continuously over the ray's cycle distance, leading to

$$\alpha^S = - \ln [R^S(\theta_m)] / D(\theta_m) .$$

The rough surface specular reflection coefficient R^S is computed as a function of frequency, grazing angle and sea-state from previous work by Spofford and Keenan.⁽¹⁷⁾ Strictly speaking, the rough surface effects should be included as a modification of the surface impedance condition and the Regge poles found in a self consistent manner. The error made in adopting the present approach is, however, consistent with present understanding of surface scattering phenomena and within the approximation of replacing the true index of refraction profile by the Furry model.

SECTION 3 MODEL EVALUATION

The virtual mode surface duct model described earlier was evaluated by comparisons with output from the parabolic equation (PE) code⁽¹⁶⁾ and the NOSC n-layer normal mode (NM) code. The test environment was a bilinear n^2 profile for a deep (1,000 foot) surface duct with a corresponding sound speed profile having a pressure gradient ($\sim .018 \text{ sec}^{-1}$) within the duct and a moderate ($\sim - .1 \text{ sec}^{-1}$) gradient below the duct. The ocean was assumed infinitely deep with a smooth, pressure-release surface and no surface loss. Incoherent transmission loss, for a monochromatic point source, was computed for a variety of source/receiver geometries.

Source frequencies of 25, 50, 100, 250, 500, and 1,000 Hz were considered which yielded propagation conditions corresponding to zero and 21 trapped modes respectively. This effectively simulated results for thinner ducts at higher frequencies. Source-receiver combinations for all depth pairs between 250 and 1,500 feet in 250-foot increments (21 distinct pairs) were chosen to cover a wide range of in-layer, cross-layer and below-layer geometries for the various source frequencies. In total, 126 different frequency/geometry propagation scenarios were examined in the comparisons.

Two types of surface duct model evaluations were made: (1) incoherent transmission-loss for all 126 scenarios, and (2) individual comparisons of modal attenuation coefficients and intensity amplitudes.

The transmission-loss evaluations were made by direct comparison of the virtual mode surface duct model results with those of the PE and NM codes. The PE code actually outputs coherent transmission-loss values, displaying characteristic interference features. These oscillations were removed by intensity averaging the PE output with an eight (8) nautical mile moving window to simulate incoherent levels.

The NM code, in addition to providing TL output, also output the individual modes used in the TL calculation. Modal attenuation coefficients and eigenfunction intensity amplitudes were available for direct comparison with the surface duct model.

3.1 PE COMPARISONS

The AESD PE code was run at six source frequencies (25, 50, 100, 250, 500, and 1,000 Hz) and for six receiver depths (250, 500, 750, 1000, 1250, and 1500 feet). The PE code is a finite depth ocean model, requiring an absorbing bottom to effectively simulate an infinitely deep ocean. The bottom was placed at 8,000 feet for the 25 Hz run and at 2,000 feet for all other frequencies. The FFT transform size used by the PE code was 2^8 for 25, 500, and 1,000 Hz runs, and 2^7 for the 50, 100, and 250 Hz runs. Due to the use of a running intensity average, PE results at ranges closer than 8 nautical miles are not reliable and are ignored. The PE code implicitly includes the leaky as well as the trapped waves and thus provides a check on the validity of truncating the virtual mode spectrum after three leaky modes.

Comparisons between the virtual mode surface duct model and PE are shown in Figures (3.1) to (3.36) for the various propagation scenarios. Good agreement with the PE code is indicated for within-, cross-, and below-layer geometries.

The 25 Hz run had no trapped modes and the three lowest leaky virtual modes were included in the virtual mode sum. Good agreement with the PE results are seen for ranges exceeding 10-15 nautical miles. Deviation between PE and model results for shorter ranges are possibly an artifact of the PE smoother and/or due to insufficient terms in the modal sum.

The 50 Hz run case corresponds to one trapped mode. The PE code predicts a higher intensity (by ~1-2 dB) at 50 nautical miles. This is probably an artifact of the PE run due to the bottom being too shallow. Such an effect occurred on earlier 25 Hz runs with shallower bottoms and arises from the non-radiation boundary condition used in the PE code. The PE code boundary condition effectively forces an increase in the pressure field within the water column, leading to higher intensities, hence less TL. Additional deviation between the PE code and the surface duct model occur at intermediate ranges (10 - 20 nm) where PE shows more loss. This trend persists for other frequencies. A plausible explanation for this, is phase cancellation leading to a deep null in this region. Since the surface duct model is not designed

to compute phased TL, such differences are to be expected. In any case, the maximum deviation is ~ 2 dB.

The 100 Hz runs exhibit the same general trends as the 50 Hz data, with the exception of much smaller offset at 50 nm. This is due to the decreasing effect of the finite depth bottom used by the PE code, and a corresponding decrease in intensity from "ghost" reflections off the bottom.

The 250, 500, and 1,000 Hz runs can be grouped as a whole for comparisons. Generally the agreement between PE and the virtual mode code is good at longer ranges. For short ranges ($r \lesssim 10$ nm) possible spectrum truncation and/or PE smoother effects are noticed. Medium ($10 \lesssim r \lesssim 25$ nm) ranges exhibit a weak null in the PE results which is not seen in the virtual mode data. This is most probably caused by phase cancellation which the virtual mode model is not treating. For sources within the duct, the PE results display a characteristic interference with range that the smoother has not completely removed. This effect is more pronounced with increasing frequency.

A volume absorption loss term α_v , of the form $\alpha_v = .125 (f/1000)^2$ dB/nm (f the frequency in Hertz), has been added to the virtual mode model results shown in Figures (3.1) to (3.36) to comply with the PE predictions.

SOURCE: FREQUENCY- 25 (HZ) , DEPTH- 250 (FT)

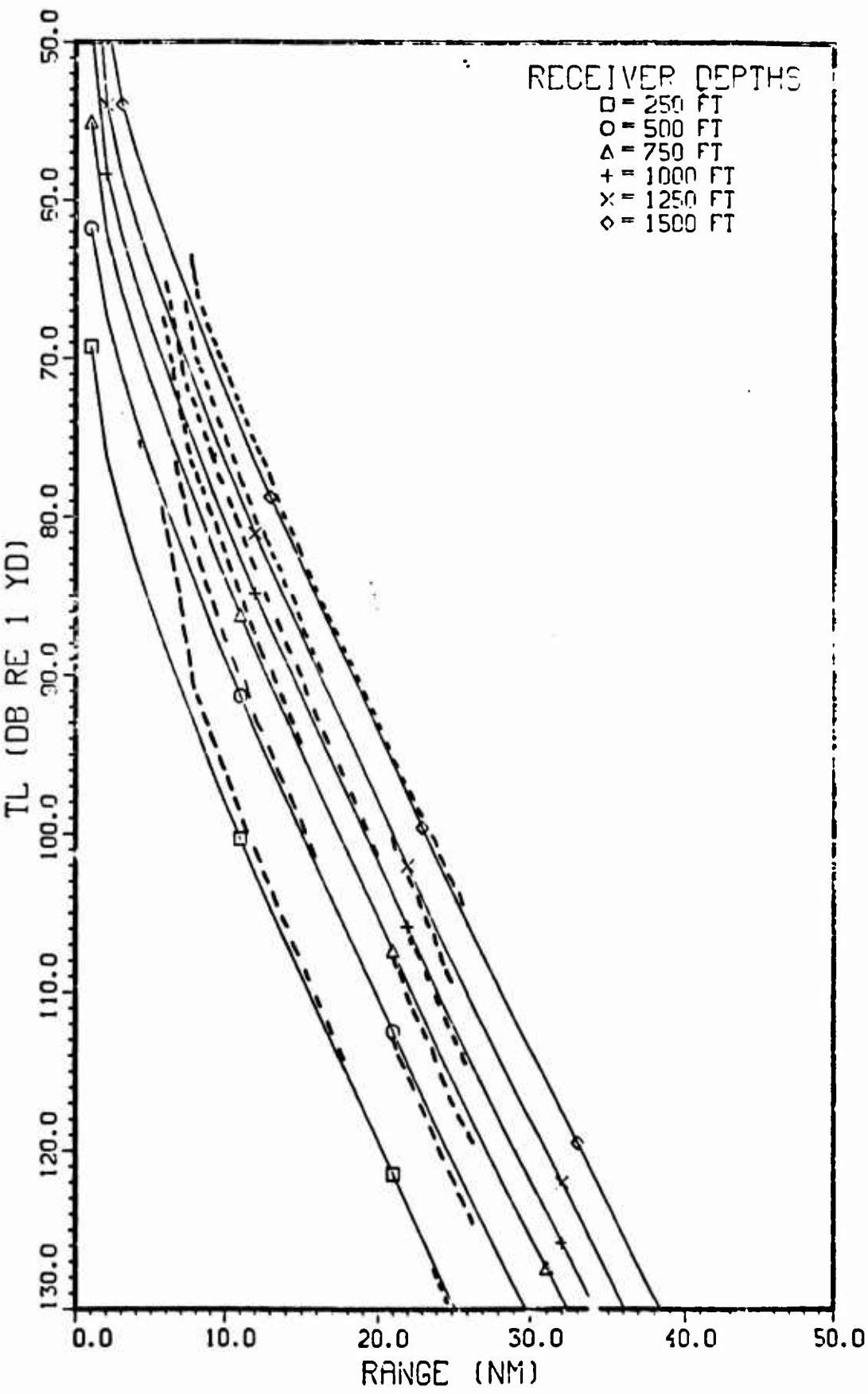


Figure 3-1 . Comparison of Surface-Duct Model (solid) with PE (dash). Consecutive curves displaced 5 db up .

PNT 2 20.00 MED 1 OCT, 1980 , SAI DISPLA VER 8.2

SOURCE: FREQUENCY- 25 (HZ) , DEPTH- 500 (FT)

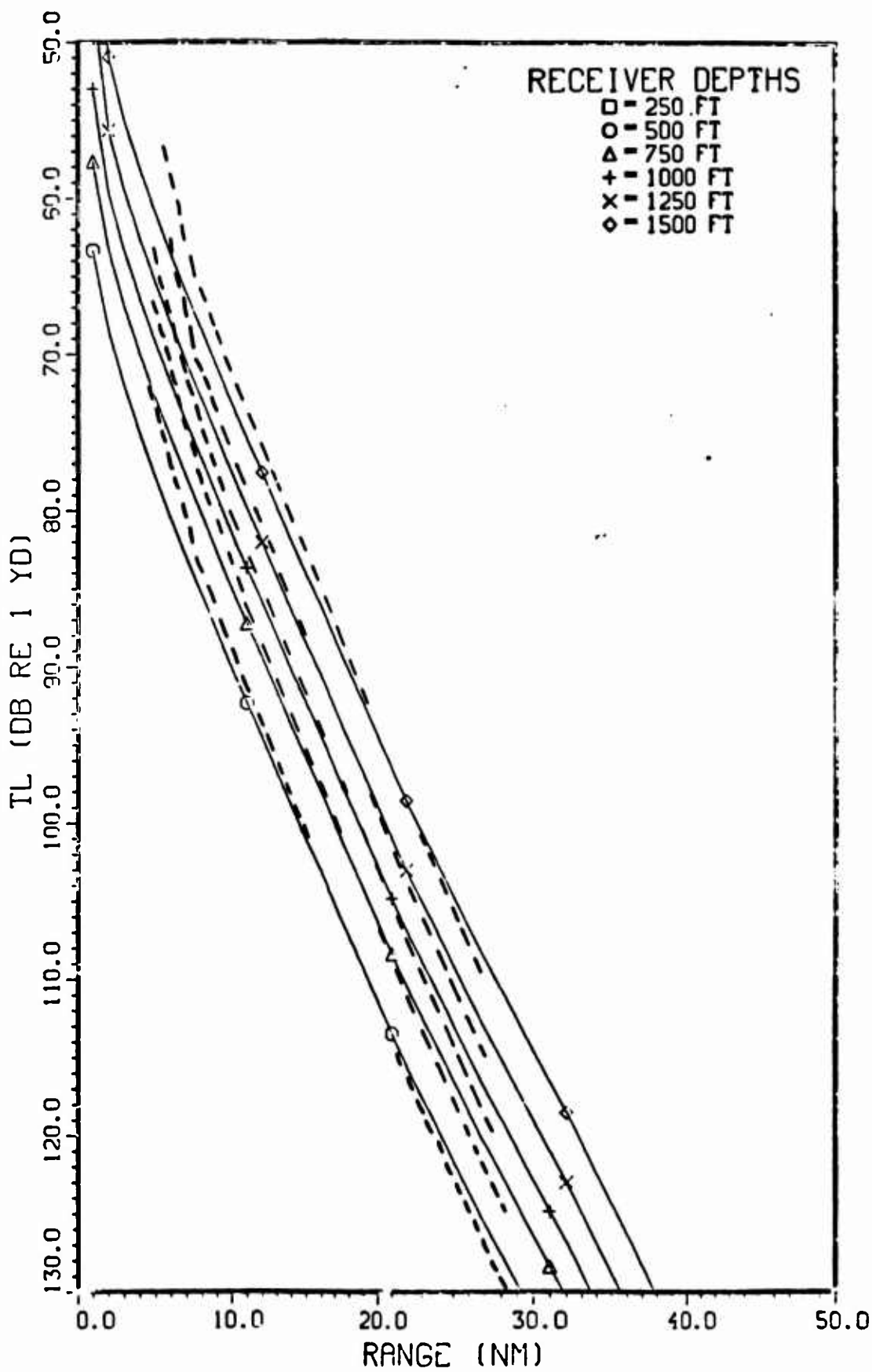


Figure 3-2 . Comparison of Surface-Duct Model (solid) with PE (dashed). Consecutive curves displaced 5 db up .

SOURCE: FREQUENCY= 25 (HZ) , DEPTH= 750 (FT)

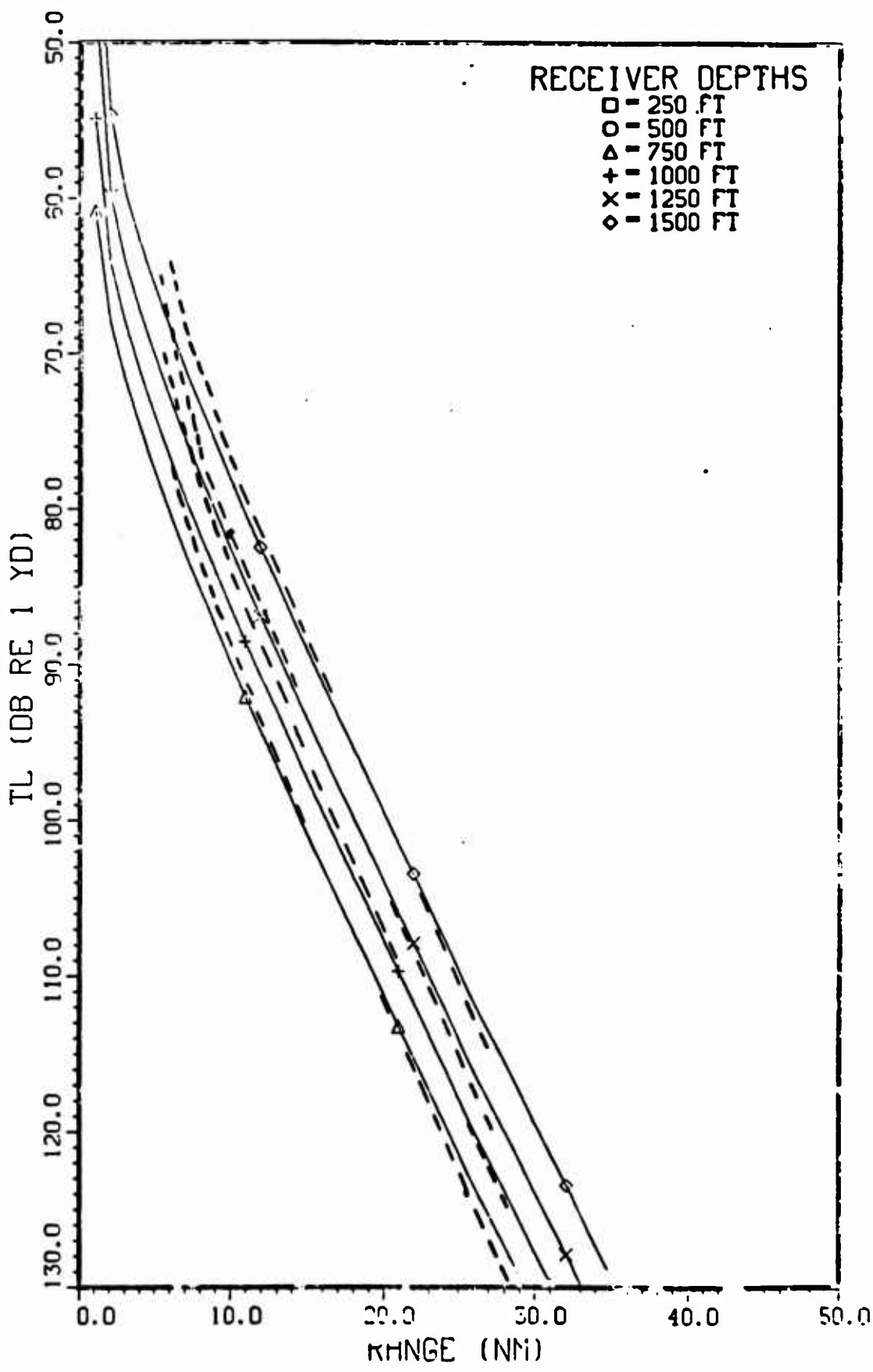


Figure 3-3 . Comparison of Surface-Duct Model (solid) with FE (dash). Consecutive curves displaced 5 db up .

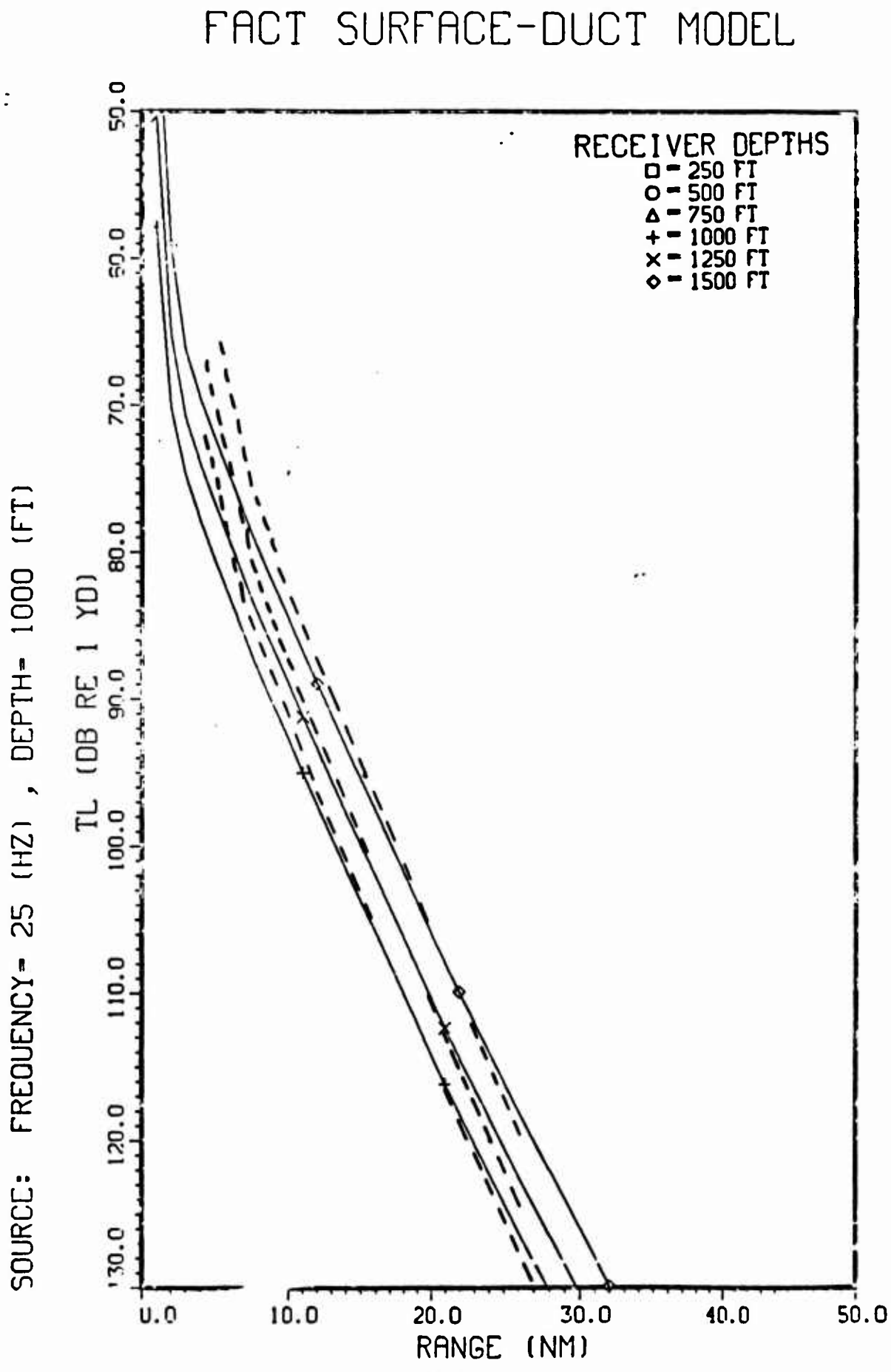


Figure 3-4 . Comparison of Surface-Duct Model (solid) with PE (dash). Consecutive curves displaced 5 db up .

SOURCE: FREQUENCY- 25 (HZ) , DEPTH- 1250 (FT)

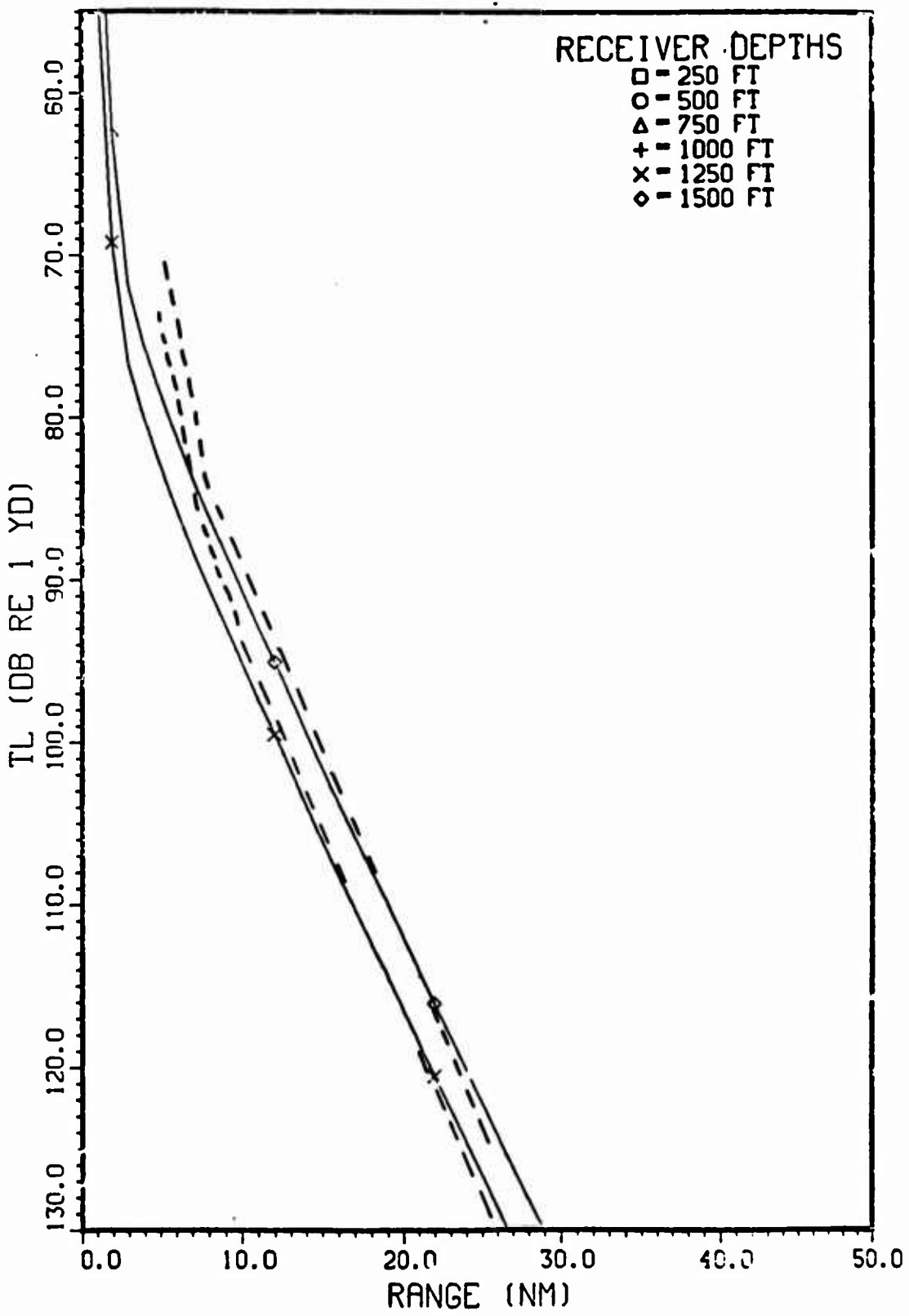


Figure 3-5 .

Comparison of Surface-Duct Model (solid) with PE (dash).
Consecutive curves displaced 5 db up .

SOURCE: FREQUENCY= 25 (HZ) , DEPTH= 1500 (FT)

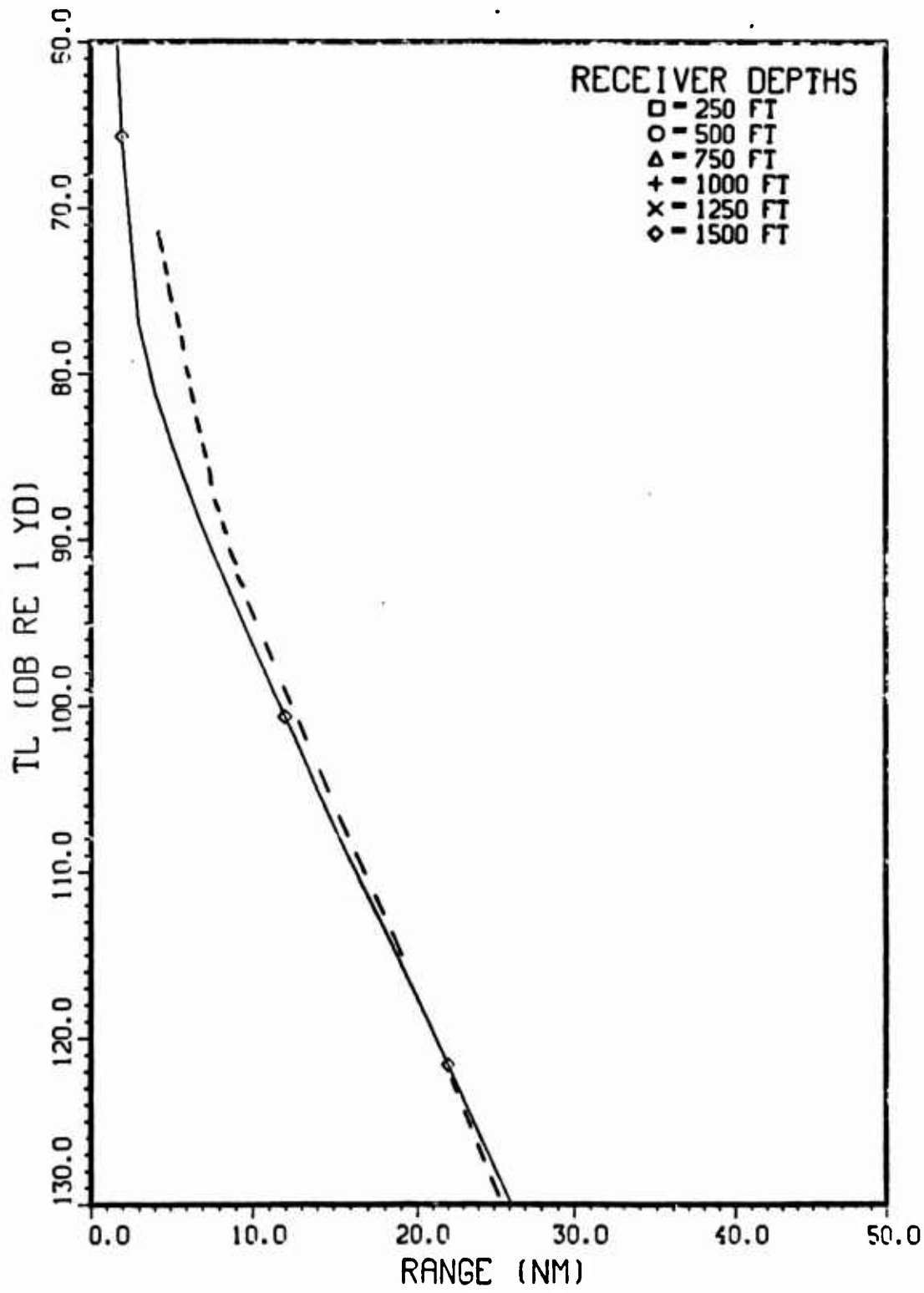


Figure 3-6. Comparison of Surface-Duct Model (solid) with PE (dash).

SOURCE: FREQUENCY- 50 (HZ) , DEPTH- 250 (FT)

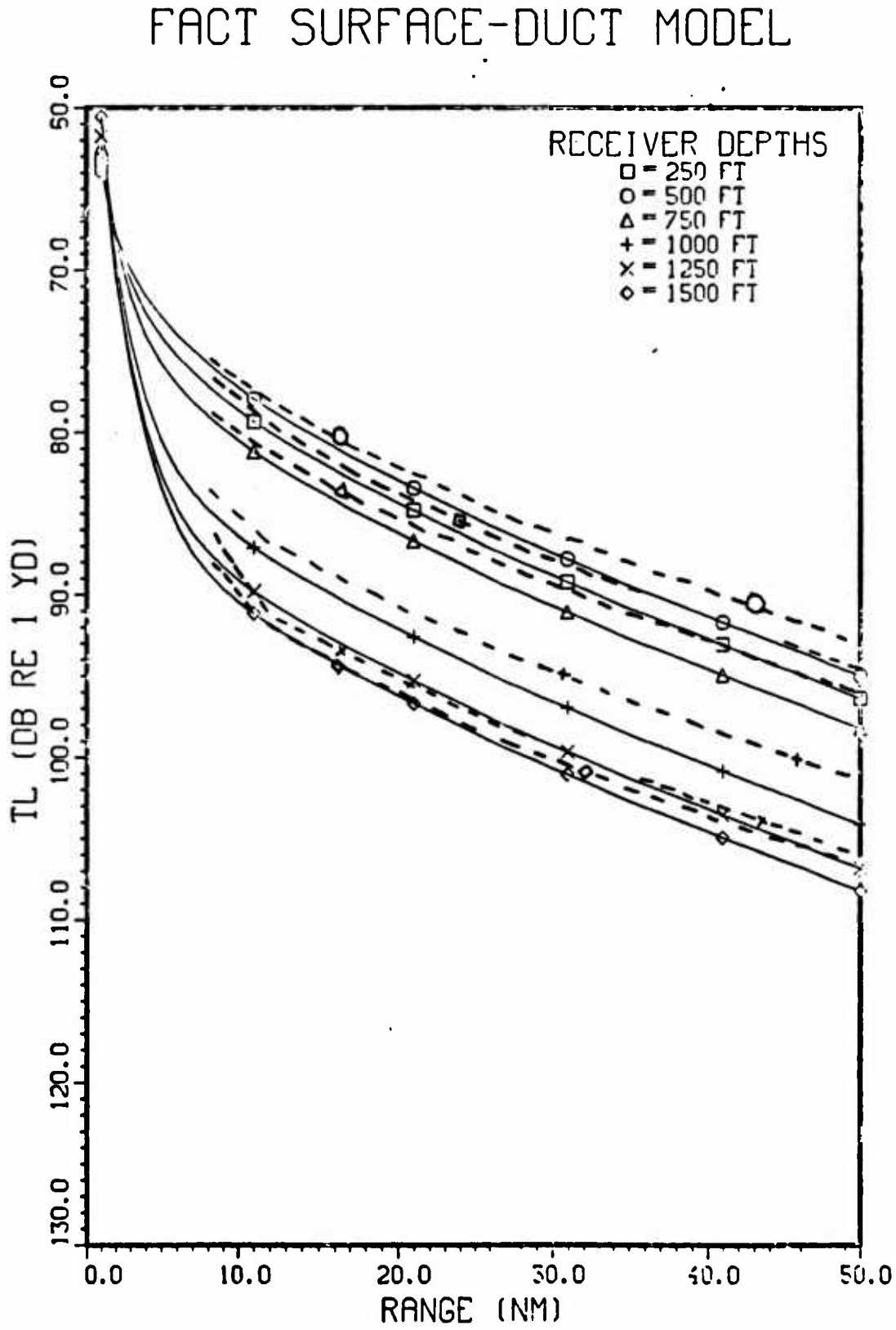


Figure 3-7 . Comparison of Surface-Duct Model (solid) with PC (dashed).

SOURCE: FREQUENCY- 50 (HZ) , DEPTH- 500 (FT)

FACT SURFACE-DUCT MODEL

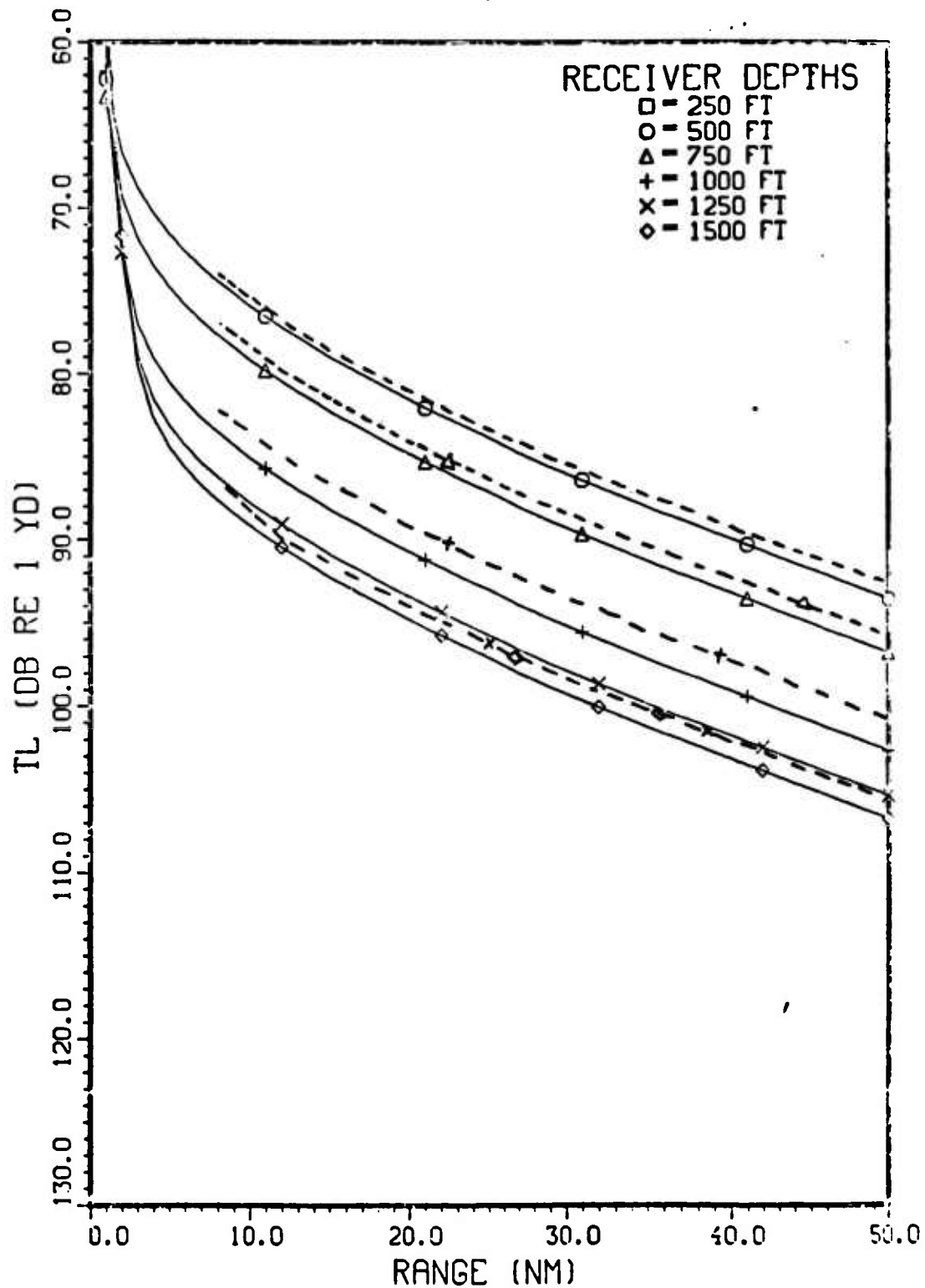


Figure 3-8 . Comparison of Surface-Duct Model (solid) with PC (dashed).

SOURCE: FREQUENCY- 50 (HZ) , DEPTH- 750 (FT)

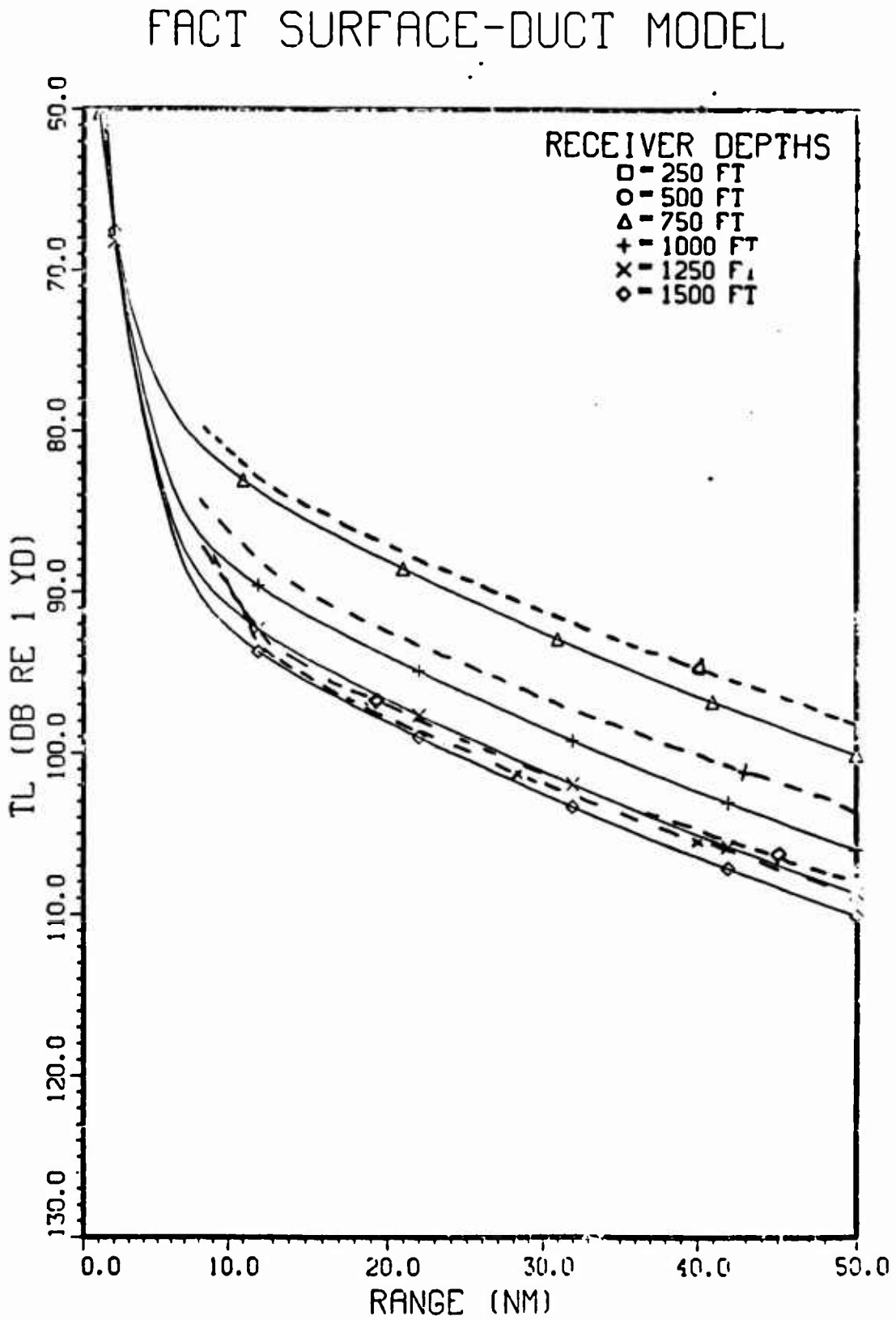


Figure 3-9 . Comparison of Surface-Duct Model (solid) with PE (dash-dot).

FACT SURFACE-DUCT MODEL

SOURCE: FREQUENCY - 50 (HZ) , DEPTH- 1000 (FT)

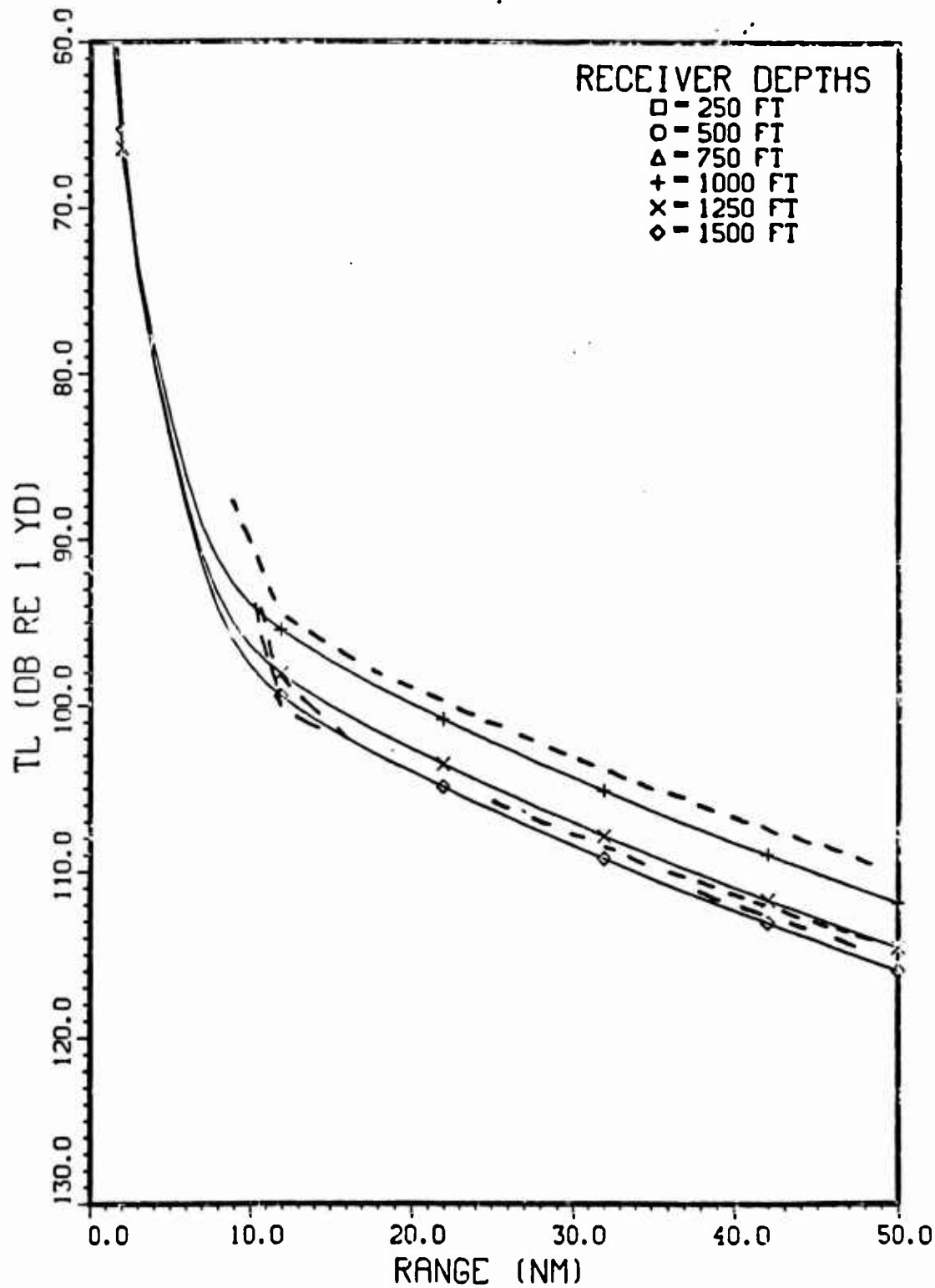


Figure 3-10 . Comparison of Surface-Duct Model (solid) with PE (dash).

SOURCE: FREQUENCY- 50 (HZ) , DEPTH- 1250 (FT)

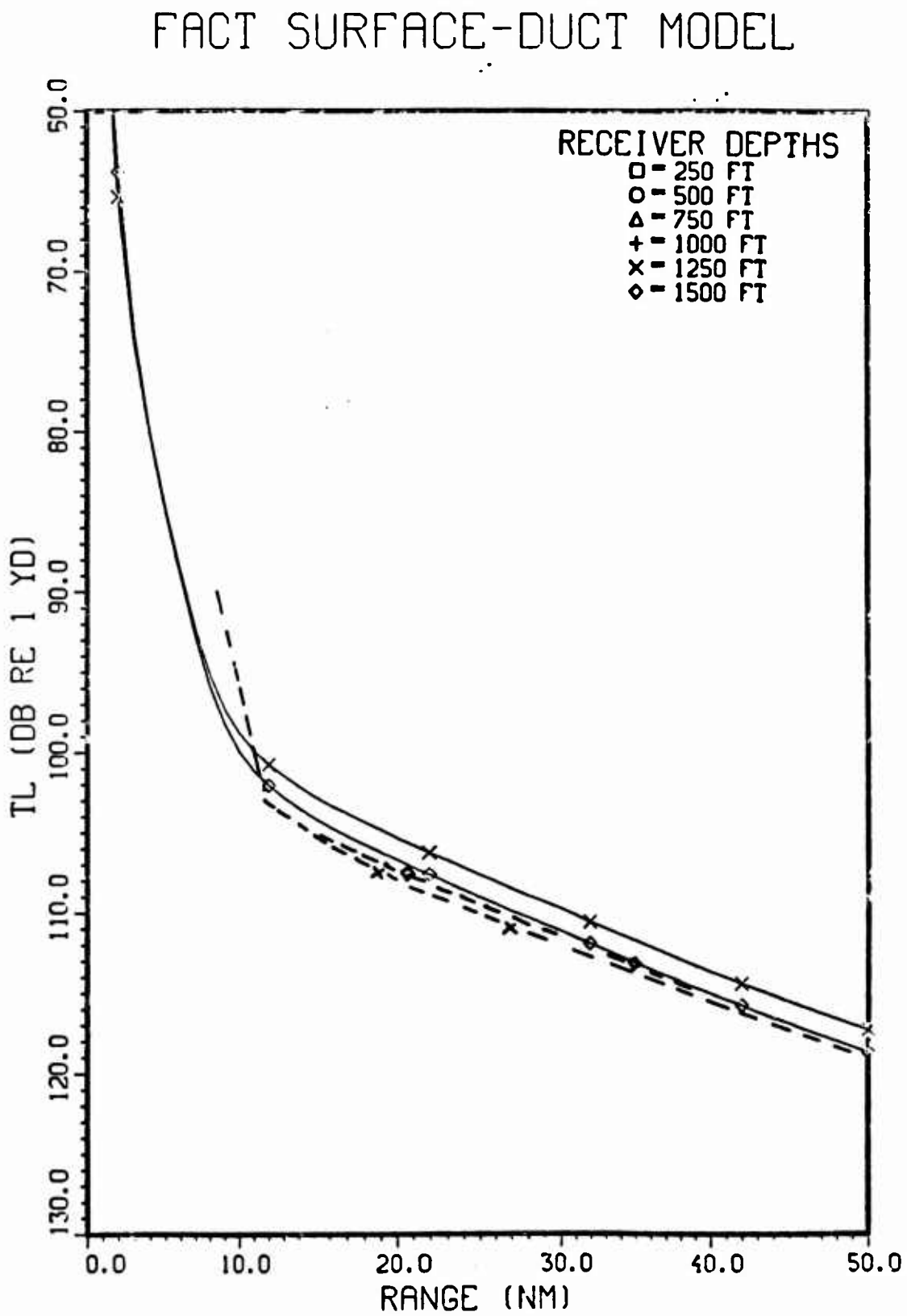


Figure 3-11 . Comparison of Surface-Duct Model (solid) with PE (dash).

SOURCE: FREQUENCY- 50 (HZ) , DEPTH- 1500 (FT)

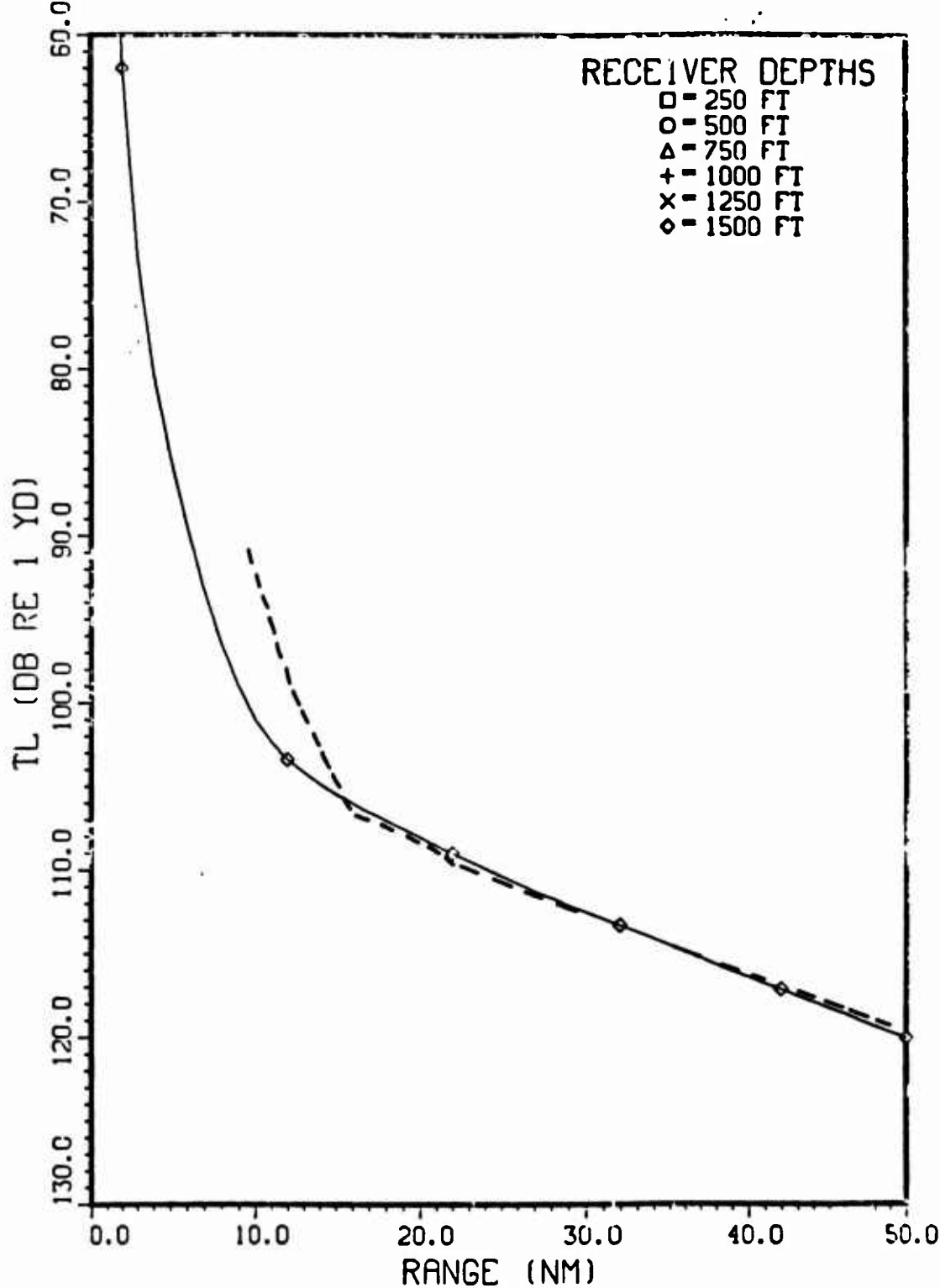


Figure 3-12 .

Comparison of Surface-Duct Model (solid) with PE (dash).

SOURCE: FREQUENCY- 100 (HZ) , DEPTH- 250 (FT)

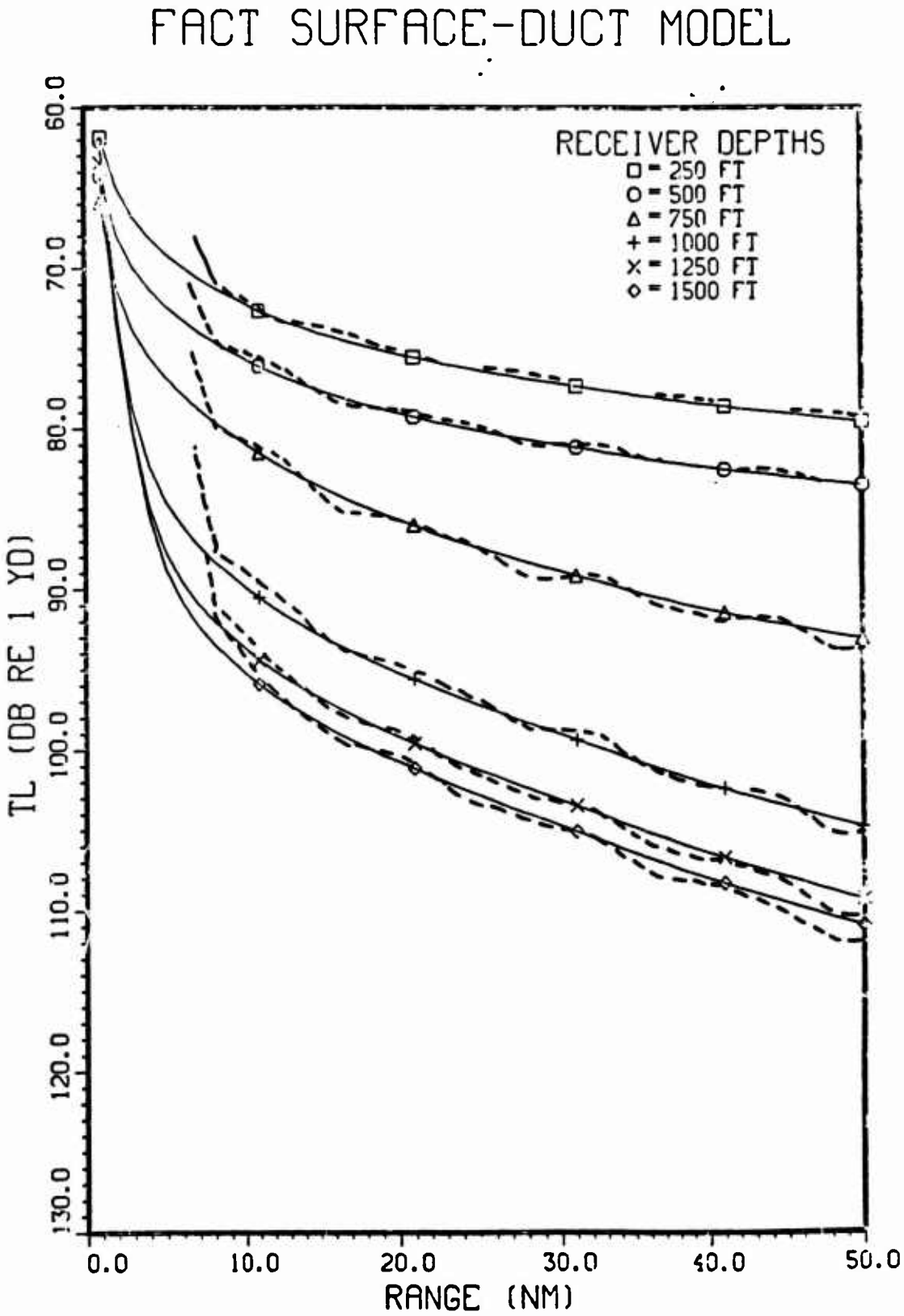


Figure 3-13 . Comparison of Surface-Duct Model (solid) with PE (dash).

FACT SURFACE-DUCT MODEL

SOURCE: FREQUENCY- 100 (HZ) , DEPTH- 500 (FT)

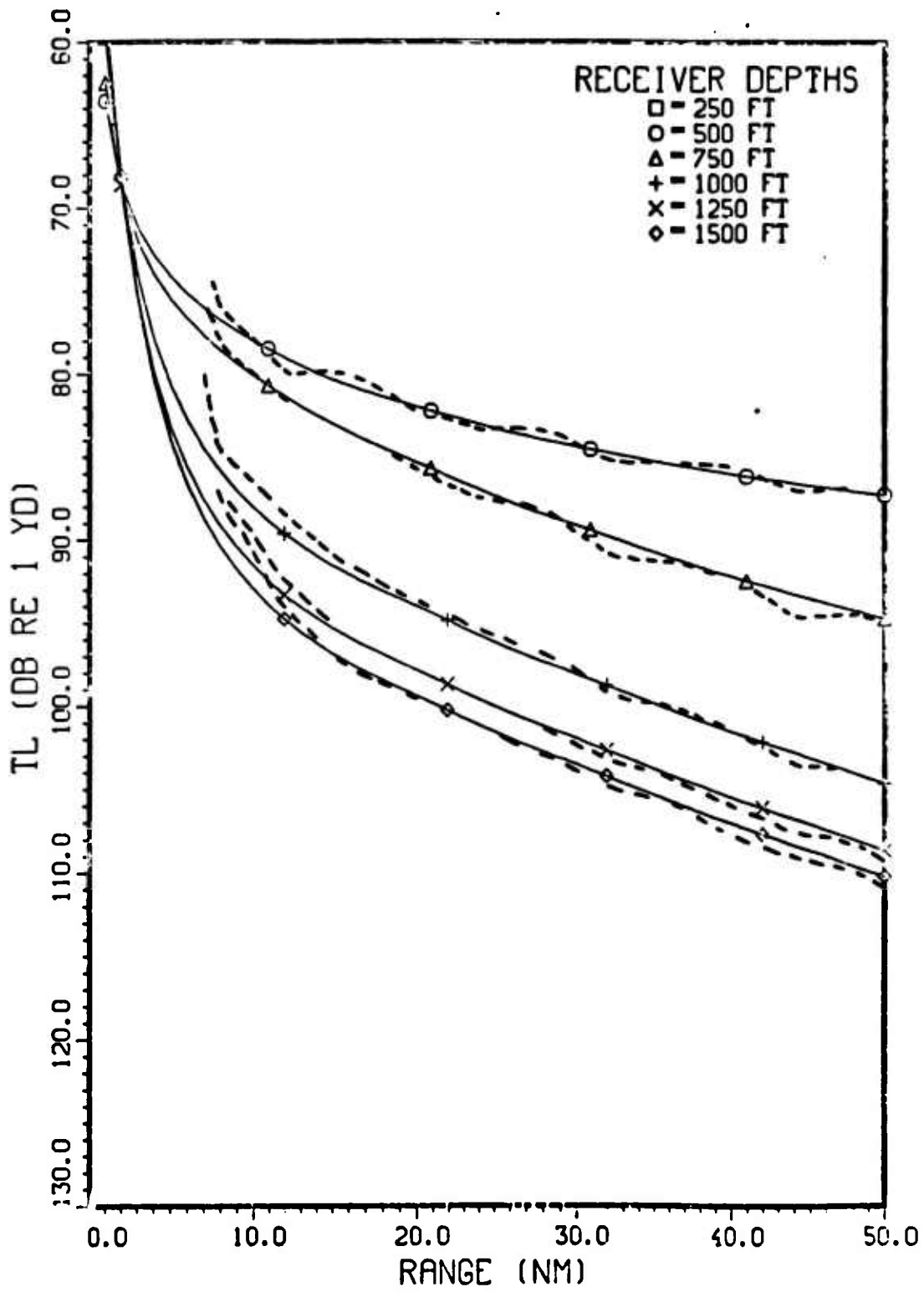


Figure 3-14 . Comparison of Surface-Duct Model (solid) with PC (dorn).

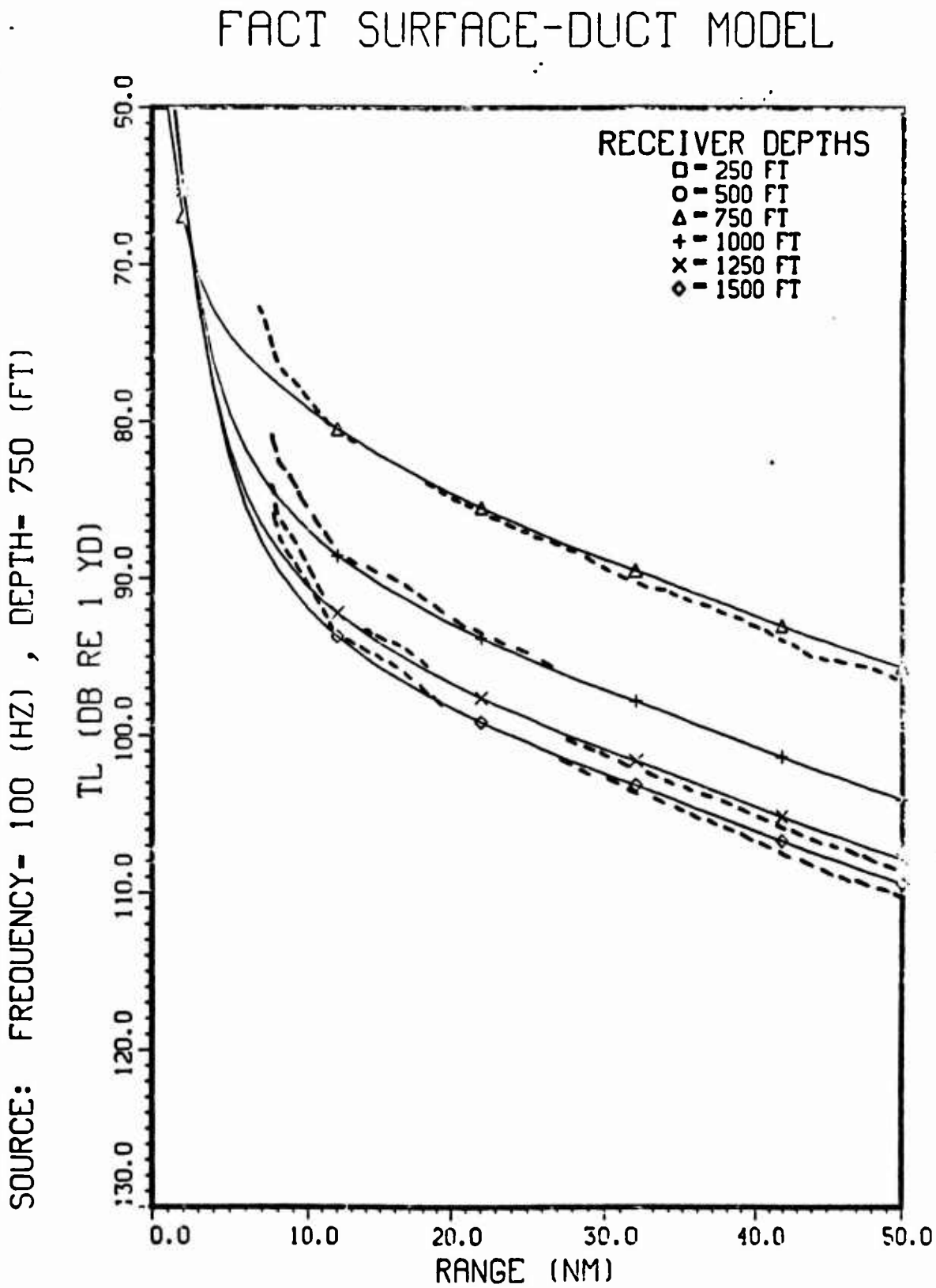


Figure 3-15 . Comparison of Surface-Duct Model (solid) with PE (dash).

SOURCE: FREQUENCY= 100 (HZ) , DEPTH= 1000 (FT)

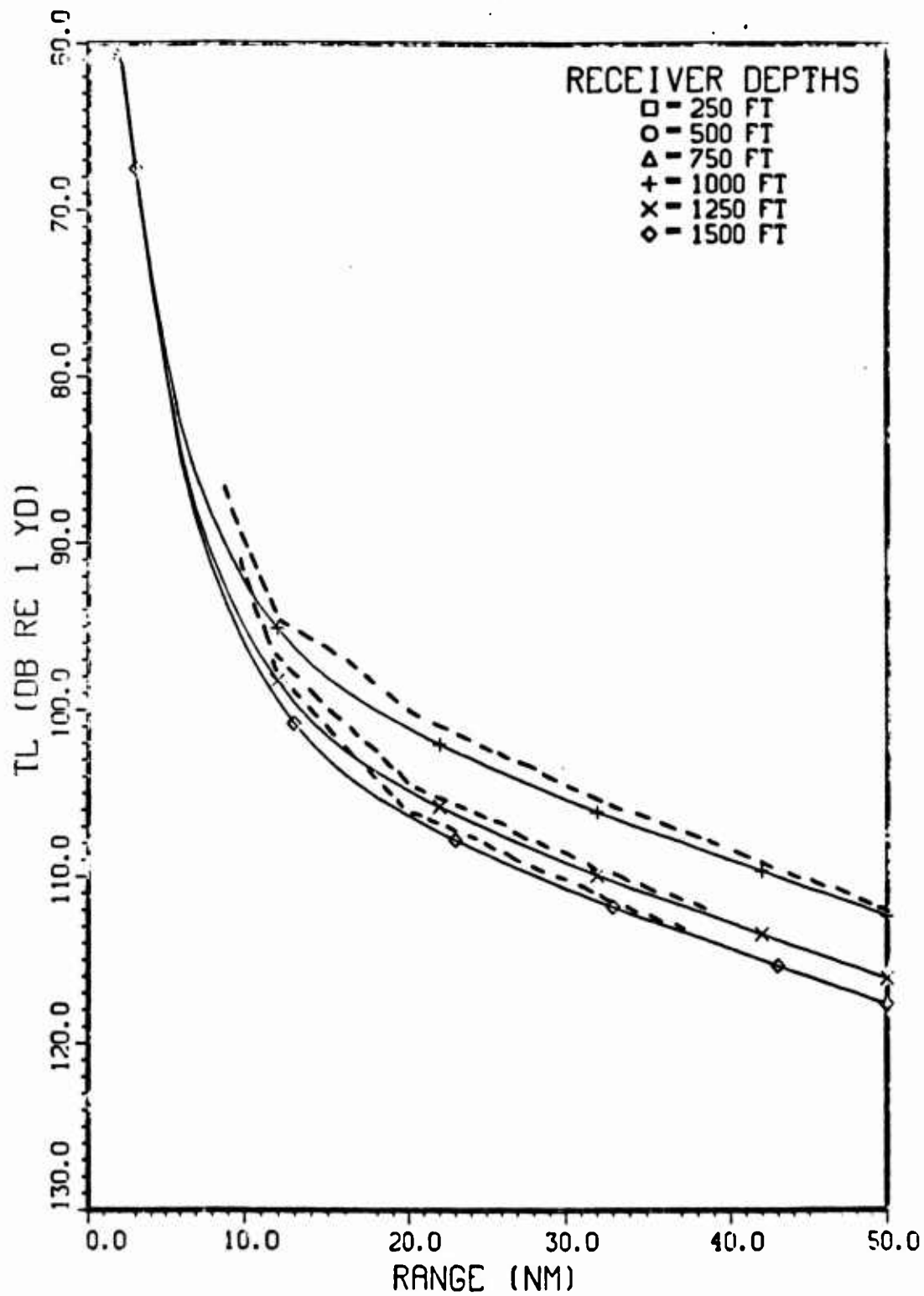


Figure 3-16 . Comparison of Surface-Duct Model (solid) with PE (dash).

SOURCE: FREQUENCY- 100 Hz DEPTH- 1250 (FT)

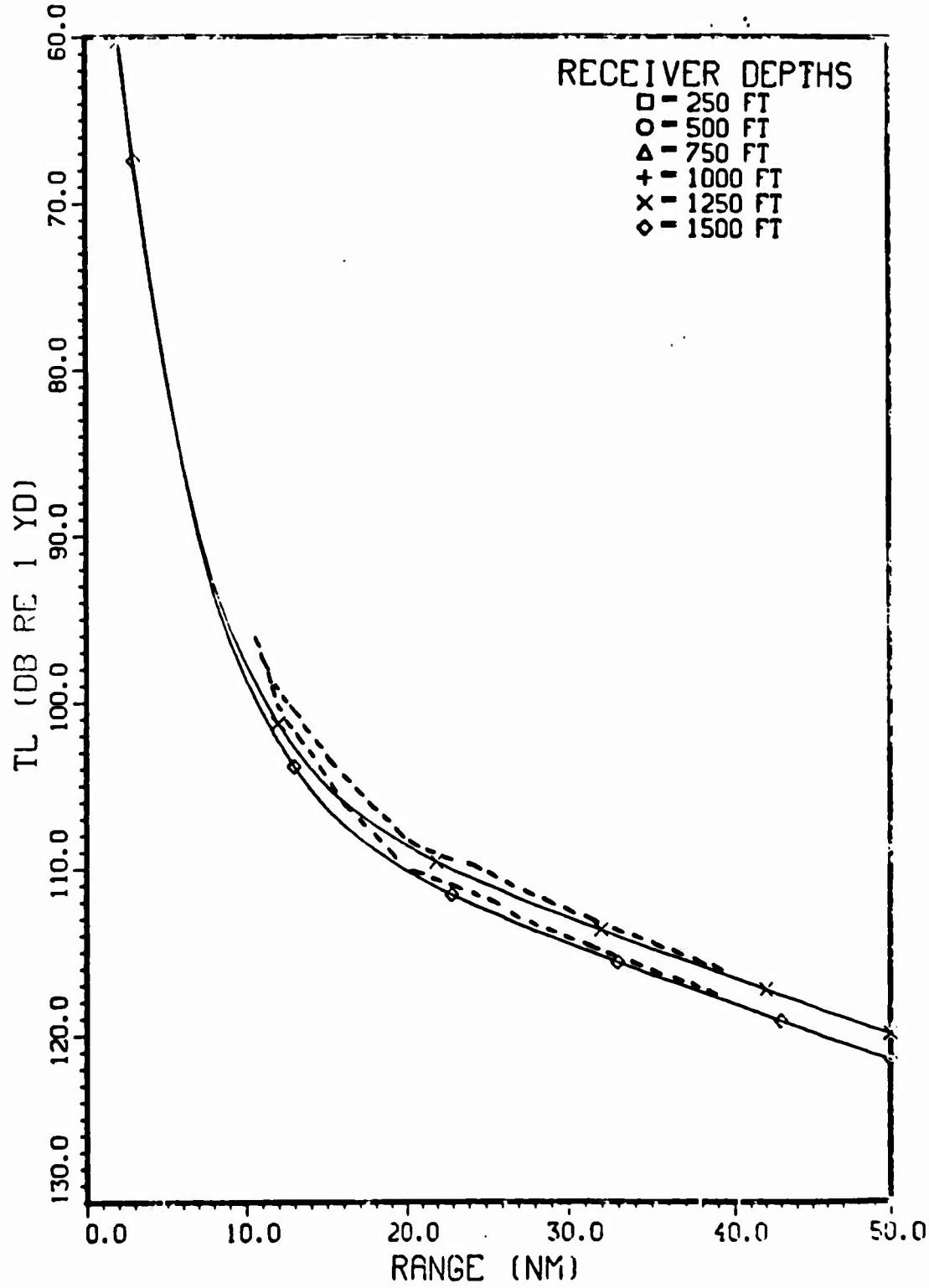


Figure 3-17 . Comparison of Surface-Duct Model (solid) with PE (dash).

SOURCE: FREQUENCY= 100 (HZ) , DEPTH= 1500 (FT)

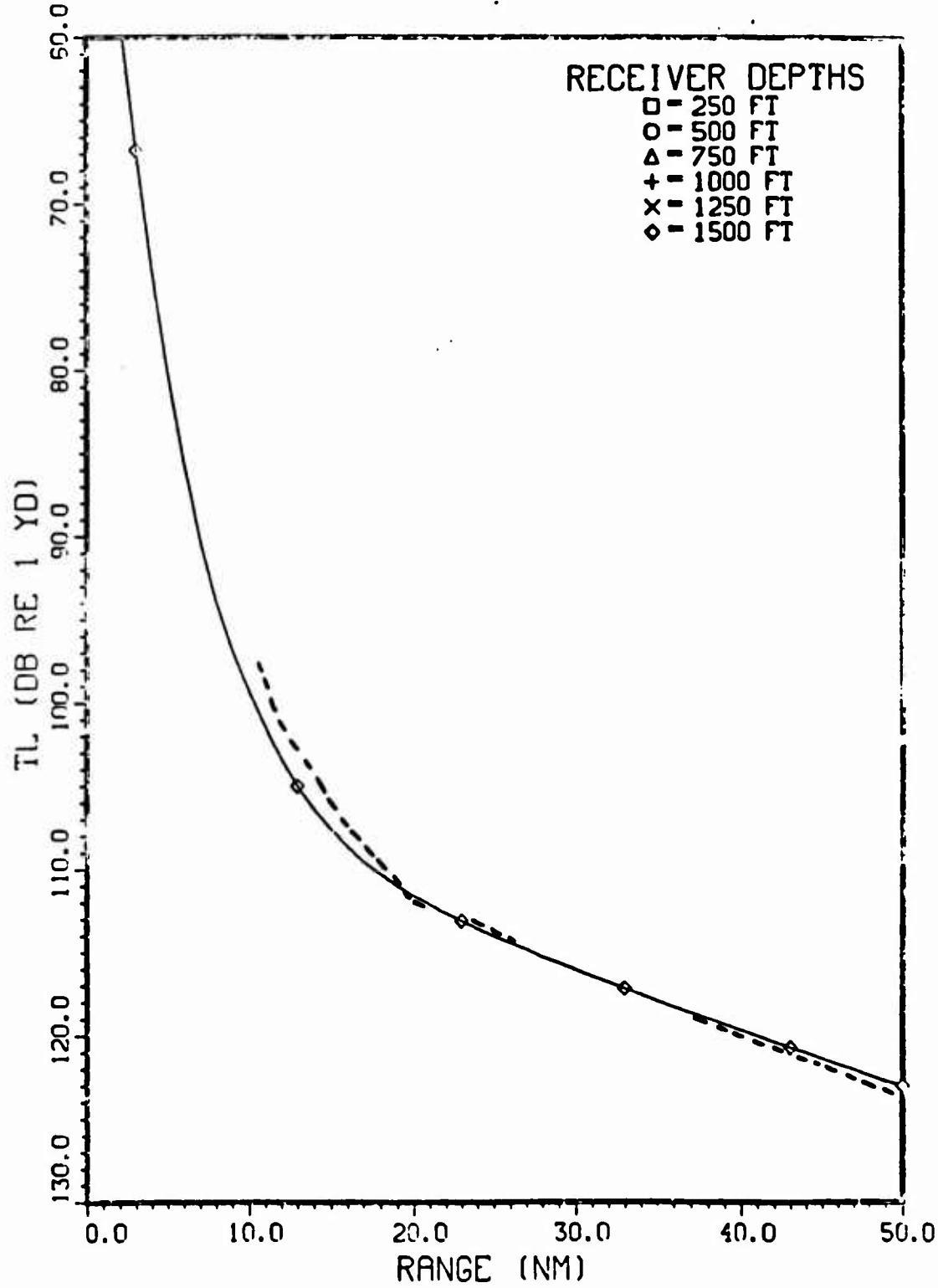


Figure 3-18 .

Comparison of Surface-Duct Model (solid) with PE (dash).

SOURCE: FREQUENCY - 250 (HZ) , DEPTH- 250 (FT)

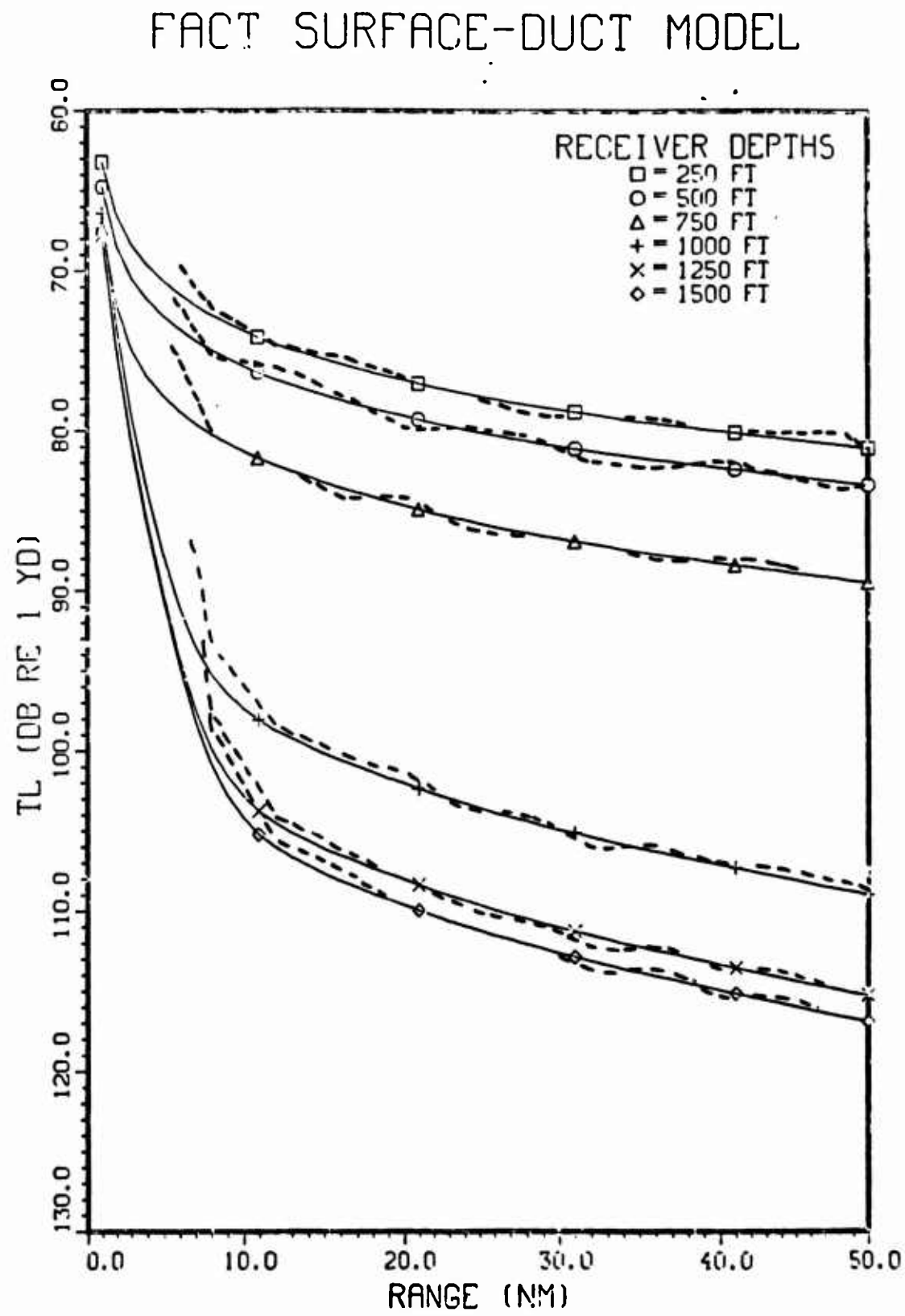


Figure 3-19 . Comparison of Surface-Duct Model (solid) with PE (dashed).

SOURCE: FREQUENCY = 250 (HZ) , DEPTH= 500 (FT)

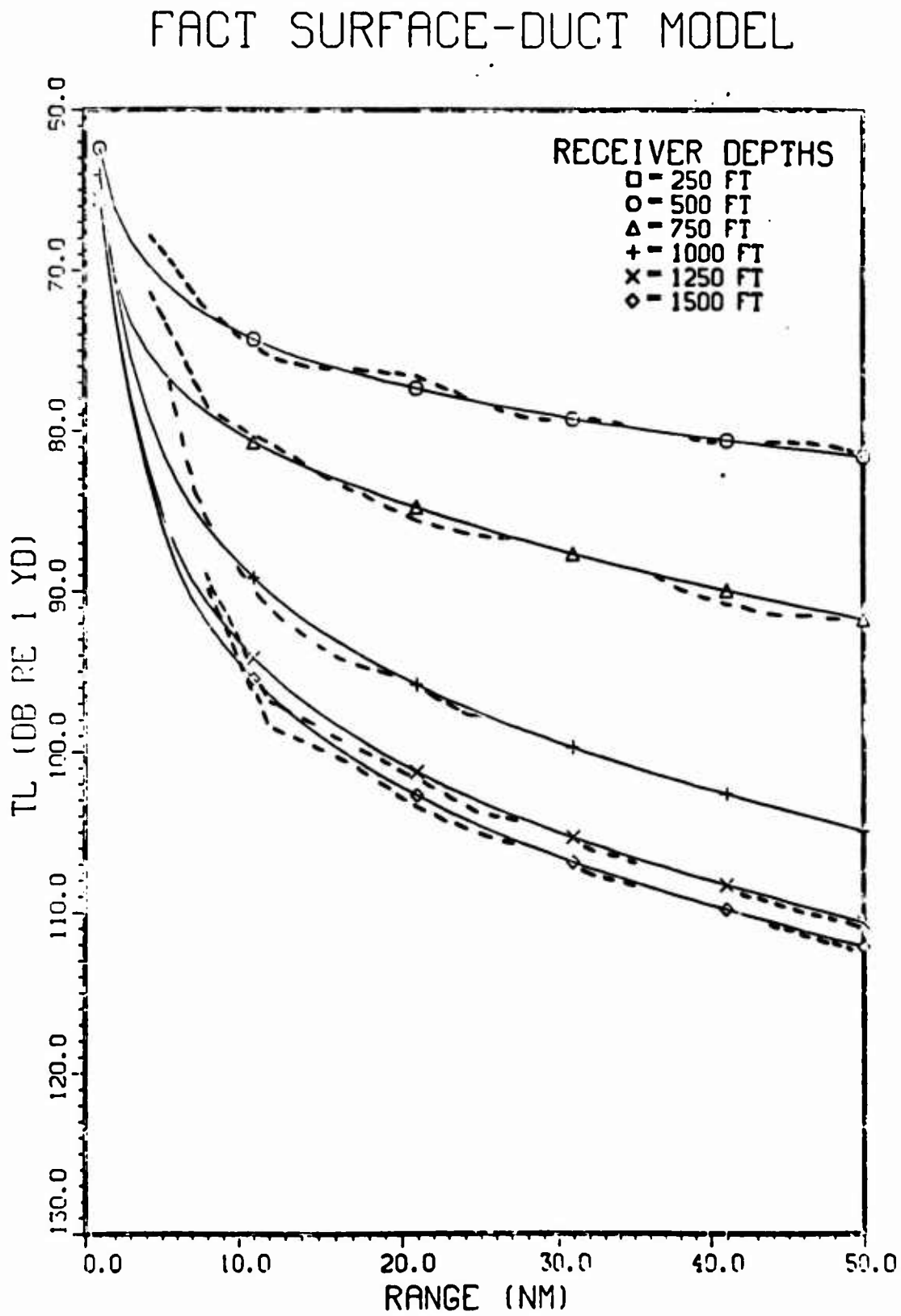


Figure 3-20 . Comparison of Surface-Duct Model (solid) with PC (dashed).

SOURCE: FREQUENCY= 250 (HZ) , DEPTH= 750 (FT)

FACT SURFACE-DUCT MODEL

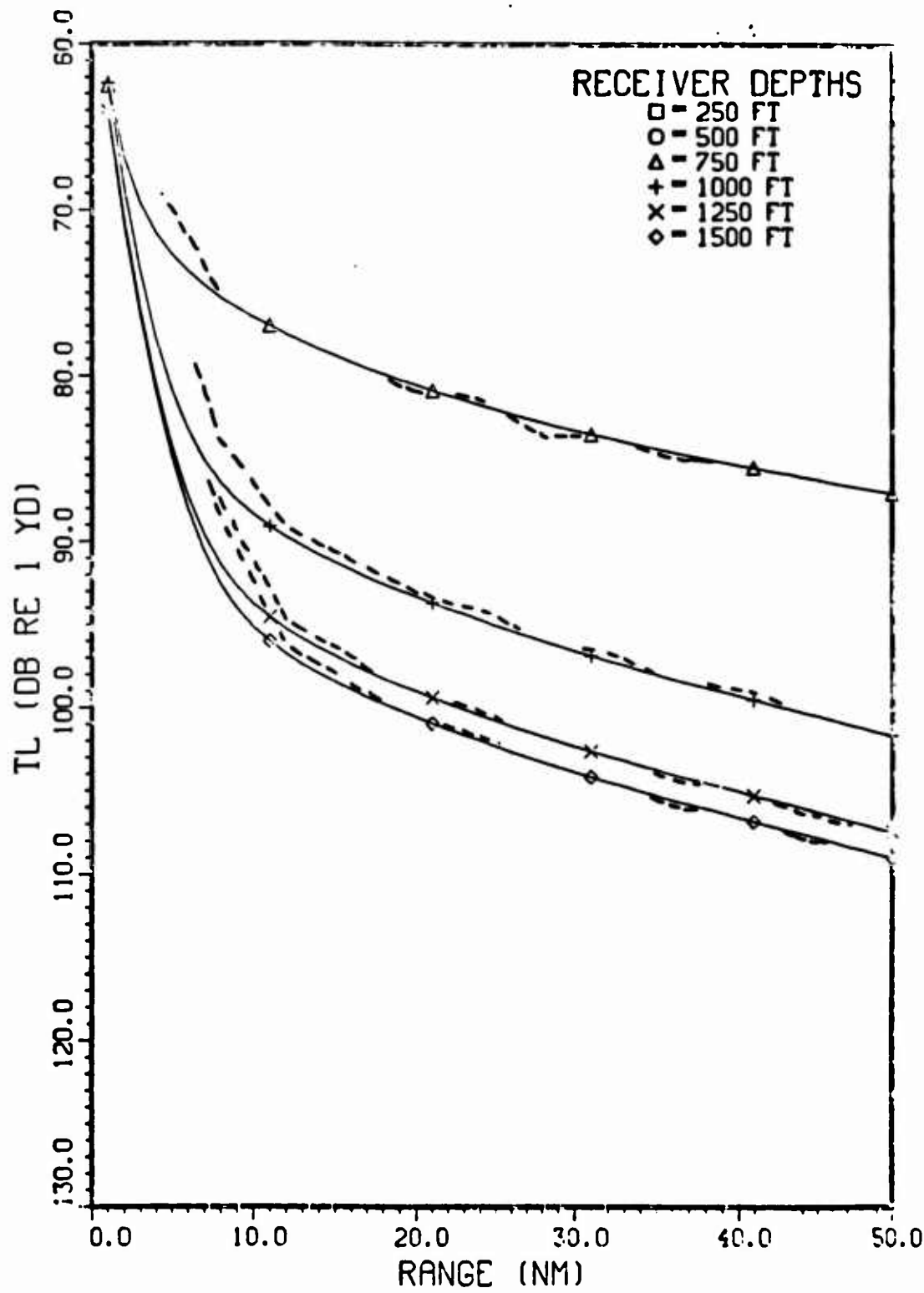


Figure 3-21 . Comparison of Surface-Duct Model (solid) with PE (dashed).

SOURCE: FREQUENCY = 250 (HZ) , DEPTH= 1000 (FT)

FACT SURFACE-DUCT MODEL

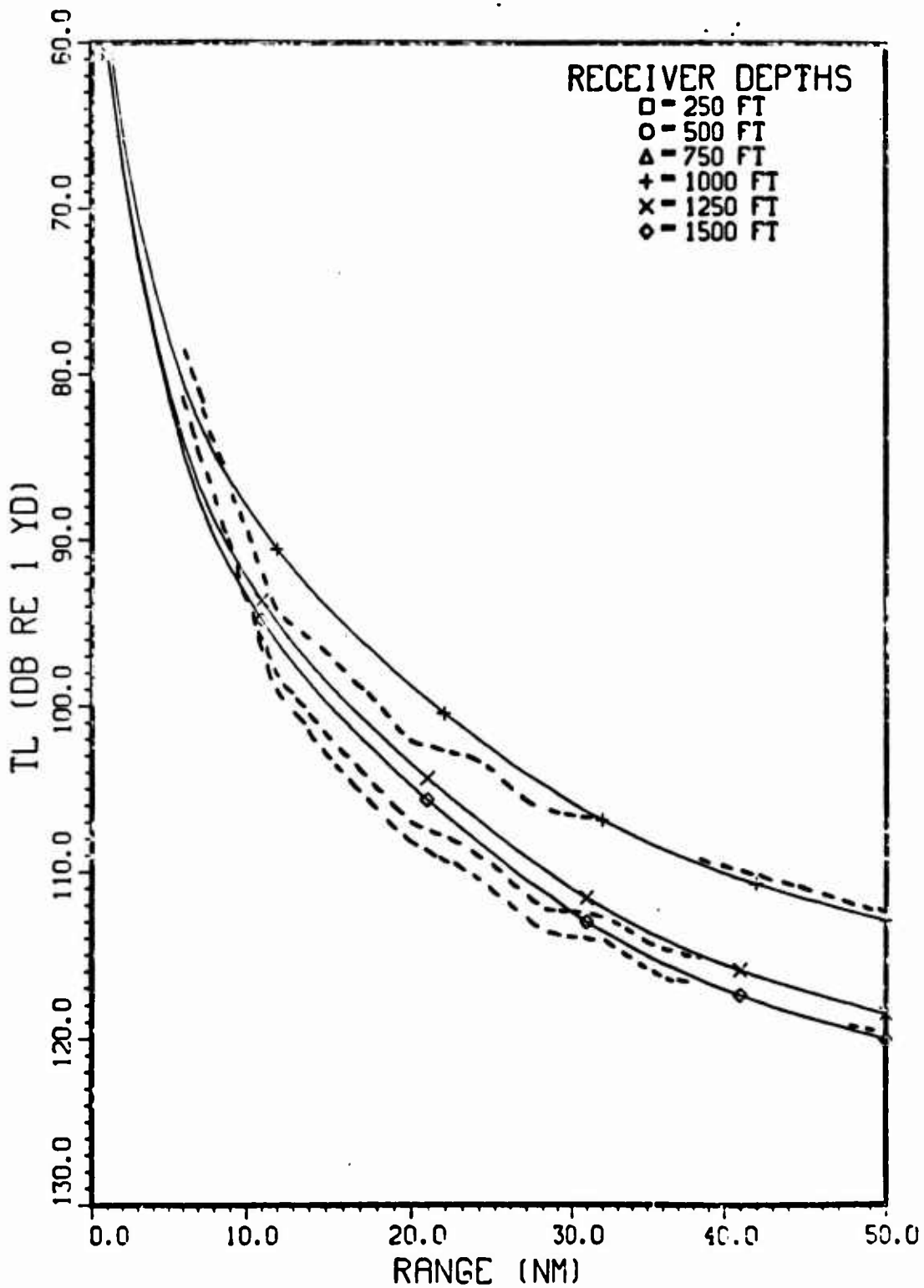


Figure 3-22 . Comparison of Surface-Duct Model (solid) with PE (dash).

SOURCE: FREQUENCY = 250 (HZ) , DEPTH= 1250 (FT)

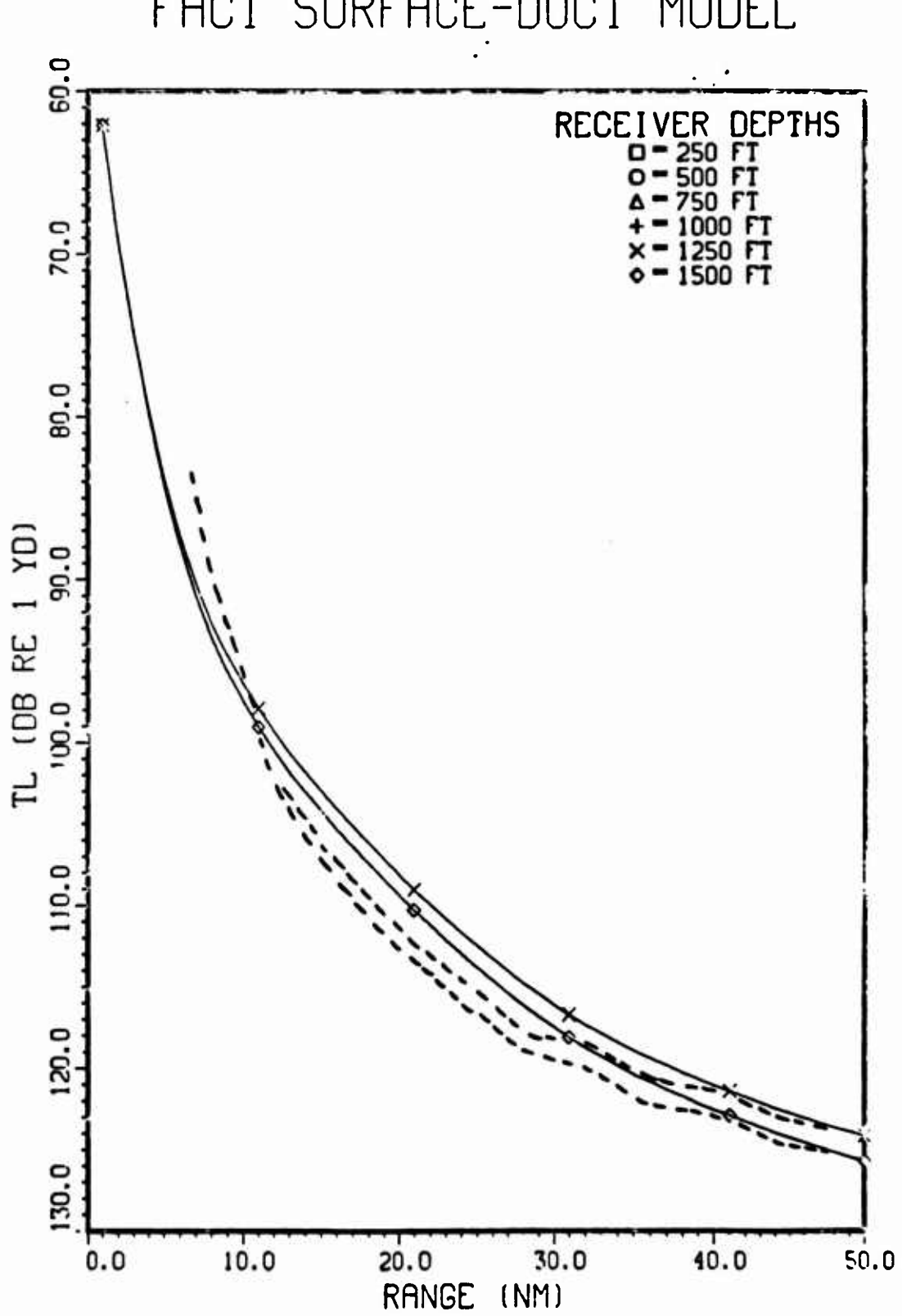


Figure 3-23 . Comparison of Surface-Duct Model (solid) with PE (dash).

FACT SURFACE-DUCT MODEL

SOURCE: FREQUENCY= 250 (HZ) , DEPTH= 1500 (FT)

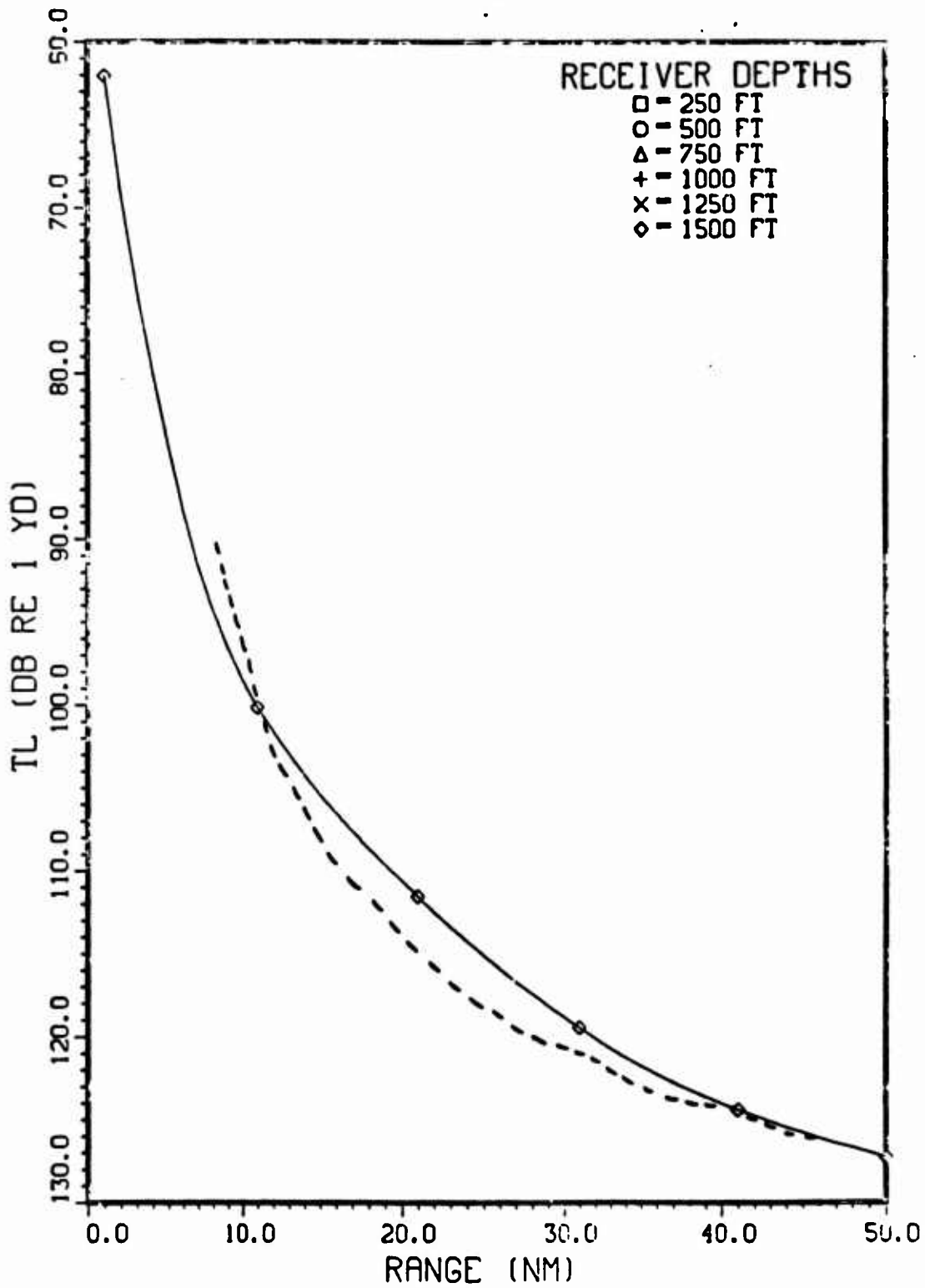


Figure 3-24 . Comparison of Surface-Duct Model (solid) with FE (dash).

SOURCE: FREQUENCY = 500 (HZ) , DEPTH= 250 (FT)

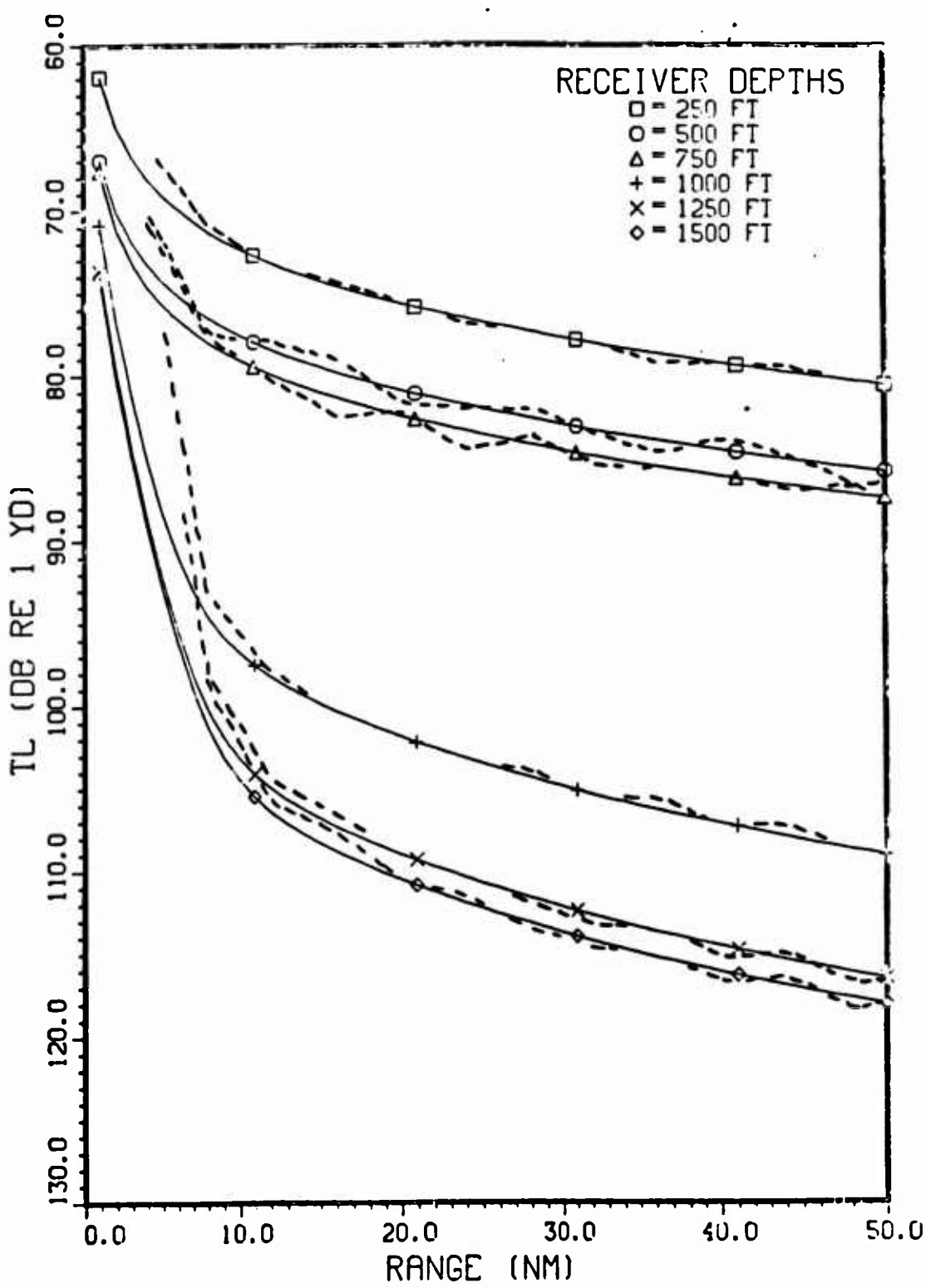


Figure 3-25 . Comparison of Surface-Duct Model (solid) with PC (dash).

SOURCE: FREQUENCY- 500 (HZ) , DEPTH- 500 (FT)

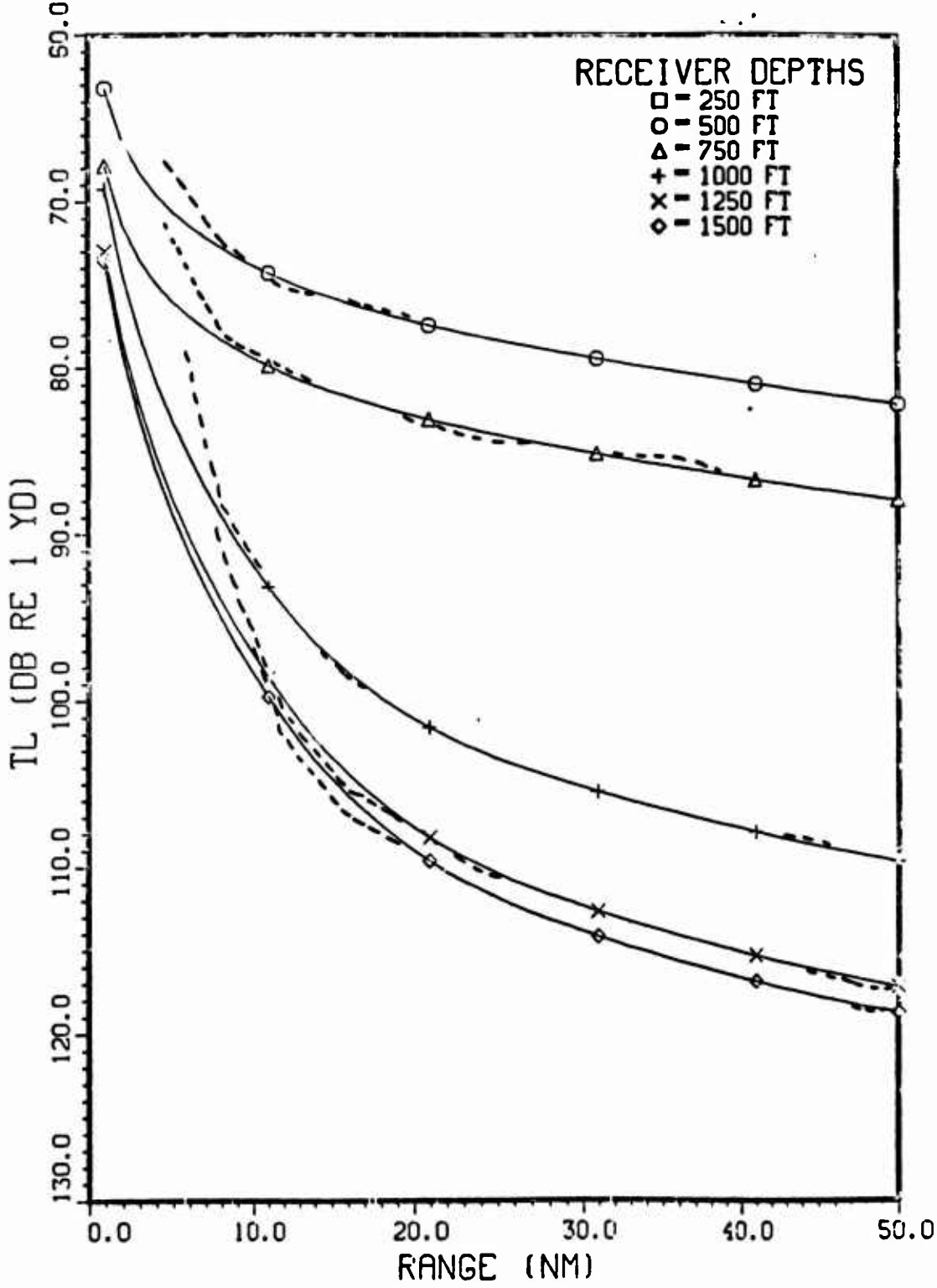


Figure 3-26 . Comparison of Surface-Duct Model (solid) with PE (dash).

SOURCE: FREQUENCY= 500 (HZ) , DEPTH= 750 (FT)

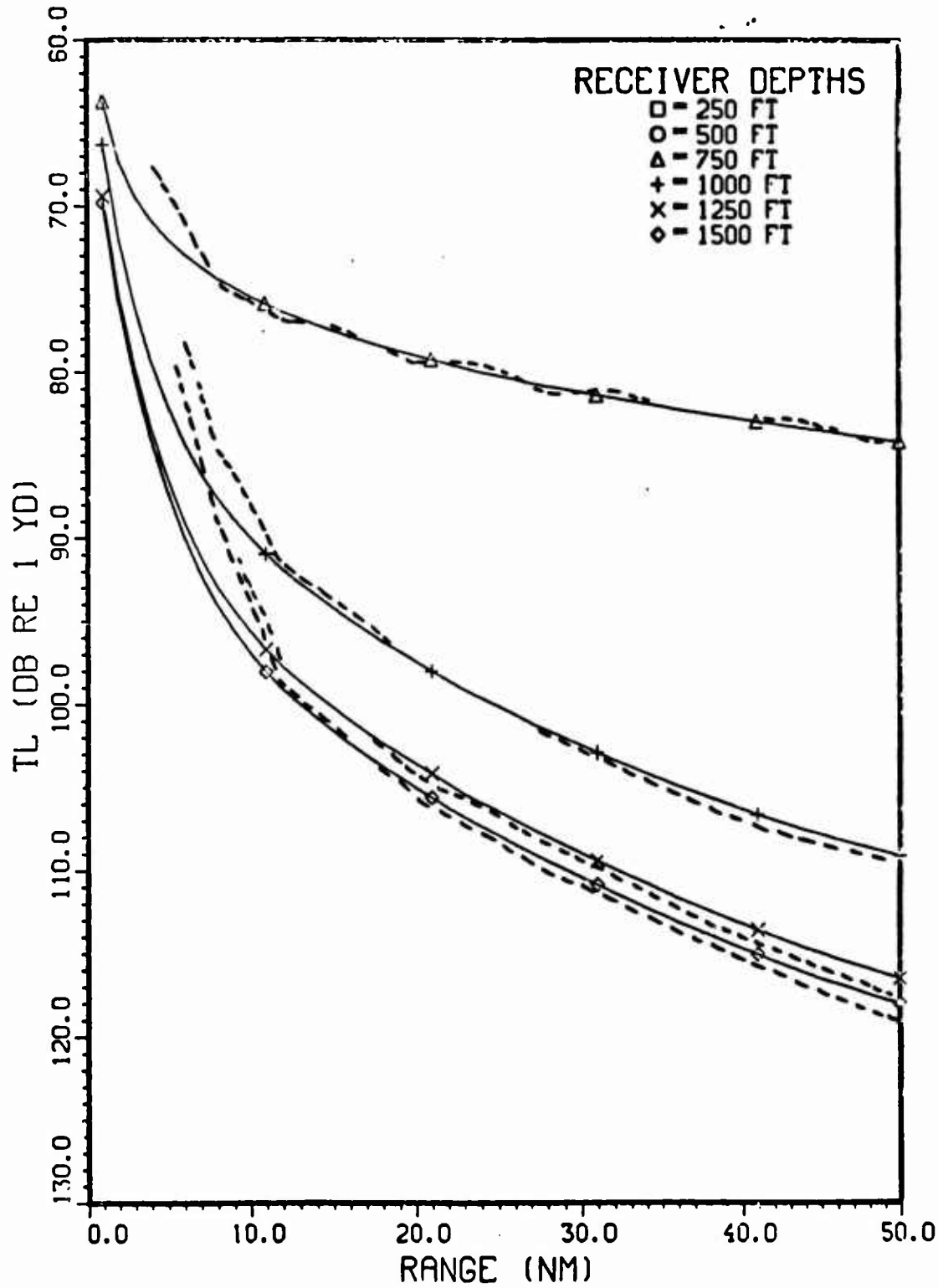


Figure 3-27 . Comparison of Surface-Duct Model (solid) with PE (dash).

PLOT 28 20.10.00 MDO 1 OCT, 1980 , SRI DISSEM VER 8.2

SOURCE: FREQUENCY- 500 (HZ) , DEPTH- 1000 (FT)

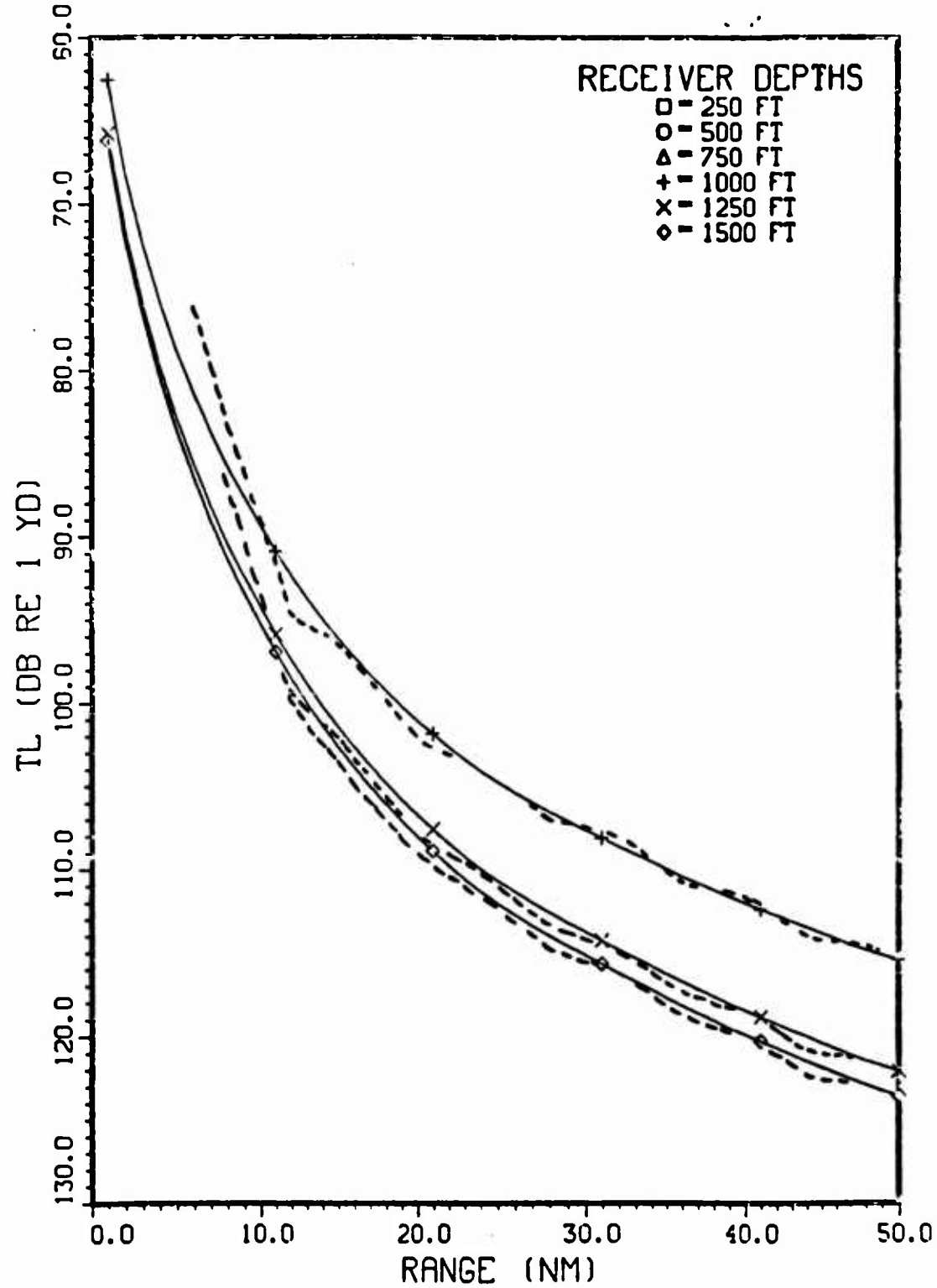


Figure 3-28 .

Comparison of Surface-Duct Model (solid) with FE (dash).

SOURCE: FREQUENCY= 500 (HZ) , DEPTH- 1250 (FT)

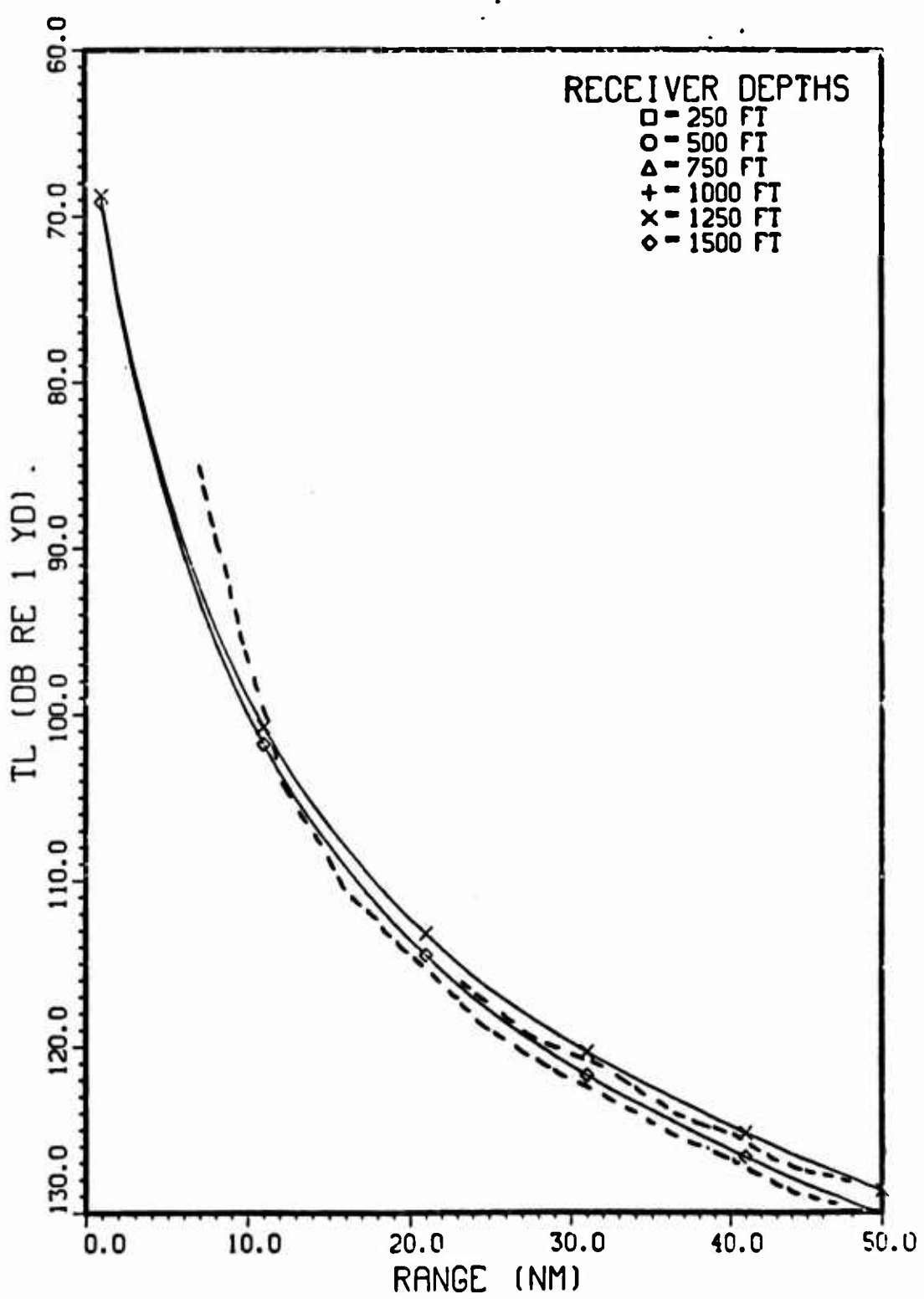


Figure 3-29 . Comparison of Surface-Duct Model (solid) with FE (dashed).

SOURCE: FREQUENCY= 500 (HZ) , DEPTH- 1500 (FT)

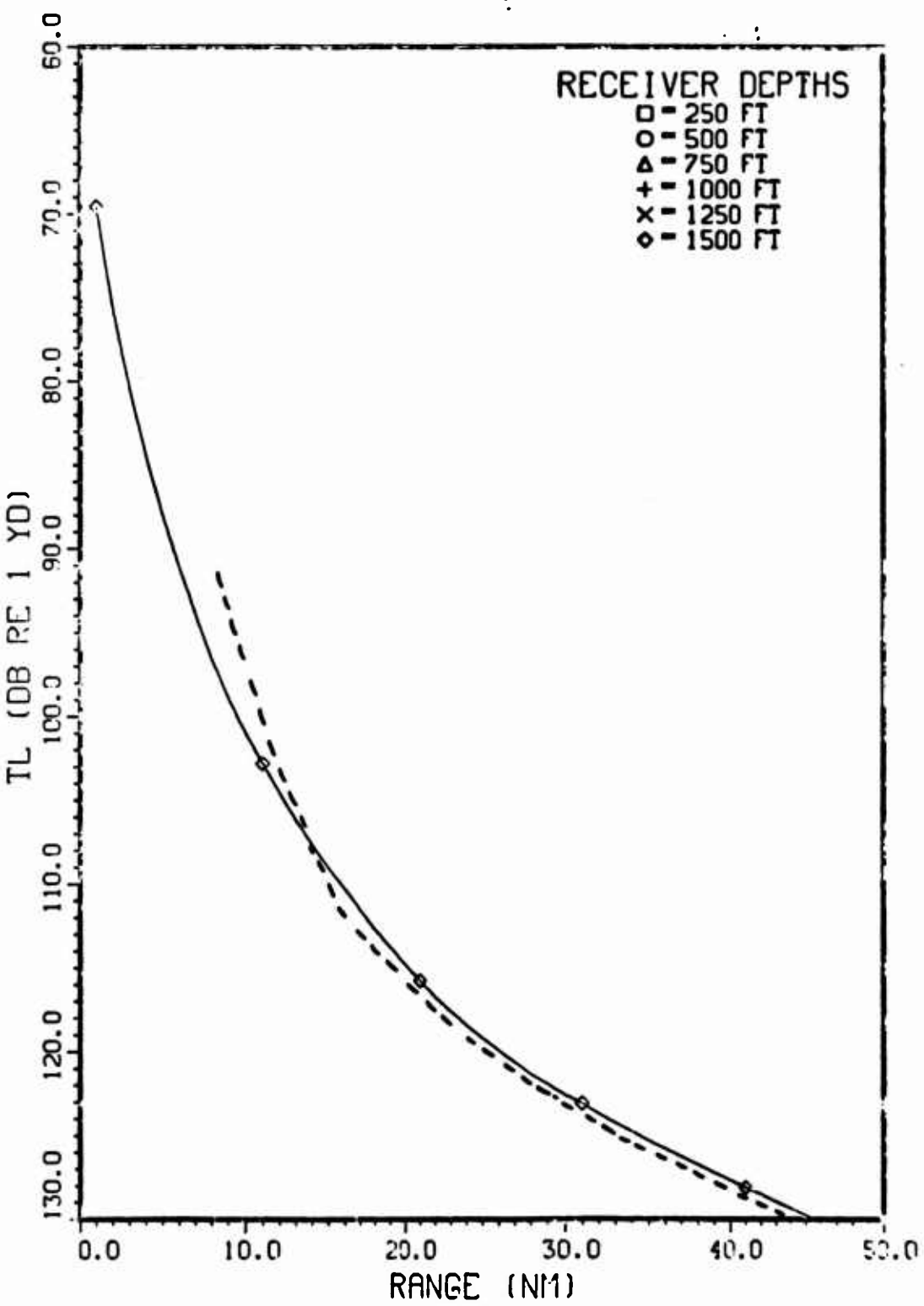


Figure 3-20 .

Comparison of Surface-Duct Model (solid) with FE (dash).

SOURCE: FREQUENCY= 1000 (HZ) , DEPTH= 250 (FT)

FACT SURFACE-DUCT MODEL

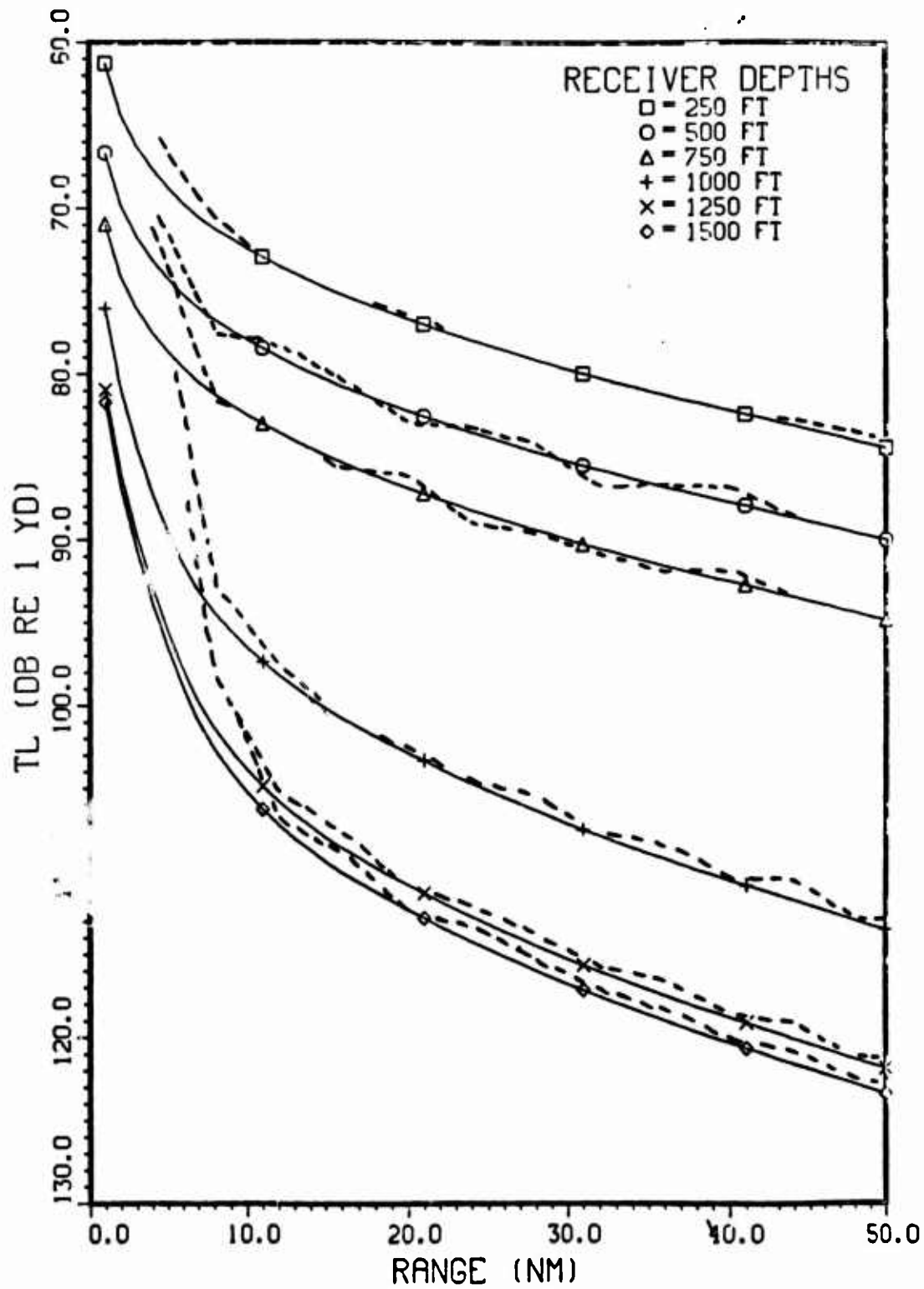


Figure 3-31 . Comparison of Surface-Duct Model (solid) with PE (dash).

FACT SURFACE-DUCT MODEL

SOURCE: FREQUENCY - 1000 (HZ) , DEPTH- 500 (FT)

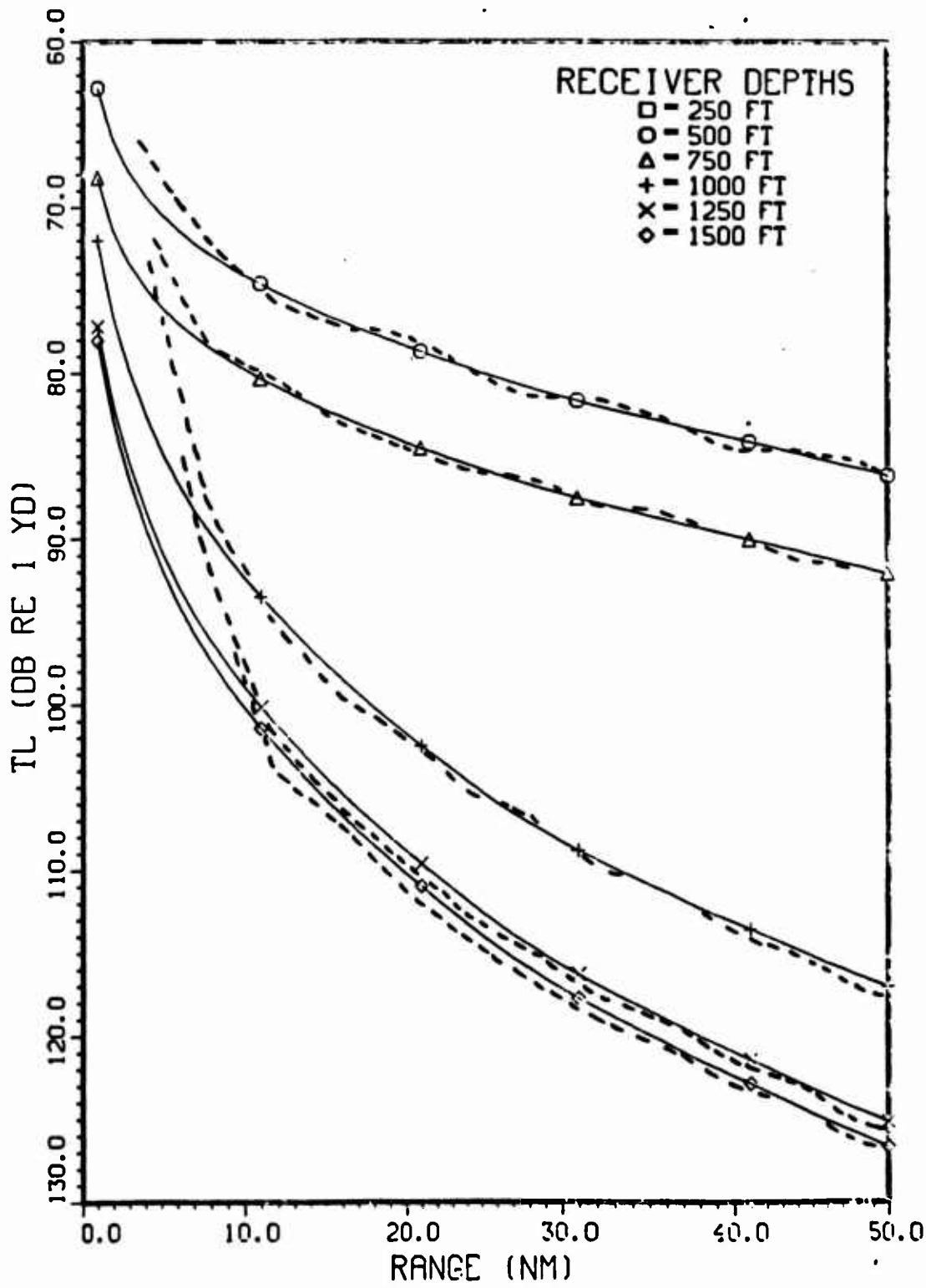


Figure 3-32 . Comparison of Surface-Duct Model (solid) with PC (dash).

FACT SURFACE-DUCT MODEL

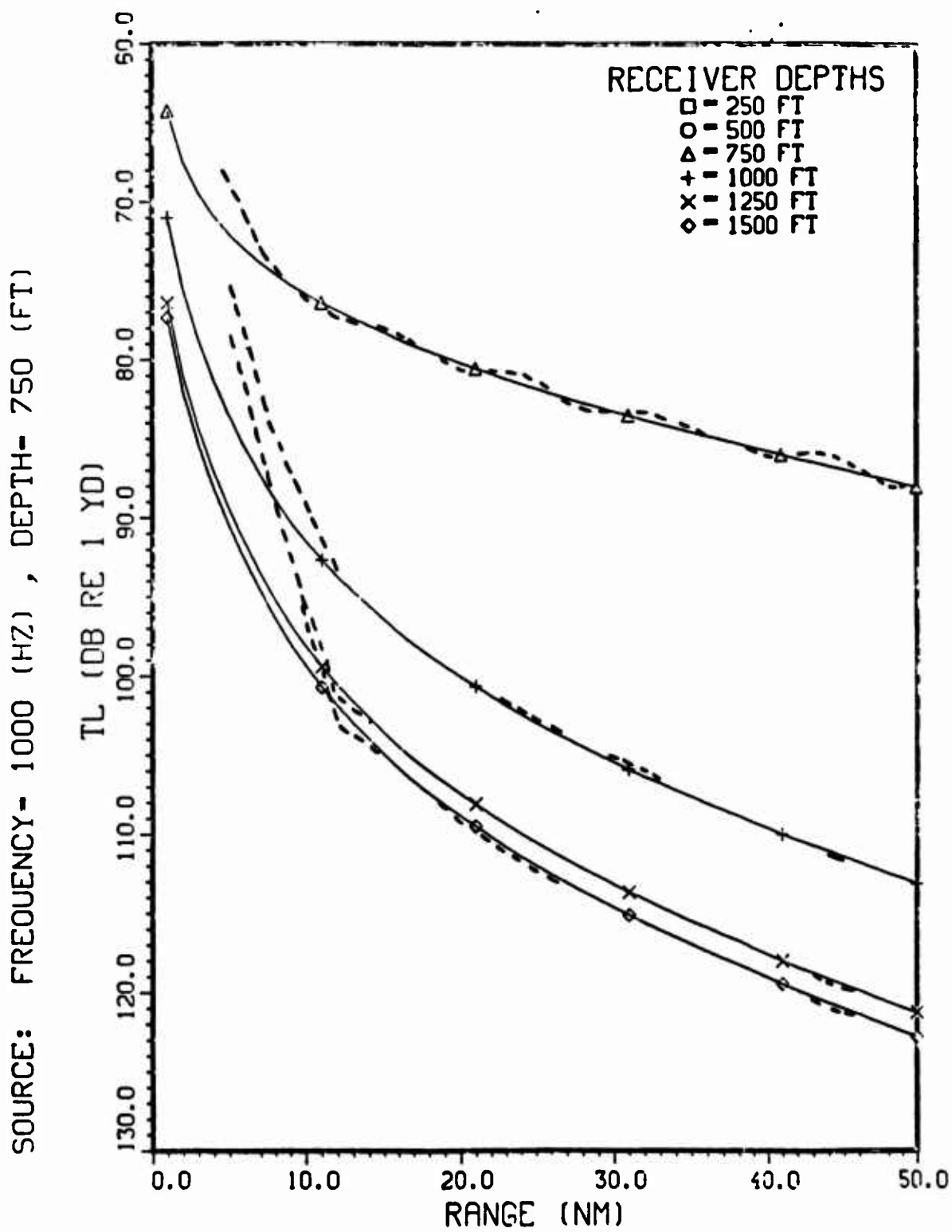


Figure 3-33 . Comparison of Surface-Duct Model (solid) with PC (dash).

SOURCE: FREQUENCY- 1000 (HZ) , DEPTH- 1000 (FT)

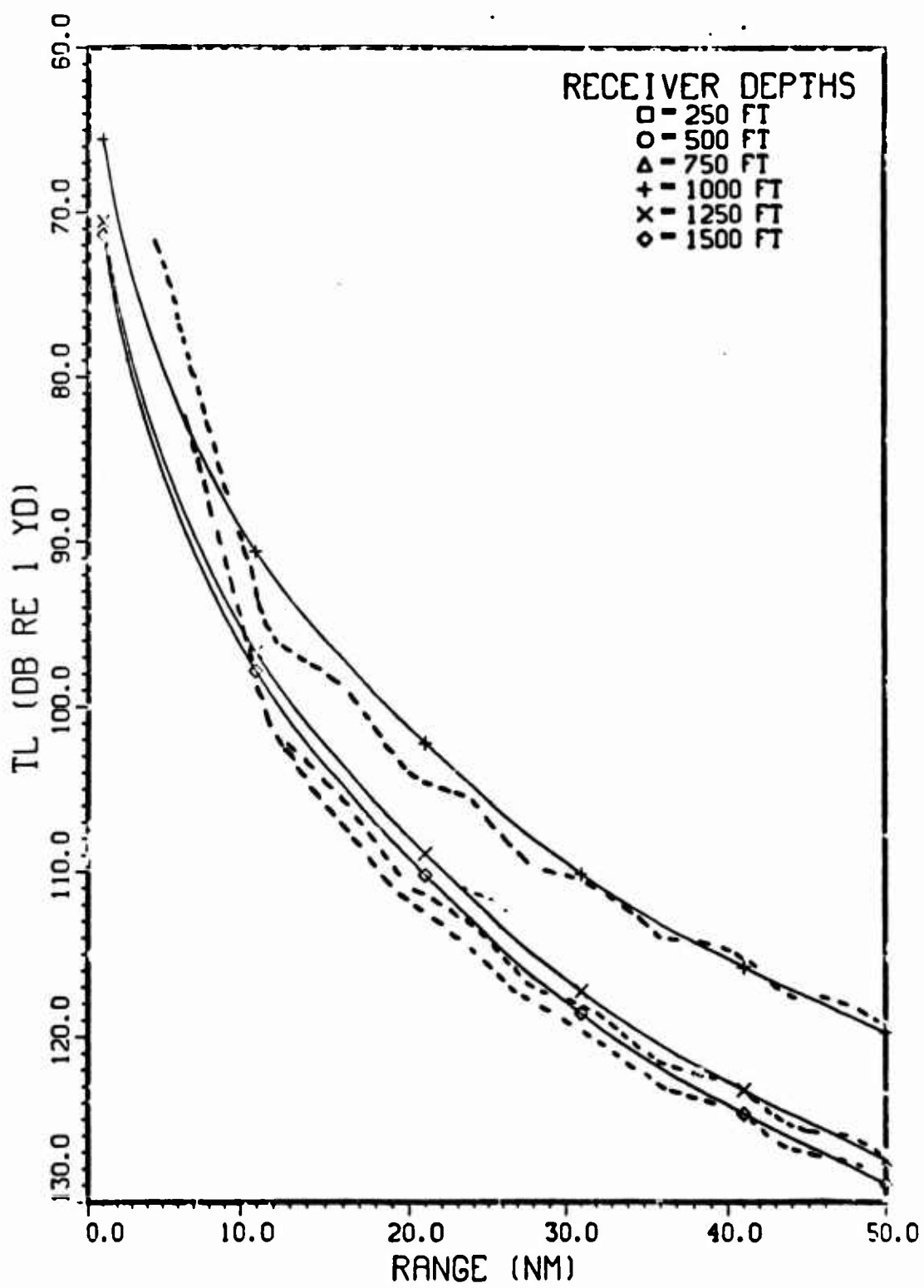


Figure 3-34 . Comparison of Surface-Duct Model (solid) with PE (dash).

SOURCE: FREQUENCY= 1000 (HZ) , DEPTH= 1250 (FT)

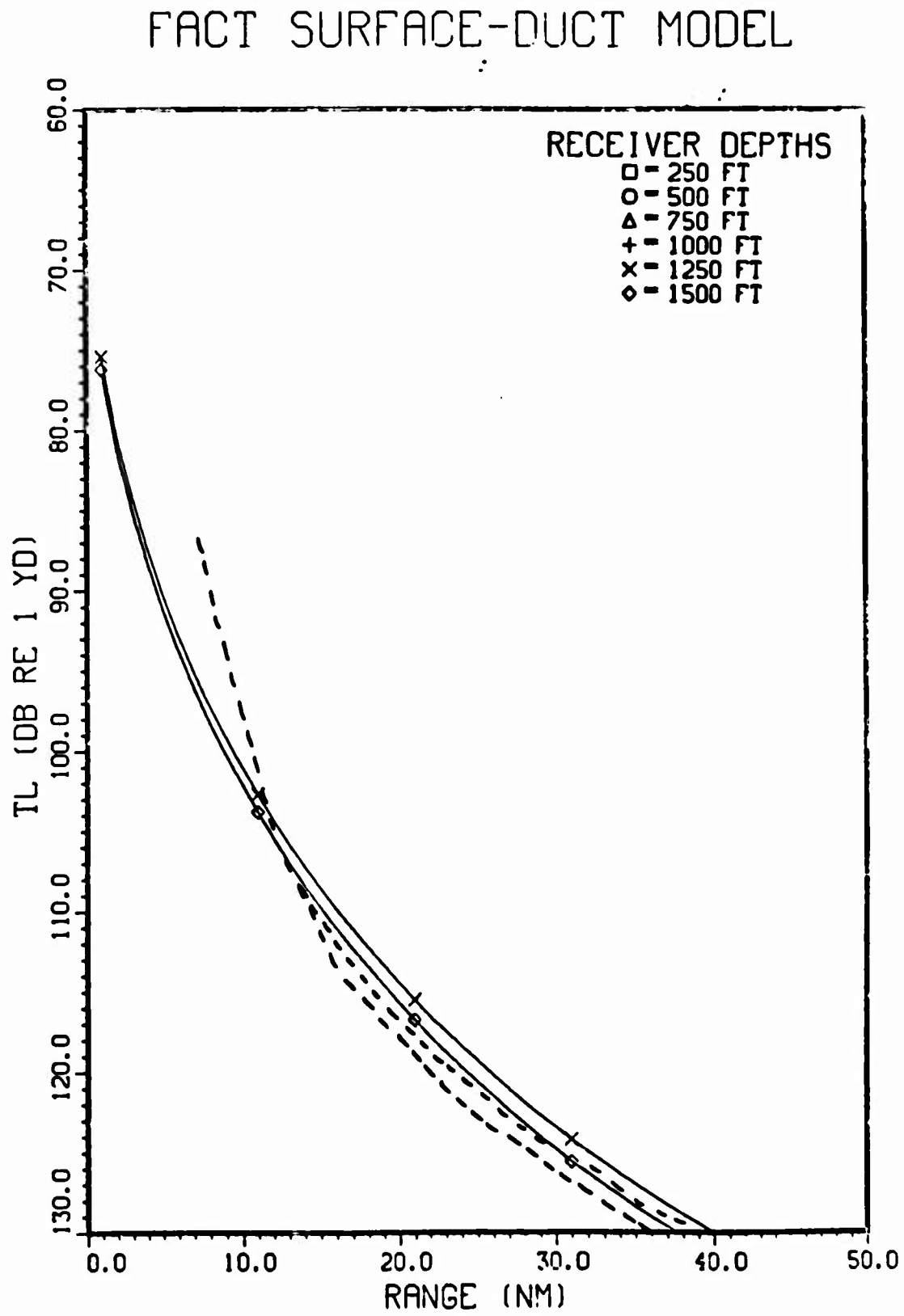


Figure 3-35 . Comparison of Surface-Duct Model (solid) with PE (dash).

SOURCE: FREQUENCY= 1000 (HZ) , DEPTH= 1500 (FT)

FACT SURFACE-DUCT MODEL

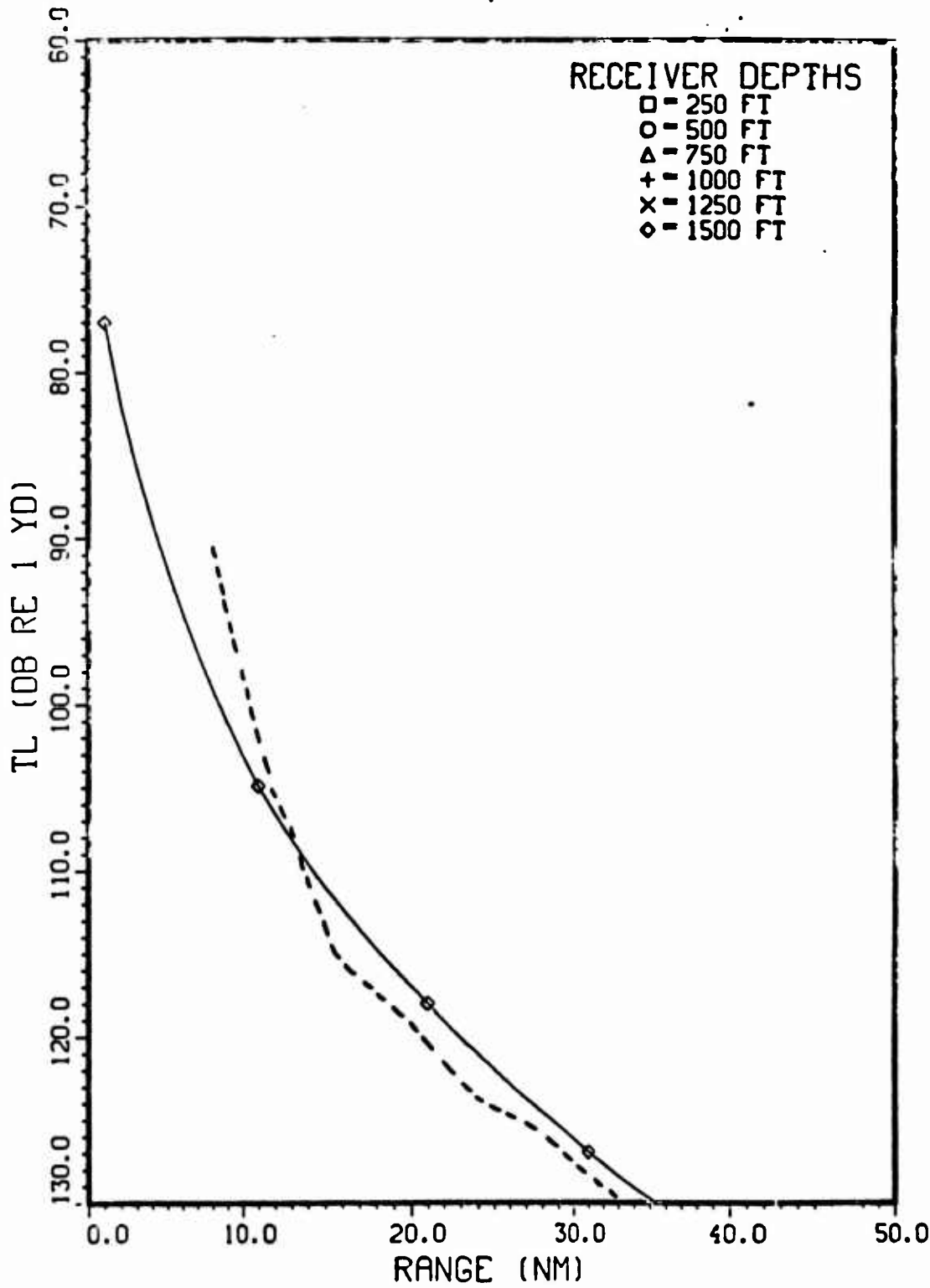


Figure 3-36 . Comparison of Surface-Duct Model (solid) with PE (dash).

3.2 NORMAL MODE COMPARISONS

A more detailed evaluation of the virtual mode surface duct model was made by comparing the predicted modal longitudinal wavenumbers λ_m and intensity amplitudes ψ_m with corresponding values computed using the NOSC n-layer normal mode code. The NM code was run with the same bilinear profile used by the surface duct model and the ocean modeled as infinitely deep. Both models (surface duct and NM) truncated the modal spectrum, hence near field TL values may be in error due to an insufficient number of modes. The imaginary part of λ_m is related to the attenuation coefficient a_m by $a_m = 2 I_m(\lambda_m)$.

The λ_m computed by the virtual mode surface duct model agree quite well with the NM results: relative error in $|I_m(\lambda_m)| \lesssim 10^{-1}$ and $|\text{Re}(\lambda_m)| \lesssim 10^{-4}$. Agreement is better for the trapped modes and gets worse for the strongly leaky waves. However, the strongly leaky modes have large attenuation coefficients and contribute little to the intensity at ranges greater than a few nautical miles.

Intensity amplitudes ψ_m are close to the NM predictions with two exceptions. First, the true ψ_m may exhibit deep nulls which are clipped in the surface duct model. The second exception involves deeply trapped modes where ψ_m is computed within or below the barrier. In the NOSC NM code, numerical difficulties in computing Hankel functions lead to a modification of the bilinear profile. The virtual mode model uses a different formulation of the ψ 's and avoids this problem. Thus computed intensity amplitudes are expected to be lower than those predicted by the NM code. This is in fact observed.

Detailed comparison of λ_m for the surface duct model predictions and the NM code results are provided for 25, 100, and 500 Hz. This corresponds to cases with zero, two, and eleven trapped modes, respectively. The λ_m are shown in Tables (3-1) with values in parenthesis being the NM results.

Table 3-1. Comparison of λ_m (NM results in parenthesis).

<u>Mode</u>	<u>$\text{Re}(\lambda_m)$</u>	<u>$I_m(\lambda_m)$</u>
	<u>$\approx 25 \text{ Hz}$</u>	
1	3.126790 E-2 (3.126250)	3.492409 E-5 (3.778848)
2	3.087473 E-2 (3.097519)	2.877695 E-4 (2.453416)
3	3.015320 E-2 (3.035346)	6.646130 E-4 (6.215050)
	<u>$\approx 100 \text{ Hz}$</u>	
1	.1254460 (.1254452)	3.310623 E-8 (3.177127)
2	.1252816 (.1252807)	4.514341 E-6 (4.761233)
3	.1251256 (.1251152)	3.782473 E-5 (3.949632)
4	.1248763 (.1248825)	1.075746 E-4 (1.041099)
5	.1245431 (.1245658)	1.917165 E-4 (1.856100)
	<u>$\approx 500 \text{ Hz}$</u>	
1	.6279464 (.6279451)	5.030603 E-33 (0.)
2	.6276678 (.6276654)	3.230407 E-27 (0.)
3	.6274396 (.6274364)	8.766610 E-23 (0.)
4	.6272378 (.6272339)	3.685180 E-16 (0.)
5	.6270533 (.6270487)	4.186859 E-14 (3.466829)
6	.6268813 (.6268761)	1.684570 E-13 (1.430650)
7	.6267190 (.6267133)	2.801780 E-11 (2.433916)
8	.6265645 (.6265582)	2.104337 E-9 (1.868979)
9	.6264166 (.6264097)	7.414939 E-8 (6.730201)
10	.6262741 (.6262668)	1.181578 E-6 (1.103277)
11	.6261333 (.6261259)	7.110299 E-6 (7.500457)
12	.6259948 (.6259753)	2.183201 E-5 (2.295352)
13	.6258225 (.6258053)	4.323009 E-5 (4.329292)
14	.6256280 (N/A)	6.543505 E-5 (N/A)

3.3 EVALUATION SUMMARY

The surface-duct model transmission-loss (TL) results were found to be in good agreement with PE and NM computations for a bilinear test case. The virtual mode model predicted the proper frequency dependence of the TL and exhibited excellent performance in predicting the depth dependence of the TL for within-, cross-, and below-layer propagation geometries. Comparison with the NM results shows good agreement for mode attenuation coefficients, giving the proper range decay of intensity.

The execution time of the surface duct model for the 126 scenarios was about 12 CPU seconds on a Digital DEC-10, including loading and I/O. For comparison, a CDC CYBER-76/175, or UNIVAC 1110 are approximately eight (8) times faster than the DEC-10, leading to projected execution times of ~2 seconds - well within the time constraint of the FACT model.

Deviations between model computed TL's and PE results are small (2 - 3 dB max) and generally occur at short ranges. These ranges are within the direct-path regime and can be adequately modeled using ray theory as is presently being done in FACT. Systematic deviations, not related to the surface duct model, are probably present in the PE data arising from the smoother and/or "ghost" bottom reflections. In any event, larger variations in the computed TL are more apt to arise from use of the bilinear approximation to the environmental index of refraction.

SECTION 4

SURFACE DUCT PROGRAM

The virtual mode surface duct model described earlier has been implemented into a FORTRAN program suitable for inclusion into the FACT model. The surface duct program is written in ANSI standard FORTRAN-77, compatible with compilers on CDC, UNIVAC and DEC computers. The surface duct model is designed to operate as a self-contained module needing only environmental specifications and desired propagation scenarios. The virtual mode calculations are automatic and require no initial conditions from the user.

The surface duct code is configured as a main control sub-program, SDUCT, and six ancillary subroutines: TRAPED, LEAKY, SMODE, AIRY, H1SQ, and REFLKT. To facilitate use as a stand-alone module, a separate driver program DRIVER is supplied which automatically calls SDUCT. A FORTRAN source listing of the surface duct model and the stand-alone driver are provided in Appendix B.

User inputs to DRIVER are provided via free-format NAMELIST inputs. The surface duct model is configured to handle up to six frequencies and six distinct source/receiver depths for a total of $6 \times 21 = 126$ distinct transmission-loss scenarios. The surface duct program is capable of using either metric or english units and automatically adjusts outputs accordingly. Transmission-loss (TL) is computed as a function of range, and optional debug flags allow individual modal values of attenuation coefficient α_m and intensity amplitude ψ_m to be printed. A sample execution, corresponding to the deep duct test case used in Section 3, is shown in Appendix C.

SECTION 5

CONCLUSIONS

The virtual mode surface duct model described in this report is proposed as a replacement to the current FACT surface duct model. The virtual mode model was compared with parabolic equations and normal mode calculations for a bilinear duct over a wide range of propagation scenarios and found to be in good agreement with each. The virtual mode model exhibited the proper frequency and depth dependence displayed by the PE code results. Model execution times are well within FACT constraints and no user interaction is required other than environmental inputs and specification of frequency/depth scenarios.

The major limitation of the surface duct model is in approximating the environmental refractive index profile by the Furry model, and future efforts should be directed toward removing this limitation. Additional work in the area of surface loss mechanisms is also warranted.

APPENDIX A

EVALUATION OF $T_+ T_-$

For real arguments, the Airy functions are real valued hence the expressions for T_+ and T_- [Eqs. (2.5)] are complex conjugates of one another and

$$T_+(E)T_-(E) = |T(E)|^2 = \pi |\psi(0, E)h_1(E) - \psi'(0, E)h_1'(E)|^2 .$$

Now $\psi(0, E)$ and $\psi'(0, E)$ are found from Eq. (2.4a) to be

$$\psi(0, E) = \frac{\pi}{s} [Ai(-w)Bi(-q_0) - Ai(-q_0)Bi(-w)] .$$

and

$$\psi'(0, E) = \frac{d\psi(0, E)}{dx} = \pi [Ai'(-w)Bi(-q_0) - Ai(-q_0)Bi'(-w)] .$$

Since w and q_0 are positive for leaky modes, the Airy functions and their derivatives can be expressed in terms of modulus and phase as

$$Ai(-w) = M(w)\cos\theta(w) , \quad Bi(-w) = M(w)\sin\theta(w) ,$$

and

$$Ai'(-w) = N(w)\cos\phi(w) , \quad Bi'(-w) = N(w)\sin\phi(w) ,$$

with similar expressions for $Ai(-q_0)$, $Bi(-q_0)$. Thus

$$\psi(0, E) = \frac{\pi}{s} M(w)M(q_0) \sin[\theta(q_0) - \theta(w)] .$$

and

$$\psi'(0, E) = \pi M(q_0)N(w) \sin[\theta(q_0) - \phi(w)] .$$

The function $h_1(E)$ and its derivative $h'_1(E)$ are

$$h_1(E) = A\phi(-E) - iB\psi(-E) = M(E)e^{-i\theta(E)}$$

and

$$h'_1(E) = -[A\phi'(-E) - iB\psi'(-E)] = -N(E)e^{-i\phi(E)}.$$

Thus the expression for $|T(E)|^2$ becomes

$$\begin{aligned} |T(E)|^2 &= \frac{\pi^3}{s^2} M^2(q_0) \left| sN(w) \sin[\theta(q_0) - \phi(w)] M(E) e^{-i\theta(E)} \right. \\ &\quad \left. + N(w) \sin[\theta(q_0) - \phi(w)] N(E) e^{-i\phi(E)} \right|^2 \end{aligned}$$

with the definitions

$$\beta = N(E)M(w)/sM(E)N(w) ,$$

$$\Delta = \phi(E) - \theta(E) ,$$

$$\delta = \phi(w) - \theta(w) ,$$

$$x = 2\theta(q_0) - \phi(w) - \theta(w) ,$$

and

$$x_{\pm} = (x \pm \delta)/2 .$$

$$|T(E)|^2 = \frac{\pi^3}{s^2} M^2(q_0) M^2(E) N^2(w) G^2(E)$$

where

$$G^2(E) = \beta^2 \sin^2(x_+) + \sin^2 x_- + 2\beta \sin x_+ \sin x_- \cos \Delta .$$

APPENDIX B
SURFACE-DUCT PROGRAM LISTING

The following is a FORTRAN listing of the virtual mode surface program and stand-alone driver.

IF SO, ALL MUSCULAR PAINS CONSIDERED WITH NO ARP

RESULTS OF DISTINCT SENSE RECEIVED NEPTUS (MAX 4) AND OF RAISE POLYNS SINU CALCULATION (MAX 50)

Concordia! Concordia! Concordia! Concordia!

כ'..... יונתן אט ווינטן

• **DE** → **DEUTSCHE PFERD**, **DEUTSCHE PFERD**
• **DE** → **DEUTSCHE PFERD**, **DEUTSCHE PFERD**

8.9.15 IN CHARGE OF THE DRAKE 1 FT TO THE RE 1 YD.

PRIVACY AND INFORMATION SECURITY IN THE FINANCIAL SERVICES INDUSTRY

ପାତାମେଲେ କେବଳ ଏହି ଦିନ

.....

मात्रा विद्या के अनुसार इन शब्दों का अर्थ है-

መ/ቤትና ማረጋገጫ በት/ሮ/የግብር/ንግድ/ንግድ

مودودی، احمد (۱۹۳۰-۱۹۷۵)،
بیوگرافی، دانشگاه علام حنفیہ، ۱۹۷۶

AND IN HAVING THEREFORE CHARGE DILECTIONS OF FOLIATION ARRAYS
IF INFLUENT VARIATIONS OCCUR.

卷之三

STRUCTURE: **STRUCTURE** IS THE WAY A SYSTEM ALLOWS CAPABILITY FOR VIRTUAL MODE CONTROL SURROUNDED -STRUCT-

LA JUNIOR, C.A.
SOCIETE AMERICANA, INC.
ACCIDENT INSURANCE
COMPANY

STATION-ALIVE DRIVE FESTA 2010FACE HUCHI MODEL

JOURNAL OF POLYMER SCIENCE: PART A-1

PAGE 1

CAIRI SURVEY OF THE 2007-08 HABITAT PREDILECTION INDEX

CONCLUDING REMARKS

卷之三

四庫全書

卷之三

THE JOURNAL OF CLIMATE

CAMBRIDGE UNIVERSITY PRESS

卷之三

-3

卷之三

فیصلہ

THE SILENT COMPILER IS A PROGRAM WHICH TAKES A SOURCE PROGRAM AS INPUT AND PRODUCES AN OBJECT PROGRAM AS OUTPUT.

ବ୍ୟାକ ପିଲାରୀ

13. *Wetland Management* 1/2
14. *Wetland Management* 1 AND 111. *Wetland Management* 15, 16

PLATES FROM THE EDITIONS OF THE MAF.

BIBLIOGRAPHY OF THE BIBLICAL STUDIES OF J. C. RABBIK

HISTORICAL AND CRITICAL STUDIES OF THE BIBLE

INPUT

100

卷之三

כטנו וארנו כמי ונתנו שנותנו

卷之三

PNT 0.7 700 FPT.1(17), MAY 1971, COMM-F

2161 1 100000 2161
2162 1 100000 2162
2163 1 100000 2163
2164 1 100000 2164
2165 1 100000 2165
2166 1 100000 2166
2167 1 100000 2167
2168 1 100000 2168
2169 1 100000 2169
2170 1 100000 2170
2171 1 100000 2171
2172 1 100000 2172
2173 1 100000 2173
2174 1 100000 2174
2175 1 100000 2175
2176 1 100000 2176
2177 1 100000 2177
2178 1 100000 2178
2179 1 100000 2179
2180 1 100000 2180
2181 1 100000 2181
2182 1 100000 2182
2183 1 100000 2183
2184 1 100000 2184
2185 1 100000 2185
2186 1 100000 2186
2187 1 100000 2187
2188 1 100000 2188
2189 1 100000 2189
2190 1 100000 2190
2191 1 100000 2191
2192 1 100000 2192
2193 1 100000 2193
2194 1 100000 2194
2195 1 100000 2195
2196 1 100000 2196
2197 1 100000 2197
2198 1 100000 2198
2199 1 100000 2199
2200 1 100000 2200

REF ID: A3A6021 / #1 2-00CT-40 PAGE 103

REF ID: A3A6021 / #1 2-00CT-40 PAGE 103

SOLICIT

PROPOSAL NO. 5216311 / XI 22-SPR-00 PAGE 1-3

STRUCTURAL MORTAR V-SAR6211 10043 22-SEPT-90 PAGE 1-3

لـ $\Delta_{\text{أدنى}} = \left(\frac{\Delta_{\text{أدنى}}}{\Delta_{\text{أدنى}}} \right) \cdot 100$ وـ $\Delta_{\text{أعلى}} = \left(\frac{\Delta_{\text{أعلى}}}{\Delta_{\text{أدنى}}} \right) \cdot 100$
 مـ $\Delta_{\text{أدنى}} = \left(\frac{\Delta_{\text{أدنى}}}{\Delta_{\text{أدنى}}} - 1 \right) \cdot 100$ وـ $\Delta_{\text{أعلى}} = \left(\frac{\Delta_{\text{أعلى}}}{\Delta_{\text{أدنى}}} - 1 \right) \cdot 100$

COUNTY FORTY-NINE MILLFIRTH ARCLF (RMUNIS) AT SURFACE

卷之三

印譜一編卷之三

卷之三

ECONOMETRIC METHODS / 1000

卷之三

THE JOURNAL OF CLIMATE

THE JOURNAL OF CLIMATE VOL. 14, NO. 10, OCTOBER 2001

REAL TESTS.

卷之三

THE JOURNAL OF PRACTICAL THEOLOGY

SIRIACAE EPIGRAPHEE CESTE DOCUMENT IS COMPTEED IN SIRIACUM. 21031.

THE JOURNAL OF CLIMATE

ALPHABET OF ALPINE AS

OPTIMAL CONTROL PROBLEMS

XII. - 10/2011

```

00226      742 PUPART(10(2),74) = 0.0
00227      1   5X, "2, "11X, "10X, "QR, "12X, "9X, "3M002, "6X, "PSI1, "6X,
00228      2   7M44/PSI0,7Y, "U030, "6Y, "PRESSURE, /
00229      X=40
00230      U7=2, "2U/PFLN12(N7)
00231      U7=0.75/4
00232      T=-7.0/5H
00233      U7 250 IX=1, NY
00234      X=Y=0.7
00235      P=S0KTPS+SO4*(CHRDE(CHR2, Y,-ln(2)))
00236      WRITE(1U(2),74C) P
00237      PUPART(1M+, 05Y, 10E13, 5)
00238      250 CONTINUE
00239      C
00240      C COMPUTE INTENSITY AMPLITUDES AT PIELD DEPTHS - m-
00241      C 255 N7 260 IZ1,N0
00242      PSIC(I)=SMONER(N7D7, X0(I), 10(2))
00243      260 CONTINUE
00244      C
00245      C NOV PUPA MIMAL AMPLITUDES & PUP EACH SOURCE/RECEIVER P PAIR
00246      C
00247      N7 270 I=1,7P
00248      I5=0E0W1F((I)) A10
00249      IR=PPEW1F((I))-10*15
00250      AWP(NU0D7,I)=WAWLWMP5((IS))OPS1(IP)
00251      I=(nEQUIC) WAFTR((IC(1),265)) IR,PERWT((I),IS,IR,PSI1(S)),PSI1(IR),
00252      1
00253      265 PUP-AUT- Intensity at point I and ITUDRS...IP,PPRMNT,IS,IR=*,413, - OSIS,PSIR
00254      1AMP=*,3(10F13.6)
00255      270 CONTINUE
00256      200 CONTINUE
00257      C
00258      C
00259      C***** BLOCK 41 *****
00260      C COMPUTE RELATIVE INTENSITY L
00261      C IF VTFOR UNITS IN USE, INTENSITY RELATIVE TO
00262      C POINT SOURCE AT 1 METER. IF ENGLISH UNITS USED,
00263      C INTENSITY RELATIVE TO POINT SOURCE AT 1 FOOT.
00264      C
00265      RANGE=0.
00266      U7 500 IR=1,MRNGC
00267      PANGC= RAIHF+F+DELTAR
00268      N7 440 IP=1,MP
00269      S1=0
00270      N7 450 "0D2=1,M4R0E3
00271      AWP((4M12, 1P)=AWP((4M12, 1P))
00272      S1=S1+SWAWP((4M12, 1P))
00273      450 CONTINUE
00274      C
00275      RFLIMIT((IR,IP,IP))= SUM/RANGE
00276      440 CMYFL4U5
00277      500 CMYFL4U5
00278      1000 CMYFL4U5
00279      RETURN
00280      END

```

SOMCET IN ENRICHED DETECTORS

• 90001 2205

त्रिलोकीय

SUPERPROGRAM CALLUP

SONG	PIRAL.	LEAKY	SPT.	TRAPPED	C99P.	AWAR.	M INO.	A10C.
ADASIN.	PIRAT.	EXP.						

common names

SAR 9721 - 22-5566-0 Page 1-5

B-14

નાગરિક

• 19014 114 : 90000 117 : 900001 120 : 900002 121

四庫全書

卷之三

卷之三

۱

SCILLARIA

卷之三

• 8

५८

CONCEPTS

P-510 47

卷之三

卷之三

```

00001 C SUBROUTINE LEAKY(MODE, IO1, REALM)
00002 C COMPUTES PARAMETERS ASSOCIATED WITH LEAKY MODES.
00003 C ENERGY - EM-. DECAY COEFFICIENT -ALPHAH-. AND
00004 C RAY EQUIVALENT PERIOD -RH-.
00005 C *****
00006 C
00007 C *****
00008 C
00009 C DIMENSION REALM( 1 )
00010 C INTEGER ERROR
00011 C COMPLEX EM,Z,J6Z,A,A2,Z2,DE,U02,DZETA,DQ,ZETA0,E0,R0,V,DRD
00012 C REAL KO,KOI,MM
00013 C LOGICAL DEBUG
00014 C COMMON/DUCT/S,S2,S3,KOH,S3D,D,CPLUS,CHINUS,H,K0
00015 C COMMON/MODES/NVM,ALPHA0,EM,DQ,MM,PSI0,U05Q
00016 C COMMON/CONST/P1,TWOP1,C1,C2,OVRFL0,SORT3,SORTP1
00017 C DATA R0/(-.36450537..6313421668)/
00018 C
00019 C
00020 C DEBUG=. FALSE.
00021 C IF( IO1.GT.0 ) DEBUG=. TRUE.
00022 C DQ=( 1 .. 1. )
00023 C SD=S*D
00024 C IP(S3D.LT.1.E-2) GO TO 300
00025 C
00026 C SIGNIFICANT DUCT IS PRESENT
00027 C
00028 C
00029 C ..... DETERMINE REAL PART OF ENERGY EIGENVALUE -EM-.
00030 C FOUND BY SATISFYING PHASE INTEGRAL CONDITION
00031 C
00032 C
00033 C B=SD*SORT(SD)/(PI*75)
00034 C T=(4*MODE-1)/(3.*XB)
00035 C IF(T.LE.1.) A=1.5*T-1.
00036 C IF(T.GT.1.) A=.25*(T+SORT(T*T-1.))**2
00037 C EOLD=A*S3D
00038 C
00039 C DO NEWTON/RAPHSON ITERATES TO FIND -EM-
00040 C
00041 DO 30 I=1,5
00042 AP= A-(( (A+1.)*SORT(A+1.)-A*SORT(A))/1.5-T)/(SORT(A+1.))-_
00043 C1=SORT(A)
00044 IF( ABS( AP-A ).LT. ABS( A ) * 1. E-3 ) GO TO 55
00045 A=AP
00046 CONTINUE
00047 35 EM=AP*S3D
00048 IF( EM.LE.0. ) RETURN
00049 C1=-5.-R*((AP+1.)*SORT(AP+1.))-AP*SORT(AP)
00050 DC1:IDC=-R*(SORT(AP+1.))-SORT(AP)
00051 IF( DEBUG ) WRITE( 101,80 ) EM,FOLD,T,AP,CHI,DC1:IDE
00052 FORMAT( ' LEAKY ... EM,EOLD,T,AP,CHI,DC1:IDE= ',0(1PE14.6) )
00053 C
00054 C COMPUTE RAY-EQUIVALENT PERIOD -RM-. ASSUME RAY TURNS AT
00055 C DUCT BOTTOM, AND NORMALIZATION -NM-
00056 C

```

LEAKY FOR

FORTRAN V.5A(621) /KI 24-SEP-86

17:54 PAGE 1-1

```

00037      DM= (SQR(T(EMR+SD)) - SQR(T(EMR))) * H/SD
00038      RM= 4.*KOH*DM
00039      RH= .5*DM
00040      C..... COMPUTE AMPLITUDE DECAY TERM FOR LEAKY MODES.
00041      C..... MODEL DECAY AS REFLECTION LOSS PER RAY-EQUIVALENT
00042      C..... PERIOD APPLIED CONTINUOUSLY.
00043      C
00044      RCOEFF= REFLKT(EMR, S2, 101)
00045      IF(RCOEFF.GT. 1.) RETURN
00046      ALPHAM= -ALOG(RCOEFF)/RM
00047      ETM= -ALPHAM/(KOH*CPLUS)
00048      EM= CMPLX(EMR, EMI)
00049      IF(EMR.GT. 1.) DROF= -.5/(-EMR)**.5 + .25/EMR**2
00050      IF(EMR.LE. 1.) DROF= -(R0**2 + EMR*(.2251235 + EMR*(.16231472*RE+
00051      EM**2 + 1169137*R0**2 + .0319463474*EM))), )
00052      IF(CABS(EM).GT. 1.5*SD) GO TO 150
00053      C
00054      SMALL_ARCURENT_REGION. EXPAND IN POWER SERIES ABOUT
00055      EM=0.
00056      C
00057      C
00058      W= -EM/S2
00059      Z= W**3/6.
00060      ZFTA0= (-W+SD)**1.5/1.5 + PI/12.
00061      W02= 4.*PI*(C1*CSIN(ZETA0)*(1.+Z*(1.+Z*(ZETA0+C2*CSIN(ZETA0+PI/3.)*
00062      W*(1.+.5*Z*(1.+Z/7.)))***2)/(8*(EM+63D)**.5),
00063      C0 TO 160
00064      DZETA= (EM+SD)**1.5- (EM+SD)**1.5/(1.5*SD)
00065      U02= (CSIN(DZETA)- 5.*SD*CCOS(DZETA))/(48.*EM*(EM+SD))**.5
00066      160  CONTINUE
00067      Z= 1.+((1.+SD)*U02*DZETA
00068      NM= CADS(Z)*IV/SD
00069      IF(EMR.GT. SD) NM= DM/2.
00070      U05Q= CARS(U02)/NM
00071      IF(DEBUG) WRITE(101,200) EM, RCOEFF, RM, NM, U02, U05Q, DRDE
00072      200  FORMAT(101,200) EM, RCOEFF, RM, '4E15.7/10X,
00073      'NM, U02, U05Q, DRDE, '6(1PE14.6))
00074      GO TO 500
00075      C*****
00076      C***** CONTINUE
00077      C
00078      C
00079      C
00080      C
00081      C
00082      C
00083      C
00084      C
00085      C
00086      C
00087      C
00088      C
00089      C
00090      C
00091      C
00092      C
00093      C
00094      C
00095      C
00096      C
00097      C
00098      C
00099      C
00100      C
00101      C
00102      C
00103      C
00104      C
00105      C
00106      C
00107      C
00108      C
00109      C
00110      C
00111      C
00112      C
00113      C
00114      C
00115      C
00116      C
00117      C
00118      C
00119      C
00120      C
00121      C
00122      C
00123      C
00124      C
00125      C
00126      C
00127      C
00128      C
00129      C
00130      C
00131      C
00132      C
00133      C
00134      C
00135      C
00136      C
00137      C
00138      C
00139      C
00140      C
00141      C
00142      C
00143      C
00144      C
00145      C
00146      C
00147      C
00148      C
00149      C
00150      C
00151      C
00152      C
00153      C
00154      C
00155      C
00156      C
00157      C
00158      C
00159      C
00160      C
00161      C
00162      C
00163      C
00164      C
00165      C
00166      C
00167      C
00168      C
00169      C
00170      C
00171      C
00172      C
00173      C
00174      C
00175      C
00176      C
00177      C
00178      C
00179      C
00180      C
00181      C
00182      C
00183      C
00184      C
00185      C
00186      C
00187      C
00188      C
00189      C
00190      C
00191      C
00192      C
00193      C
00194      C
00195      C
00196      C
00197      C
00198      C
00199      C
00200      C
00201      C
00202      C
00203      C
00204      C
00205      C
00206      C
00207      C
00208      C
00209      C
00210      C
00211      C
00212      C
00213      C
00214      C
00215      C
00216      C
00217      C
00218      C
00219      C
00220      C
00221      C
00222      C
00223      C
00224      C
00225      C
00226      C
00227      C
00228      C
00229      C
00230      C
00231      C
00232      C
00233      C
00234      C
00235      C
00236      C
00237      C
00238      C
00239      C
00240      C
00241      C
00242      C
00243      C
00244      C
00245      C
00246      C
00247      C
00248      C
00249      C
00250      C
00251      C
00252      C
00253      C
00254      C
00255      C
00256      C
00257      C
00258      C
00259      C
00260      C
00261      C
00262      C
00263      C
00264      C
00265      C
00266      C
00267      C
00268      C
00269      C
00270      C
00271      C
00272      C
00273      C
00274      C
00275      C
00276      C
00277      C
00278      C
00279      C
00280      C
00281      C
00282      C
00283      C
00284      C
00285      C
00286      C
00287      C
00288      C
00289      C
00290      C
00291      C
00292      C
00293      C
00294      C
00295      C
00296      C
00297      C
00298      C
00299      C
00300      C
00301      C
00302      C
00303      C
00304      C
00305      C
00306      C
00307      C
00308      C
00309      C
00310      C
00311      C
00312      C
00313      C
00314      C
00315      C
00316      C
00317      C
00318      C
00319      C
00320      C
00321      C
00322      C
00323      C
00324      C
00325      C
00326      C
00327      C
00328      C
00329      C
00330      C
00331      C
00332      C
00333      C
00334      C
00335      C
00336      C
00337      C
00338      C
00339      C
00340      C
00341      C
00342      C
00343      C
00344      C
00345      C
00346      C
00347      C
00348      C
00349      C
00350      C
00351      C
00352      C
00353      C
00354      C
00355      C
00356      C
00357      C
00358      C
00359      C
00360      C
00361      C
00362      C
00363      C
00364      C
00365      C
00366      C
00367      C
00368      C
00369      C
00370      C
00371      C
00372      C
00373      C
00374      C
00375      C
00376      C
00377      C
00378      C
00379      C
00380      C
00381      C
00382      C
00383      C
00384      C
00385      C
00386      C
00387      C
00388      C
00389      C
00390      C
00391      C
00392      C
00393      C
00394      C
00395      C
00396      C
00397      C
00398      C
00399      C
00400      C
00401      C
00402      C
00403      C
00404      C
00405      C
00406      C
00407      C
00408      C
00409      C
00410      C
00411      C
00412      C
00413      C
00414      C
00415      C
00416      C
00417      C
00418      C
00419      C
00420      C
00421      C
00422      C
00423      C
00424      C
00425      C
00426      C
00427      C
00428      C
00429      C
00430      C
00431      C
00432      C
00433      C
00434      C
00435      C
00436      C
00437      C
00438      C
00439      C
00440      C
00441      C
00442      C
00443      C
00444      C
00445      C
00446      C
00447      C
00448      C
00449      C
00450      C
00451      C
00452      C
00453      C
00454      C
00455      C
00456      C
00457      C
00458      C
00459      C
00460      C
00461      C
00462      C
00463      C
00464      C
00465      C
00466      C
00467      C
00468      C
00469      C
00470      C
00471      C
00472      C
00473      C
00474      C
00475      C
00476      C
00477      C
00478      C
00479      C
00480      C
00481      C
00482      C
00483      C
00484      C
00485      C
00486      C
00487      C
00488      C
00489      C
00490      C
00491      C
00492      C
00493      C
00494      C
00495      C
00496      C
00497      C
00498      C
00499      C
00500      C
00501      C
00502      C
00503      C
00504      C
00505      C
00506      C
00507      C
00508      C
00509      C
00510      C
00511      C
00512      C
00513      C
00514      C
00515      C
00516      C
00517      C
00518      C
00519      C
00520      C
00521      C
00522      C
00523      C
00524      C
00525      C
00526      C
00527      C
00528      C
00529      C
00530      C
00531      C
00532      C
00533      C
00534      C
00535      C
00536      C
00537      C
00538      C
00539      C
00540      C
00541      C
00542      C
00543      C
00544      C
00545      C
00546      C
00547      C
00548      C
00549      C
00550      C
00551      C
00552      C
00553      C
00554      C
00555      C
00556      C
00557      C
00558      C
00559      C
00560      C
00561      C
00562      C
00563      C
00564      C
00565      C
00566      C
00567      C
00568      C
00569      C
00570      C
00571      C
00572      C
00573      C
00574      C
00575      C
00576      C
00577      C
00578      C
00579      C
00580      C
00581      C
00582      C
00583      C
00584      C
00585      C
00586      C
00587      C
00588      C
00589      C
00590      C
00591      C
00592      C
00593      C
00594      C
00595      C
00596      C
00597      C
00598      C
00599      C
00600      C
00601      C
00602      C
00603      C
00604      C
00605      C
00606      C
00607      C
00608      C
00609      C
00610      C
00611      C
00612      C
00613      C
00614      C
00615      C
00616      C
00617      C
00618      C
00619      C
00620      C
00621      C
00622      C
00623      C
00624      C
00625      C
00626      C
00627      C
00628      C
00629      C
00630      C
00631      C
00632      C
00633      C
00634      C
00635      C
00636      C
00637      C
00638      C
00639      C
00640      C
00641      C
00642      C
00643      C
00644      C
00645      C
00646      C
00647      C
00648      C
00649      C
00650      C
00651      C
00652      C
00653      C
00654      C
00655      C
00656      C
00657      C
00658      C
00659      C
00660      C
00661      C
00662      C
00663      C
00664      C
00665      C
00666      C
00667      C
00668      C
00669      C
00670      C
00671      C
00672      C
00673      C
00674      C
00675      C
00676      C
00677      C
00678      C
00679      C
00680      C
00681      C
00682      C
00683      C
00684      C
00685      C
00686      C
00687      C
00688      C
00689      C
00690      C
00691      C
00692      C
00693      C
00694      C
00695      C
00696      C
00697      C
00698      C
00699      C
00700      C
00701      C
00702      C
00703      C
00704      C
00705      C
00706      C
00707      C
00708      C
00709      C
00710      C
00711      C
00712      C
00713      C
00714      C
00715      C
00716      C
00717      C
00718      C
00719      C
00720      C
00721      C
00722      C
00723      C
00724      C
00725      C
00726      C
00727      C
00728      C
00729      C
00730      C
00731      C
00732      C
00733      C
00734      C
00735      C
00736      C
00737      C
00738      C
00739      C
00740      C
00741      C
00742      C
00743      C
00744      C
00745      C
00746      C
00747      C
00748      C
00749      C
00750      C
00751      C
00752      C
00753      C
00754      C
00755      C
00756      C
00757      C
00758      C
00759      C
00760      C
00761      C
00762      C
00763      C
00764      C
00765      C
00766      C
00767      C
00768      C
00769      C
00770      C
00771      C
00772      C
00773      C
00774      C
00775      C
00776      C
00777      C
00778      C
00779      C
00780      C
00781      C
00782      C
00783      C
00784      C
00785      C
00786      C
00787      C
00788      C
00789      C
00790      C
00791      C
00792      C
00793      C
00794      C
00795      C
00796      C
00797      C
00798      C
00799      C
00800      C
00801      C
00802      C
00803      C
00804      C
00805      C
00806      C
00807      C
00808      C
00809      C
00810      C
00811      C
00812      C
00813      C
00814      C
00815      C
00816      C
00817      C
00818      C
00819      C
00820      C
00821      C
00822      C
00823      C
00824      C
00825      C
00826      C
00827      C
00828      C
00829      C
00830      C
00831      C
00832      C
00833      C
00834      C
00835      C
00836      C
00837      C
00838      C
00839      C
00840      C
00841      C
00842      C
00843      C
00844      C
00845      C
00846      C
00847      C
00848      C
00849      C
00850      C
00851      C
00852      C
00853      C
00854      C
00855      C
00856      C
00857      C
00858      C
00859      C
00860      C
00861      C
00862      C
00863      C
00864      C
00865      C
00866      C
00867      C
00868      C
00869      C
00870      C
00871      C
00872      C
00873      C
00874      C
00875      C
00876      C
00877      C
00878      C
00879      C
00880      C
00881      C
00882      C
00883      C
00884      C
00885      C
00886      C
00887      C
00888      C
00889      C
00890      C
00891      C
00892      C
00893      C
00894      C
00895      C
00896      C
00897      C
00898      C
00899      C
00900      C
00901      C
00902      C
00903      C
00904      C
00905      C
00906      C
00907      C
00908      C
00909      C
00910      C
00911      C
00912      C
00913      C
00914      C
00915      C
00916      C
00917      C
00918      C
00919      C
00920      C
00921      C
00922      C
00923      C
00924      C
00925      C
00926      C
00927      C
00928      C
00929      C
00930      C
00931      C
00932      C
00933      C
00934      C
00935      C
00936      C
00937      C
00938      C
00939      C
00940      C
00941      C
00942      C
00943      C
00944      C
00945      C
00946      C
00947      C
00948      C
00949      C
00950      C
00951      C
00952      C
00953      C
00954      C
00955      C
00956      C
00957      C
00958      C
00959      C
00960      C
00961      C
00962      C
00963      C
00964      C
00965      C
00966      C
00967      C
00968      C
00969      C
00970      C
00971      C
00972      C
00973      C
00974      C
00975      C
00976      C
00977      C
00978      C
00979      C
00980      C
00981      C
00982      C
00983      C
00984      C
00985      C
00986      C
00987      C
00988      C
00989      C
00990      C
00991      C
00992      C
00993      C
00994      C
00995      C
00996      C
00997      C
00998      C
00999      C
01000      C
01001      C
01002      C
01003      C
01004      C
01005      C
01006      C
01007      C
01008      C
01009      C
01010      C
01011      C
01012      C
01013      C
01014      C
01015      C
01016      C
01017      C
01018      C
01019      C
01020      C
01021      C
01022      C
01023      C
01024      C
01025      C
01026      C
01027      C
01028      C
01029      C
01030      C
01031      C
01032      C
01033      C
01034      C
01035      C
01036      C
01037      C
01038      C
01039      C
01040      C
01041      C
01042      C
01043      C
01044      C
01045      C
01046      C
01047      C
01048      C
01049      C
01050      C
01051      C
01052      C
01053      C
01054      C
01055      C
01056      C
01057      C
01058      C
01059      C
01060      C
01061      C
01062      C
01063      C
01064      C
01065      C
01066      C
01067      C
01068      C
01069      C
01070      C
01071      C
01072      C
01073      C
01074      C
01075      C
01076      C
01077      C
01078      C
01079      C
01080      C
01081      C
01082      C
01083      C
01084      C
01085      C
01086      C
01087      C
01088      C
01089      C
01090      C
01091      C
01092      C
01093      C
01094      C
01095      C
01096      C
01097      C
01098      C
01099      C
01100      C
01101      C
01102      C
01103      C
01104      C
01105      C
01106      C
01107      C
01108      C
01109      C
01110      C
01111      C
01112      C
01113      C
01114      C
01115      C
01116      C
01117      C
01118      C
01119      C
01120      C
01121      C
01122      C
01123      C
01124      C
01125      C
01126      C
01127      C
01128      C
01129      C
01130      C
01131      C
01132      C
01133      C
01134      C
01135      C
01136      C
01137      C
01138      C
01139      C
01140      C
01141      C
01142      C
01143      C
01144      C
01145      C
01146      C
01147      C
01148      C
01149      C
01150      C
01151      C
01152      C
01153      C
01154      C
01155      C
01156      C
01157      C
01158      C
01159      C
01160      C
01161      C
01162      C
01163      C
01164      C
01165      C
01166      C
01167      C
01168      C
01169      C
01170      C
01171      C
01172      C
01173      C
01174      C
01175      C
01176      C
01177      C
01178      C
01179      C
01180      C
01181      C
01182      C
01183      C
01184      C
01185      C
01186      C
01187      C
01188      C
01189      C
01190      C
01191      C
01192      C
01193      C
01194      C
01195      C
01196      C
01197      C
01198      C
01199      C
01200      C
01201      C
01202      C
01203      C
01204      C
01205      C
01206      C
01207      C
01208      C
01209      C
01210      C
01211      C
01212      C
01213      C
01214      C
01215      C
01216      C
01217      C
01218      C
01219      C
01220      C
01221      C
01222      C
01223      C
01224      C
01225      C
01226      C
01227      C
01228      C
01229      C
01230      C
01231      C
01232      C
01233      C
01234      C
01235      C
01236      C
01237      C
01238      C
01239      C
01240      C
01241      C
01242      C
01243      C
01244      C
01245      C
01246      C
01247      C
01248      C
01249      C
01250      C
01251      C
01252      C
01253      C
01254      C
01255      C
01256      C
01257      C
01258      C
01259      C
01260      C
01261      C
01262      C
01263      C
01264      C
01265      C
01266      C
01267      C
01268      C
01269      C
01270      C
01271      C
01272      C
01273      C
01274      C
01275      C
01276      C
01277      C
01278      C
01279      C
01280      C
01281      C
01282      C
01283      C
01284      C
01285      C
01286      C
01287      C
01288      C
01289      C
01290      C
01291      C
01292      C
01293      C
01294      C
01295      C
01296      C
01297      C
01298      C
01299      C
01300      C
01301      C
01302      C
01303      C
01304      C
01305      C
01306      C
01307      C
01308      C
01309      C
01310      C
01311      C
01312      C
01313      C
01314      C
01315      C
01316      C
01317      C
01318      C
01319      C
01320      C
01321      C
01322      C
01323      C
01324      C
01325      C
01326      C
01327      C
01328      C
01329      C
01330      C
01331      C
01332      C
01333      C
01334      C
01335      C
01336      C
01337      C
01338      C
01339      C
01340      C
01341      C
01342      C
01343      C
01344      C
01345      C
01346      C
01347      C
01348      C
01349      C
01350      C
01351      C
01352      C
01353      C
01354      C
01355      C
01356      C
01357      C
01358      C
01359      C
01360      C
01361      C
01362      C
01363      C
01364      C
01365      C
01366      C
01367      C
01368      C
01369      C
01370      C
0
```

```

00113      T= (2.5810567+ .27929556*(PI*FLOAT(MODE)**2)/D**3
00114      E0= (PI*FLOAT(MODE)/D)**2*(T*(1.+5.*Z)+ 7.74317/D*x*3+ 3.*Z2+
1. *Z+1.)
00115      EB=REAL(E0)
00116      EI=AIMAG(E0)
00117      IF(DEBUG) WRITE(101,320) MODE,T,Z,Z2,E0
00118      320 FORMAT('LEVEL 2 LEAKY... M:DE,T,Z,Z2,E0= ',14.6E14,7)
00119      IF(S.LT.1.E-6) GO TO 400
00120
00121      C
00122      C GRADIENT IS NON-ZERO. FUT EFFECTIVE THICKNESS OF DUCT IS SMALL.
00123      C COMPUTE FIRST ORDER PERTURBATION TO S=0 ENERGY.
00124      C
00125      Z= CSQRT(E0)*D
00126      J0Z= CSIN(Z)/Z
00127      DE= (S3D*D/4.)*(J0Z*J0Z-1.)
00128      EM= E0+DE
00129      IF(DEBUG) WRITE(101,340) Z,J0Z,DE
00130      340 FORMAT(' LEVEL 2 LEAKY... Z,J0Z,DE= ',6E15,7)
00131      C
00132      C COMPUTE RAY-EQUIVALENT PERIOD -RM-
00133      C IF ENERGY IS POSITIVE ( ABOVE BARRIER), ASSUME RAY TURNS AT
00134      C BOTTOM OF DUCT.
00135      C
00136      400  RM=0.
00137      IF(S.EQ.0.) GO TO 500
00138      EM=REAL(EM)
00139      RM=SQRT(EM+S3D)
00140      IF(EM.GE.0.) RM=(RM-SQRT(EM))*4.*SQRT(1.-CPLUS*H*(EM+S3D))/
00141      B-17
00142      500 CONTINUE
00143      RETURN
00144      END
00145

```

COMMON BLOCKS

```

/DUCT/(+12)
S      +0      S2      +1      S3      +2      KOH      +3      S3D      +4
D      +5      CPLUS   +6      CMINUS  +7      H        +10     K0       +11
/MODES/(+11)
RM      +0      ALRMA0  +1      EM      +2      DQ      +4      M       +6
PSI0    +7      USGSQ  +10
/CONST/(+7)
PI      +0      TWOPI   +1      C1      +2      C2      +3      OVFLO  +4
SORT3  +5      SORTPI  +6

```

SUBPROGRAMS CALLED

```

REAL:   CABS,   SORT,   CTRIX,   CSORT,   ALOC.
CCOS:   FLOAT,   AIMAG,   REFLKT,   CSIN.

```

LEAKY LEAKY.FOR FORTTRAN V.5A(621) /KI 24-SEP-80 17:54 PAGE 1-3

SCALARS AND ARRAYS ["*" NO EXPLICIT DEFINITION - "X" NOT REFERENCED]

DE	1	DEBUG	3	Z	4	*SD	6	W	7
*AP	11	*T	12	DRDE	13	*EMR	15	*CHI	16
*B	17	*101	20	*REALEM		*RCOEFF	21	*ER	22
*ALPHAN	23	E0	24	A2	26	DZETA	36	*MODE	32
*DM	33	A	34	.S00000	36	ERROR	37	*EMI	40
*EOLD	41	*RM	42	J0Z	43	*I	45	Z2	46
*DCII/DR.	50	ZETAO	51	U02	53	R0	55	*EI	57

TEMPORARIES

.A0016	133	.000000	134	.000001	135	.000002	136	.000003	137	.000004	140
.Q0005	141										

LEAKY [NO ERRORS DETECTED]

١٥٧٦
مکالمہ حسنیہ
و ملکیہ علیاً

SUSPECTED CALIFN

COSU. PEARL. GART. RANS. PROG. EVP.
A111. CSIN. CNS. A111.

SCALAR IN ARRAYS & NEW NP POLICIT OF FIRMING & NEW NOT REPC RE NCED 1

	07	2	050000	3	07	4	0	5	
DRPMC	1	07	068	11	0701	12	0101	13	
ENK	7	07TA	16	075TA	17	P	0707	23	
OO	14	0AR5Q	74	II	25	0700	27	PSI	30
SPRNG	31	0P	33	0C	34	0ETA0	35	0U2	37
AESRA	40								

TEMPERATURE

	A0011 75	A0011 76	A0016 77	A0002 100	A0007 101	A0004 102
AU010	75	A0006 104	A0007 105	A0000 105	A0001 107	A0002 110
AU005	103					
AU003	111					

SUSPECT & NP ERRORS DETERMIN 3

SISTEMI DI TIPI ALGEBRAICI (X, A, B, T, A1B, H1D, H1E)

14. EPISODE: COMPUTES ANY FUNCTIONS AND DERIVATIVES FOR REAL ARGUMENTS.

METHODS
A COMBINATORY OF CONVERGENT POWER SERIES FOR SMALL ARGUMENTS,
WITH ASYMPTOTIC EXPANSIONS FOR LARGE POSITIVE
AND NEGATIVE ARGUMENTS.
REFs ARHANOUTZ AND STEGUN, HANDBOOK OF MATHEMATICAL
FUNCTIONS.

三月三日

ICFAC AUTISTICS DIV SCIENCE APPLICATIONS, INC.

SILVERSTEIN CALL HOME

ARITHMETIC FUNCTIONS

- x.....ARGUMENT OF ANY FUNCTION
- A1,A2,...,A100...ANY FUNCTION (OUTPUT)
- A1,P1,P2,...,P100...ANY FUNCTION, DIFFERENTIALS
- M1,M2,...,M100...ANY ALG. COMPUTE
- S1,S2,...,S100...ANY ALG. COMPUTE
- A1,H1,A2,H2,...,A100,H100...COMPUTE

P. 27

ט' ט' ט' ט' ט'

78 $\frac{1}{1000} \cdot \frac{1}{n}$
 $TF(1.0 - F_1, P_1) \approx 10^{-30}$
 $F_1 = 1.0 - 1.0^{1.0} \cdot 2^{0.7} \cdot (1.0 + 2^{1.2}) \cdot (1.0 + (2/22)^2) \cdot (1.0 + (2/26)^2) \approx C1$
 $F_2 = 1.0 - 1.0^{1.0} \cdot 2^{0.7} \cdot (1.0 + (7/7)^2) \cdot (1.0 + (22/15)^2) \cdot (1.0 + (27/26)^2) \approx C2$
 $A12 F = F_2$
 $A12 S = S_2$
 $A12 S_{12} T \approx (1 + C)$
 80 $TF(1.0 - F_1, P_1) \approx 10^{-19}N$
 $F_1 = 1.0 - 1.0^{1.0} \cdot 2^{0.7} \cdot (1.0 + 1.25^2) \cdot (1.0 + (7/14)^2) \cdot (1.0 + (2/26)^2) \approx C1$
 $F_2 = 1.0 - 1.0^{1.0} \cdot 2^{0.7} \cdot (1.0 + (7/10)^2) \cdot (1.0 + 0.25^2) \cdot (1.0 + (7/12.5)^2) \approx C2$
 $A12 F = F_2$

سیاه و سفید

SUGAR 10

SIN. 14

SCALARS AND ARRAYS. (See NOT EXPLICIT DEFINITION - "Z" NOT REFERENCED)

*CIP	1	*F0001	2	*T	1	*F0003	4	*F0002	5
*F0001	6	*F0000	7	*TWTYA	10	N	11	*START	12
*ETA	13	*I	14	*AI	15	*WIP	16	*FP	17
N	20	*E	21	*M000F	22	*VRFLO	23	*AIP	24
*C2	25	*X	26	*SAHTZ	27	*PMI	30	*F	31
*C1	32	*U	33						

TERMINATORS

*ENDFILE
*EOT
*EOF

AIRY 1 AIRY 1 AIRY 1 AIRY 1

STRUCTURE AND USES

SQRT.
ASIN.
ATAN
COS.

SCALARS AND ARRAYS & HOW TO EXPLICIT DEFINITION & HOW NOT REFERENCED

DEFUNC	1	DEFUN	?
OF	7	OF	10
CAT	14	CAT	15
AIN	21	AIN	22
CCL	30	CCL	31

FUNCTIONS

AUD10	56	AUD11	57	AUD12	60
AUD12	54	AUD02	65	AUD01	66
AUD07	72	AUD000	73	AUD001	74

PRFLKT & HOW GROUPS DEFEND

PI	4	PI	5
PI	11	PI	12
REFLKT	17	REFLKT	18
R	25	R	26

Transcript

.A0016 21 .A0002 22 .A0001 23 .A0004 24 .A0005 25 .A0000 26
.20001 27

MIC 0 & NO RECORDS RECEIVED 1

APPENDIX C

SAMPLE EXECUTION

The following is transmission-loss (TL) output for the test case considered in Section 3. The values have been scaled by a factor of 10 and volume attenuation [$\alpha = .125 (f/1000)^2$ dB/nm] subtracted.*

* The virtual-mode model does not include volume loss. However, the PE runs used in section 3 did, so I added volume loss to the values shown in the following paper to get the results plotted in section 3. The TL values in this appendix have been converted to dB re \equiv .

	75 (Hz)	750	250	750	250	500	500	500	500	750	750	750	1000	1000	1250	1250	1500	1500	1500	1500
H (Hz)	750	750	750	750	750	750	750	750	750	750	750	750	750	750	750	750	750	750	750	750
H (Hz)	61.6	64.7	65.9	64.9	67.4	62.6	61.6	62.6	60.7	59.1	60.0	56.1	55.9	54.0	51.6	51.1	50.2	50.5	49.4	49.1
H (Hz)	2.00	66.0	64.0	71.3	71.3	71.4	63.5	60.7	64.2	64.6	67.0	65.3	64.7	60.7	60.5	59.9	60.3	59.5	58.6	2.00
H (Hz)	3.00	66.4	64.4	71.4	71.6	60.3	60.7	71.1	71.4	71.9	75.7	75.1	71.6	72.4	67.4	67.4	67.4	67.4	66.8	3.00
H (Hz)	4.00	66.1	71.1	75.5	67.4	84.8	65.4	72.0	77.0	80.2	71.0	70.7	77.0	77.0	67.5	67.5	67.5	67.5	67.4	4.00
H (Hz)	5.00	66.1	72.3	76.4	61.5	87.7	89.7	74.1	75.4	80.6	83.1	83.9	74.5	70.5	81.9	82.4	79.8	74.7	74.7	73.9
H (Hz)	6.00	66.0	71.2	77.4	61.1	90.5	90.6	75.1	76.6	82.7	95.6	95.6	75.7	71.8	94.3	94.3	91.6	95.5	95.5	6.00
H (Hz)	7.00	70.6	71.0	76.7	67.7	90.9	62.7	76.0	77.7	94.4	87.5	89.7	75.8	77.5	96.7	87.8	85.9	90.4	90.6	1.00
H (Hz)	8.00	71.2	74.6	74.5	61.7	91.5	61.1	76.7	74.5	90.1	90.3	77.7	84.9	88.2	95.5	95.3	90.7	91.4	92.8	3.00
H (Hz)	9.00	71.7	76.1	60.2	67.1	92.1	92.5	77.4	77.4	91.7	90.4	91.7	79.4	86.0	92.5	90.8	90.4	93.4	93.9	8.00
H (Hz)	10.00	72.2	75.6	81.6	91.5	91.7	65.7	78.0	60.0	91.5	92.0	79.2	97.0	90.5	91.0	91.0	95.4	96.2	96.9	9.00
H (Hz)	11.00	72.6	74.1	74.1	61.5	91.2	64.4	95.0	74.5	80.7	84.0	92.5	93.0	94.7	90.5	91.7	90.5	90.4	90.4	10.00
H (Hz)	12.00	72.0	72.0	61.1	65.0	91.1	65.0	79.6	70.0	80.6	91.7	94.7	90.5	91.6	91.7	90.5	90.4	10.23	10.13	12.00
H (Hz)	13.00	73.4	74.9	92.6	91.8	91.5	95.5	97.7	79.5	91.0	90.3	94.0	95.5	91.1	90.2	92.9	94.4	95.3	10.50	13.00
H (Hz)	14.00	73.7	77.3	93.1	60.7	92.4	92.2	67.0	79.0	92.4	90.0	94.7	94.2	91.6	93.6	97.6	95.1	97.2	10.00	14.00
H (Hz)	15.00	74.0	77.6	93.6	62.8	92.8	92.7	68.1	90.3	93.0	91.5	95.1	96.9	92.2	90.4	94.1	95.7	98.1	10.16	15.00
H (Hz)	16.00	74.1	77.0	94.0	61.7	97.3	94.8	90.6	97.5	97.5	97.0	95.8	97.4	82.7	90.9	94.7	94.2	94.8	10.24	10.59
H (Hz)	17.00	74.6	74.2	94.4	61.8	97.8	95.0	91.0	97.0	97.0	97.5	96.3	97.0	91.5	95.2	96.7	90.5	10.31	10.46	17.00
H (Hz)	18.00	74.0	74.5	94.4	61.1	94.2	95.2	95.8	91.3	94.4	91.0	96.8	94.1	81.7	97.0	95.7	10.00	10.37	10.52	18.00
H (Hz)	19.00	75.1	76.4	95.3	61.7	96.7	10.07	91.6	94.0	94.0	91.5	97.0	97.0	94.2	97.4	96.2	97.4	10.90	11.03	19.00
H (Hz)	20.00	75.0	76.0	95.6	61.7	96.1	90.7	91.0	95.3	94.0	97.9	90.4	94.6	97.0	94.6	97.0	94.6	10.43	10.59	20.00
H (Hz)	21.00	75.6	70.2	96.0	64.6	91.7	91.7	92.2	55.7	94.4	97.4	97.4	97.4	97.4	97.4	97.4	97.4	10.61	10.63	21.00
H (Hz)	22.00	76.9	70.5	96.4	60.0	100.0	101.4	92.5	96.1	64.8	98.7	100.2	85.5	97.6	99.1	10.20	10.59	10.71	10.96	11.11
H (Hz)	23.00	76.0	70.7	96.7	64.7	96.4	10.4	92.6	96.5	95.3	90.1	10.07	95.9	94.2	99.0	99.6	10.25	10.63	10.79	11.00
H (Hz)	24.00	76.2	70.9	96.9	61.7	96.1	96.0	93.0	93.0	95.7	90.1	10.11	96.4	94.7	99.4	10.00	10.67	10.67	10.92	24.00
H (Hz)	25.00	76.4	80.1	97.4	67.7	10.7	91.2	92.2	93.7	97.7	96.1	100.0	91.5	96.4	97.1	97.1	97.1	10.71	10.71	25.00
H (Hz)	26.00	76.5	80.3	97.7	67.6	10.7	91.5	93.5	97.7	96.5	100.4	101.0	87.2	95.5	99.3	10.09	10.75	10.75	11.13	26.00
H (Hz)	27.00	76.7	80.5	97.0	67.0	10.7	91.7	93.7	97.7	96.9	100.8	10.23	87.6	95.0	96.7	10.12	10.42	10.79	10.95	27.00
H (Hz)	28.00	76.0	80.0	97.3	67.3	97.3	96.8	93.0	93.0	97.3	97.3	101.1	10.27	99.0	96.3	10.01	10.16	10.45	10.93	28.00
H (Hz)	29.00	76.0	80.0	97.4	67.4	97.4	96.9	93.0	93.0	97.4	97.4	101.1	10.27	99.0	96.3	10.01	10.16	10.45	10.93	29.00
H (Hz)	30.00	76.0	80.0	97.4	67.4	97.4	96.9	93.0	93.0	97.4	97.4	101.1	10.27	99.0	96.3	10.01	10.16	10.45	10.93	30.00
H (Hz)	31.00	76.0	80.0	97.4	67.4	97.4	96.9	93.0	93.0	97.4	97.4	101.1	10.27	99.0	96.3	10.01	10.16	10.45	10.93	31.00
H (Hz)	32.00	76.5	80.5	97.5	67.5	97.5	96.9	93.0	93.0	97.5	97.5	101.1	10.27	99.0	96.3	10.01	10.16	10.45	10.93	32.00
H (Hz)	33.00	76.0	80.0	97.6	67.6	97.6	96.9	93.0	93.0	97.6	97.6	101.1	10.27	99.0	96.3	10.01	10.16	10.45	10.93	33.00
H (Hz)	34.00	76.0	80.0	97.6	67.6	97.6	96.9	93.0	93.0	97.6	97.6	101.1	10.27	99.0	96.3	10.01	10.16	10.45	10.93	34.00
H (Hz)	35.00	76.0	80.0	97.6	67.6	97.6	96.9	93.0	93.0	97.6	97.6	101.1	10.27	99.0	96.3	10.01	10.16	10.45	10.93	35.00
H (Hz)	36.00	76.0	80.0	97.6	67.6	97.6	96.9	93.0	93.0	97.6	97.6	101.1	10.27	99.0	96.3	10.01	10.16	10.45	10.93	36.00
H (Hz)	37.00	76.0	80.0	97.6	67.6	97.6	96.9	93.0	93.0	97.6	97.6	101.1	10.27	99.0	96.3	10.01	10.16	10.45	10.93	37.00
H (Hz)	38.00	76.0	80.0	97.6	67.6	97.6	96.9	93.0	93.0	97.6	97.6	101.1	10.27	99.0	96.3	10.01	10.16	10.45	10.93	38.00
H (Hz)	39.00	76.0	80.0	97.6	67.6	97.6	96.9	93.0	93.0	97.6	97.6	101.1	10.27	99.0	96.3	10.01	10.16	10.45	10.93	39.00
H (Hz)	40.00	76.0	80.0	97.6	67.6	97.6	96.9	93.0	93.0	97.6	97.6	101.1	10.27	99.0	96.3	10.01	10.16	10.45	10.93	40.00
H (Hz)	41.00	76.0	80.0	97.6	67.6	97.6	96.9	93.0	93.0	97.6	97.6	101.1	10.27	99.0	96.3	10.01	10.16	10.45	10.93	41.00
H (Hz)	42.00	76.0	80.0	97.6	67.6	97.6	96.9	93.0	93.0	97.6	97.6	101.1	10.27	99.0	96.3	10.01	10.16	10.45	10.93	42.00
H (Hz)	43.00	76.0	80.0	97.6	67.6	97.6	96.9	93.0	93.0	97.6	97.6	101.1	10.27	99.0	96.3	10.01	10.16	10.45	10.93	43.00
H (Hz)	44.00	76.0	80.0	97.6	67.6	97.6	96.9	93.0	93.0	97.6	97.6	101.1	10.27	99.0	96.3	10.01	10.16	10.45	10.93	44.00
H (Hz)	45.00	76.0	80.0	97.6	67.6	97.6	96.9	93.0	93.0	97.6	97.6	101.1	10.27	99.0	96.3	10.01	10.16	10.45	10.93	45.00
H (Hz)	46.00	76.0	80.0	97.6	67.6	97.6	96.9	93.0	93.0	97.6	97.6	101.1	10.27	99.0	96.3	10.01	10.16	10.45	10.93	46.00
H (Hz)	47.00	76.0	80.0	97.6	67.6	97.6	96.9	93.0	93.0	97.6	97.6	101.1	10.27	99.0	96.3	10.01	10.16	10.45	10.93	47.00
H (Hz)	48.00	76.0	80.0	97.6	67.6	97.6	96.9	93.0	93.0	97.6	97.6	101.1	10.27	99.0	96.3	10.01	10.16	10.45	10.93	48.00
H (Hz)	49.00	76.0	80.0	97.6	67.6	97.6	96.9	93.0	93.0	97.6	97.6	101.1	10.27	99.0	96.3	10.01	10.16	10.45	10.93	49.00
H (Hz)	50.00	76.0	80.0	97.6	67.6	97.6	96.9	93.0	93.0	97.6	97.6	101.1	10.27	99.0	96.3	10.01	10.16	10.45	10.93	50.00

	75 (FT)	250	250	250	250	500	500	500	500	500	500	500	500	750	750	750	1000	1000	1000	1000	1000	1000	1250	1250	1250	1500	1500	1500	
0.00	673	673	673	673	677	677	677	677	677	677	677	677	677	656	656	656	674	674	674	674	674	674	640	640	640	621	621	621	
1.00	641	721	715	715	661	661	703	703	725	725	670	684	704	710	657	675	676	692	692	692	692	692	692	632	632	632	2.00	2.00	2.00
2.00	664	704	740	701	807	807	751	751	778	778	695	714	764	707	729	711	747	747	747	747	747	747	740	740	740	3.00	3.00	3.00	
3.00	667	714	766	818	856	856	749	749	820	825	714	774	906	910	747	771	771	796	796	796	796	796	796	400	400	400	4.00	4.00	4.00
4.00	706	724	774	879	903	903	706	706	913	913	659	777	900	949	780	811	811	841	841	841	841	841	841	500	500	500	500	500	500
5.00	706	724	774	879	903	903	706	706	913	913	659	777	900	949	780	811	811	841	841	841	841	841	841	500	500	500	500	500	500
6.00	715	717	794	911	942	942	715	715	932	932	974	984	971	971	932	971	971	981	981	981	981	981	981	600	600	600	600	600	600
7.00	717	743	795	935	974	974	722	722	947	947	903	945	951	905	746	851	851	829	829	829	829	829	829	700	700	700	700	700	700
8.00	745	921	921	921	1045	1045	747	747	912	912	900	951	964	900	957	957	905	949	949	949	949	949	949	1200	1200	1200	1200	1200	1200
9.00	777	730	902	856	856	1009	728	728	960	960	909	920	953	964	914	925	944	944	944	944	944	944	935	935	935	935	935	935	
10.00	762	765	907	964	1016	1027	734	734	972	972	920	933	975	927	940	964	964	964	964	964	964	964	964	964	964	964	964	964	964
11.00	767	912	912	976	1025	1047	718	901	942	931	944	965	994	937	951	979	979	922	933	933	933	933	933	1000	1000	1000	1000	1000	1000
12.00	767	917	917	971	1029	1047	718	901	942	931	944	965	994	937	951	979	979	922	933	933	933	933	933	1000	1000	1000	1000	1000	1000
13.00	768	925	925	971	1051	1066	751	917	969	950	973	982	994	974	982	982	982	982	982	982	982	982	982	982	982	982	982	982	982
14.00	752	774	920	992	1056	1071	754	921	961	957	991	974	996	970	976	976	976	976	976	976	976	976	976	976	976	976	976	976	976
15.00	765	775	912	952	1011	1041	754	925	962	953	994	975	994	975	975	975	975	975	975	975	975	975	975	975	975	975	975	975	975
16.00	759	780	915	975	1026	1055	761	919	960	951	997	977	996	977	977	977	977	977	977	977	977	977	977	977	977	977	977	977	977
17.00	761	781	913	973	1005	1049	763	931	961	950	998	976	995	976	976	976	976	976	976	976	976	976	976	976	976	976	976	976	976
18.00	763	783	914	974	1011	1053	766	917	962	951	995	975	995	975	975	975	975	975	975	975	975	975	975	975	975	975	975	975	975
19.00	766	786	914	977	1027	1067	769	914	963	951	997	977	997	977	977	977	977	977	977	977	977	977	977	977	977	977	977	977	977
20.00	766	786	914	977	1027	1067	770	914	963	951	997	977	997	977	977	977	977	977	977	977	977	977	977	977	977	977	977	977	977
21.00	769	791	914	977	1027	1067	771	914	963	951	997	977	997	977	977	977	977	977	977	977	977	977	977	977	977	977	977	977	977
22.00	772	792	915	977	1027	1067	774	915	963	951	997	977	997	977	977	977	977	977	977	977	977	977	977	977	977	977	977	977	977
23.00	774	794	917	979	1010	1050	776	917	963	951	997	977	997	977	977	977	977	977	977	977	977	977	977	977	977	977	977	977	977
24.00	776	796	919	979	1023	1066	778	919	963	951	997	977	997	977	977	977	977	977	977	977	977	977	977	977	977	977	977	977	977
25.00	778	800	919	979	1015	1055	780	920	963	951	997	977	997	977	977	977	977	977	977	977	977	977	977	977	977	977	977	977	977
26.00	781	801	921	979	1021	1064	783	921	963	951	997	977	997	977	977	977	977	977	977	977	977	977	977	977	977	977	977	977	977
27.00	782	802	921	979	1021	1064	784	922	963	951	997	977	997	977	977	977	977	977	977	977	977	977	977	977	977	977	977	977	977
28.00	784	803	921	979	1021	1064	786	922	963	951	997	977	997	977	977	977	977	977	977	977	977	977	977	977	977	977	977	977	977
29.00	786	805	921	979	1021	1064	788	922	963	951	997	977	997	977	977	977	977	977	977	977	977	977	977	977	977	977	977	977	977
30.00	788	806	921	979	1021	1064	790	922	963	951	997	977	997	977	977	977	977	977	977	977	977	977	977	977	977	977	977	977	977
31.00	790	807	921	979	1021	1064	792	922	963	951	997	977	997	977	977	977	977	977	977	977	977	977	977	977	977	977	977	977	977
32.00	792	809	921	979	1021	1064	794	922	963	951	997	977	997	977	977	977	977	977	977	977	977	977	977	977	977	977	977	977	977
33.00	794	811	921	979	1021	1064	796	922	963	951	997	977	997	977	977	977	977	977	977	977	977	977	977	977	977	977	977	977	977
34.00	796	813	921	979	1021	1064	798	922	963	951	997	977	997	977	977	977	977	977	977	977	977	977	977	977	977	977	977	977	977
35.00	798	815	921	979	1021	1064	800	922	963	951	997	977	997	977	977	977	977	977	977	977	977	977	977	977	977	977	977	977	977
36.00	800	817	921	979	1021	1064	802	922	963	951	997	977	997	977	977	977	977	977	977	977	977	977	977	977	977	977	977	977	977
37.00	802	819	921	979	1021	1064	804	922	963	951	997	977	997	977	977	977	977	977	977	977	977	977	977	977	977	977	977	977	977
38.00	804	821	921	979	1021	1064	806	922	963	951	997	977	997	977	977	977	977	977	977	977	977	977	977	977	977	977	977	977	977
39.00	806	823	921	979	1021	1064	808	922	963	951	997	977	997	977	977	977	977	977	977	977	977	977	977	977	977	977	977	977	977
40.00	808	825	921	979	1021	1064	810	922	963	951	997	977	997	977	977	977	977	977	977	977	977	977	977	977	977	977	977	977	977
41.00	810	827	921	979	1021	1064	812	922	963	951	997	977	997	977	977	977	977	977	977	977	977	977	977	977	977	977	977	977	977
42.00	812	829	921	979	1021	1064	814	922	963	951	997	977	997	977	977	977	977	977	977	977	977	977	977	977	977	977	977	977	977
43.00	814	831	921	97																									

		REFERENCE = 500.00 H.F. MEASURE = 0.0 H.F.										REFERENCE = 90.540000E+00 H.F. MEASURE = 90.540000E+00 H.F.										
		500					500					500					500					
		500		500			500		500			500		500			500		500			
		610	610	610	610	610	610	610	610	610	610	610	610	610	610	610	610	610	610	610	610	
2.00	620	701	712	706	706	706	706	706	706	706	706	706	706	706	706	706	706	706	706	706	706	
3.00	630	720	720	714	714	714	714	714	714	714	714	714	714	714	714	714	714	714	714	714	714	
4.00	640	731	746	736	736	736	736	736	736	736	736	736	736	736	736	736	736	736	736	736	736	
5.00	650	746	757	746	746	746	746	746	746	746	746	746	746	746	746	746	746	746	746	746	746	
6.00	660	751	765	695	695	695	695	695	695	695	695	695	695	695	695	695	695	695	695	695	695	
7.00	706	754	773	620	601	601	601	601	601	601	601	601	601	601	601	601	601	601	601	601	601	
8.00	712	764	779	615	1602	1611	726	726	726	726	726	726	726	726	726	726	726	726	726	726	726	
9.00	717	903	716	1056	1056	1056	1056	1056	1056	1056	1056	1056	1056	1056	1056	1056	1056	1056	1056	1056	1056	
10.00	718	770	785	657	1018	1018	733	733	733	733	733	733	733	733	733	733	733	733	733	733	733	
11.00	721	775	790	652	1012	1012	754	754	754	754	754	754	754	754	754	754	754	754	754	754	754	
12.00	721	790	793	675	1013	1013	741	741	741	741	741	741	741	741	741	741	741	741	741	741	741	
13.00	721	917	917	1049	1049	1049	1049	1049	1049	1049	1049	1049	1049	1049	1049	1049	1049	1049	1049	1049	1049	
14.00	726	917	917	1049	1049	1049	1049	1049	1049	1049	1049	1049	1049	1049	1049	1049	1049	1049	1049	1049	1049	
15.00	727	914	914	1049	1049	1049	1049	1049	1049	1049	1049	1049	1049	1049	1049	1049	1049	1049	1049	1049	1049	
16.00	745	707	913	1067	1067	1067	751	751	751	751	751	751	751	751	751	751	751	751	751	751	751	
17.00	764	916	1067	1077	1067	764	916	916	916	916	916	916	916	916	916	916	916	916	916	916	916	
18.00	765	917	917	1067	1067	1067	774	917	917	917	917	917	917	917	917	917	917	917	917	917	917	
19.00	765	920	920	1067	1067	1067	774	920	920	920	920	920	920	920	920	920	920	920	920	920	920	
20.00	765	921	921	1067	1067	1067	774	921	921	921	921	921	921	921	921	921	921	921	921	921	921	
21.00	766	926	1072	1069	1105	774	921	1016	1067	1096	793	926	1042	1056	1019	1076	1060	1132	1145	1159	20.00	
22.00	761	921	921	1069	1069	1069	777	921	1021	1068	1102	795	925	1048	1062	1026	1084	1097	1141	1154	1167	22.00
23.00	761	915	915	1078	1078	1078	779	926	1026	1003	1104	798	921	1053	1047	1014	1092	1105	1149	1162	1176	23.00
24.00	765	918	918	1073	1073	1073	781	921	1030	1066	1113	900	926	1059	1073	1040	1099	1113	1157	1171	1184	24.00
25.00	760	920	920	1073	1073	1073	781	920	1034	1103	1119	902	921	1064	1078	1047	1107	1120	1165	1178	1192	25.00
26.00	760	921	921	1073	1073	1073	781	921	1034	1103	1119	902	921	1064	1078	1047	1107	1121	1172	1195	1209	26.00
27.00	771	924	924	1073	1073	1073	787	924	944	1042	1112	1127	906	1011	1075	1099	1120	1133	1179	1192	1206	27.00
28.00	774	926	926	1073	1073	1073	789	926	946	1045	1114	1131	906	1014	1070	1095	1107	1131	1173	1199	1213	28.00
29.00	775	927	927	1073	1073	1073	791	927	946	1049	1116	1131	907	1017	1071	1103	1119	1153	1167	1194	1224	29.00
30.00	777	927	927	1073	1073	1073	793	927	946	1051	1121	1136	910	1020	1075	1105	1131	1166	1196	1230	1257	30.00
31.00	774	927	927	1073	1073	1073	794	927	947	1052	1124	1137	911	1021	1076	1106	1131	1167	1197	1231	1251	31.00
32.00	780	927	927	1073	1073	1073	796	927	951	1057	1126	1145	916	1023	1079	1103	1136	1171	1221	1244	1259	32.00
33.00	780	927	927	1073	1073	1073	797	927	951	1057	1126	1145	916	1023	1079	1103	1136	1171	1221	1244	1259	33.00
34.00	781	928	928	1073	1073	1073	798	928	952	1058	1126	1147	917	1024	1082	1111	1145	1179	1225	1249	1264	34.00
35.00	785	930	930	1073	1073	1073	799	929	953	1058	1126	1147	918	1024	1083	1112	1146	1180	1230	1254	1272	35.00
36.00	786	930	930	1073	1073	1073	800	930	953	1058	1126	1147	918	1024	1083	1112	1146	1180	1230	1254	1272	36.00
37.00	787	931	931	1073	1073	1073	801	931	953	1058	1126	1147	919	1024	1083	1112	1147	1181	1231	1254	1272	37.00
38.00	787	931	931	1073	1073	1073	802	931	953	1058	1126	1147	919	1024	1083	1112	1147	1181	1231	1254	1272	38.00
39.00	787	931	931	1073	1073	1073	803	931	953	1058	1126	1147	919	1024	1083	1112	1147	1181	1231	1254	1272	39.00
40.00	787	931	931	1073	1073	1073	804	931	953	1058	1126	1147	919	1024	1083	1112	1147	1181	1231	1254	1272	40.00
41.00	787	931	931	1073	1073	1073	805	931	953	1058	1126	1147	919	1024	1083	1112	1147	1181	1231	1254	1272	41.00
42.00	788	931	931	1073	1073	1073	806	931	953	1058	1126	1147	919	1024	1083	1112	1147	1181	1231	1254	1272	42.00
43.00	788	931	931	1073	1073	1073	807	931	953	1058	1126	1147	919	1024	1083	1112	1147	1181	1231	1254	1272	43.00
44.00	789	931	931	1073	1073	1073	808	931	953	1058	1126	1147	919	1024	1083	1112	1147	1181	1231	1254	1272	44.00
45.00	789	931	931	1073	1073	1073	809	931	953	1058	1126	1147	919	1024	1083	1112	1147	1181	1231	1254	1272	45.00
46.00	790	931	931	1073	1073	1073	810	931	953	1058	1126	1147	919	1024	1083	1112	1147	1181	1231	1254	1272	46.00
47.00	790	931	931	1073	1073	1073	811	931	953	1058	1126	1147	919	1024	1083	1112	1147	1181	1231	1254	1272	47.00
48.00	791	931	931	1073	1073	1073	812	931	953	1058	1126	1147	919	1024	1083	1112	1147	1181	1231	1254	1272	48.00
49.00	791	931	931	1073	1073	1073	813	931	953	1058	1126	1147	919	1024	1083	1112	1147	1181	1231	1254	1272	49.00
50.00	792	931	931	1073	1073	1073	814	931	953	1058	1126	1147	919	1024	1083	1112	1147	1181	1231	1254	1272	50.00

CUWUHTI = 6,54000; 6,00000 MU

R (cm)		250	260	270	280	290	300	310	320	330	340	350	360	370	380	390	400	410	420	430	440	450	460	470	480	490	500	510	520	530	540	550	560	570	580	590	600	610	620	630	640	650	660	670	680	690	700	710	720	730	740	750	760	770	780	790	800	810	820	830	840	850	860	870	880	890	900	910	920	930	940	950	960	970	980	990	1000	1010	1020	1030	1040	1050	1060	1070	1080	1090	1100	1110	1120	1130	1140	1150	1160	1170	1180	1190	1200	1210	1220	1230	1240	1250	1260	1270	1280	1290	1300	1310	1320	1330	1340	1350	1360	1370	1380	1390	1400	1410	1420	1430	1440	1450	1460	1470	1480	1490	1500	1510	1520	1530	1540	1550	1560	1570	1580	1590	1600	1610	1620	1630	1640	1650	1660	1670	1680	1690	1700	1710	1720	1730	1740	1750	1760	1770	1780	1790	1800	1810	1820	1830	1840	1850	1860	1870	1880	1890	1900	1910	1920	1930	1940	1950	1960	1970	1980	1990	2000	2010	2020	2030	2040	2050	2060	2070	2080	2090	2100	2110	2120	2130	2140	2150	2160	2170	2180	2190	2200	2210	2220	2230	2240	2250	2260	2270	2280	2290	2300	2310	2320	2330	2340	2350	2360	2370	2380	2390	2400	2410	2420	2430	2440	2450	2460	2470	2480	2490	2500	2510	2520	2530	2540	2550	2560	2570	2580	2590	2600	2610	2620	2630	2640	2650	2660	2670	2680	2690	2700	2710	2720	2730	2740	2750	2760	2770	2780	2790	2800	2810	2820	2830	2840	2850	2860	2870	2880	2890	2900	2910	2920	2930	2940	2950	2960	2970	2980	2990	3000	3010	3020	3030	3040	3050	3060	3070	3080	3090	3100	3110	3120	3130	3140	3150	3160	3170	3180	3190	3200	3210	3220	3230	3240	3250	3260	3270	3280	3290	3300	3310	3320	3330	3340	3350	3360	3370	3380	3390	3400	3410	3420	3430	3440	3450	3460	3470	3480	3490	3500	3510	3520	3530	3540	3550	3560	3570	3580	3590	3600	3610	3620	3630	3640	3650	3660	3670	3680	3690	3700	3710	3720	3730	3740	3750	3760	3770	3780	3790	3800	3810	3820	3830	3840	3850	3860	3870	3880	3890	3900	3910	3920	3930	3940	3950	3960	3970	3980	3990	4000	4010	4020	4030	4040	4050	4060	4070	4080	4090	4100	4110	4120	4130	4140	4150	4160	4170	4180	4190	4200	4210	4220	4230	4240	4250	4260	4270	4280	4290	4300	4310	4320	4330	4340	4350	4360	4370	4380	4390	4400	4410	4420	4430	4440	4450	4460	4470	4480	4490	4500	4510	4520	4530	4540	4550	4560	4570	4580	4590	4600	4610	4620	4630	4640	4650	4660	4670	4680	4690	4700	4710	4720	4730	4740	4750	4760	4770	4780	4790	4800	4810	4820	4830	4840	4850	4860	4870	4880	4890	4900	4910	4920	4930	4940	4950	4960	4970	4980	4990	5000
R (cm)		1.00	1.12	1.24	1.36	1.48	1.60	1.72	1.84	1.96	2.08	2.20	2.32	2.44	2.56	2.68	2.80	2.92	3.04	3.16	3.28	3.40	3.52	3.64	3.76	3.88	3.90	4.02	4.14	4.26	4.38	4.50	4.62	4.74	4.86	4.98	5.10	5.22	5.34	5.46	5.58	5.70	5.82	5.94	6.06	6.18	6.30	6.42	6.54	6.66	6.78	6.90	7.02	7.14	7.26	7.38	7.50	7.62	7.74	7.86	7.98	8.10	8.22	8.34	8.46	8.58	8.70	8.82	8.94	9.06	9.18	9.30	9.42	9.54	9.66	9.78	9.90	10.02	10.14	10.26	10.38	10.50	10.62	10.74	10.86	10.98	11.10	11.22	11.34	11.46	11.58	11.70	11.82	11.94	12.06	12.18	12.30	12.42	12.54	12.66	12.78	12.90	13.02	13.14	13.26	13.38	13.50	13.62	13.74	13.86	13.98	14.10	14.22	14.34	14.46	14.58	14.70	14.82	14.94	15.06	15.18	15.30	15.42	15.54	15.66	15.78	15.90	16.02	16.14	16.26	16.38	16.50	16.62	16.74	16.86	16.98	17.10	17.22	17.34	17.46	17.58	17.70	17.82	17.94	18.06	18.18	18.30	18.42	18.54	18.66	18.78	18.90	19.02	19.14	19.26	19.38	19.50	19.62	19.74	19.86	19.98	20.10	20.22	20.34	20.46	20.58	20.70	20.82	20.94	21.06	21.18	21.30	21.42	21.54	21.66	21.78	21.90	22.02	22.14	22.26	22.38	22.50	22.62	22.74	22.86	22.98	23.10	23.22	23.34	23.46	23.58	23.70	23.82	23.94	24.06	24.18	24.30	24.42	24.54	24.66	24.78	24.90	25.02	25.14	25.26	25.38	25.50	25.62	25.74	25.86	25.98	26.10	26.22	26.34	26.46	26.58	26.70	26.82	26.94	27.06	27.18	27.30	27.42	27.54	27.66	27.78	27.90	28.02	28.14	28.26	28.38	28.50	28.62	28.74	28.86	28.98	29.10	29.22	29.34	29.46	29.58	29.70	29.82	29.94	30.06	30.18	30.30	30.42	30.54	30.66	30.78	30.90	31.02	31.14	31.26	31.38	31.50	31.62	31.74	31.86	31.98	32.10	32.22	32.34	32.46	32.58	32.70	32.82	32.94	33.06	33.18	33.30	33.42	33.54	33.66	33.78	33.90	34.02	34.14	34.26	34.38	34.50	34.62	34.74	34.86	34.98	35.10	35.22	35.34	35.46	35.58	35.70	35.82	35.94	36.06	36.18	36.30	36.42	36.54	36.66	36.78	36.90	37.02	37.14	37.26	37.38	37.50	37.62	37.74	37.86	37.98	38.10	38.22	38.34	38.46	38.58	38.70	38.82	38.94	39.06	39.18	39.30	39.42	39.54	39.66	39.78	39.90	40.02	40.14	40.26	40.38	40.50	40.62	40.74	40.86	40.98	41.10	41.22	41.34	41.46	41.58	41.70	41.82	41.94	42.06	42.18	42.30	42.42	42.54	42.66	42.78	42.90	43.02	43.14	43.26	43.38	43.50	43.62	43.74	43.86	43.98	44.10	44.22	44.34	44.46	44.58	44.70	44.82	44.94	45.06	45.18	45.30	45.42	45.54	45.66	45.78	45.90	46.02	46.14	46.26																																																																																																	

REFERENCES

1. C. W. Spofford, "The FACT Model, Volume 1," Maury Center Report 109, (November 1974).
2. C. S. Clay, "Sound Propagation in a Half Channel and Surface Duct," Technical Notes on Sound Propagation in the Sea II, Meteorology International, Inc., Monterey, CA, (1968).
3. F. M. Labianca, "Critique of C. S. Clay's 'Sound Transmission in a Half Channel and Surface Duct'," Reference 8 in Continuation of LRAPP, February 1972, Bell Laboratories.
4. H. E. Morris, "Comparison of Propagation Prediction Models with SUDS I Acoustic Data," NUC-TP-377, (April 1974).
5. H. W. Marsh and M. Schulkin, Report on the Status of Project AMOS, U. S. Naval Underwater Sound Laboratory, New London, Conn., May 1977.
6. H. P. Bucker, "Sound Propagation in a Channel with Lossy Boundaries," J. Acoust. Soc. Am., Vol. 48, 1187-1194, (1970). This is an extension, to include rough surface effects, of the normal mode code of Pedersen and Gordon, Reference 12.
7. F. M. Labianca, "Normal Modes, Virtual Modes, and Alternative Representations in the Theory of Surface-Duct Sound Propagation," J. Acoust. Soc. Am., Vol. 53, 1137-1147, (1973).
8. C. W. Spofford, "Improved Surface Duct Model for FACT," Science Applications, Inc. Report No. SAI-78-687-WA, (1977).
9. W. H. Furry, "The Bi-linear Modified-Index Profile," in Propagation of Short Radio Waves, edited by D. E. Kerr, McGraw-Hill, (1951).
10. H. W. Marsh, "Theory of Anomalous Propagation of Acoustic Waves in the Ocean," U. S. Naval Underwater Sound Laboratory Report No. 111, (1950).
11. M. Hall, "Mode Theory of Wave Propagation in a Bilinear Medium: the WKB Approximation," J. Acoust. Soc. Am., Vol. 60, 810-814, (1976).
12. M. A. Pedersen and D. F. Gordon, "Normal-Mode Theory Applied to Short-Range Propagation in an Underwater Acoustic Surface Duct," J. Acoust. Soc. Am., Vol. 37, 105-118, (1965); M. A. Pedersen and D. F. Gordon, "Theoretical Investigation of a Double Family of Normal Modes in an Underwater Acoustic Surface Duct," ibid, Vol. 47, 304-326, (1970).

13. The form of Eq. (2.6) is equivalent to Labianca's Eq. (23.a) (Ref. 7) if the following identifications between Labianca's notation and the present are made

$$k^2 \lambda = \kappa^2 = (E + s^3 D)/H^2$$

$$\phi(Z, \lambda) = \psi(x, E)$$

$$A(\lambda) \pm iB(\lambda) = T_{\pm}(E) .$$

The factor of H arises from use of the dimension-less variable x instead of Z in the delta-function source term.

14. The intensity is normalized against a value of $4\pi r_0^2$ at unit distance r_0 (i.e., one foot or one meter).
15. M. Abramowitz and I. A. Stegun, Handbook of Mathematical Functions, Chapter 10, Dover Publications, (1965).
16. H. K. Brock, "The AESD PARABOLIC Equation Model," NORDA Tech Note 12, (1978).
17. R. E. Keenan and C. W. Spofford, "Rough Surface Loss for FACT," SAI Report No. SAI-78-688-WA, (November 1977).